

**Pathophysiology of early-onset isolated dystonia in a DYT-TOR1A  
rat model with trauma-induced dystonia-like movements**

\*

**Pathophysiologie der früh beginnenden, isolierten Dystonie in  
einem DYT-TOR1A Rattenmodell mit Trauma-induzierten  
Dystonie-ähnlichen Bewegungen**



Doctoral thesis for a doctoral degree  
at the Graduate School of Life Sciences,  
Julius-Maximilians-Universität Würzburg,  
Section Neuroscience

submitted by

**Susanne Knorr**

from

Würzburg

Würzburg 2019

**Submitted on: 16.12.2019**

**Members of the *Promotionskomitee*:**

**Chairperson: Prof. Dr. Matthias Gamer**

**Primary Supervisor: Prof. Dr. Jens Volkmann**

**Supervisor (Second): Prof. Dr. Rudolf Martini**

**Supervisor (Third): PD Dr. Chi Wang Ip**

**Supervisor (Fourth): PD Dr. Robert Blum**

**Date of Public Defence:**

**Date of Receipt of Certificates:**

### *Affidavit*

I hereby confirm that my thesis entitled “Pathophysiology of early-onset isolated dystonia in a DYT-TOR1A rat model with trauma-induced dystonia-like movements” is the result of my own work. I did not receive any help or support from commercial consultants. All sources and / or materials applied are listed and specified in the thesis.

Furthermore, I confirm that this thesis has not yet been submitted as part of another examination process neither in identical nor in similar form.

Würzburg, 16.12.2019

---

Susanne Knorr

### *Eidesstattliche Erklärung*

Hiermit erkläre ich an Eides statt, die Dissertation „Pathophysiologie der früh beginnenden, isolierten Dystonie in einem DYT-TOR1A Rattenmodell mit Trauma-induzierten Dystonie-ähnlichen Bewegungen“ eigenständig, d.h. insbesondere selbstständig und ohne Hilfe eines kommerziellen Promotionsberaters, angefertigt und keine anderen, als die von mir angegebenen Quellen und Hilfsmittel verwendet zu haben.

Ich erkläre außerdem, dass die Dissertation weder in gleicher noch in ähnlicher Form bereits in einem anderen Prüfungsverfahren vorgelegen hat.

Würzburg, 16.12.2019

---

Susanne Knorr

*„Der Sinn des Lebens besteht nicht darin,  
ein erfolgreicher Mensch zu sein,  
sondern ein wertvoller.“*

**Albert Einstein**

**Table of contents**

Table of contents .....	1
Abstract .....	5
Zusammenfassung .....	6
1 Introduction.....	8
1.1 Dystonia .....	8
1.2 DYT nomenclature.....	11
1.3 Pathophysiology of Dystonia .....	11
1.3.1 Basal ganglia .....	15
1.3.2 Striatal interneurons.....	17
1.3.3 Dopaminergic and serotonergic neurotransmitters .....	18
1.4 Relevance of environmental factors in dystonia .....	21
1.5 Treatment of dystonia.....	21
1.6 DYT-TOR1A dystonia.....	23
1.7 TorsinA.....	23
1.8 DYT-TOR1A animal models .....	25
1.8.1 Transgenic $\Delta$ ETorA DYT-TOR1A rat model.....	26
1.9 Aim of the study.....	28
2 Material and Methods.....	30
2.1 Material.....	30
2.1.1 Devices .....	30
2.1.2 Consumables .....	31
2.1.3 Chemicals, reagents and pharmaceuticals .....	32
2.1.4 Buffers and solutions .....	35
2.1.5 Antibodies .....	38
2.1.6 Commercial kits .....	39
2.1.7 Primer sequences .....	39
2.1.8 TaqMan Gene Expression Assays.....	40

2.1.9	Software.....	41
2.2	Methods.....	42
2.2.1	Animal model.....	42
2.2.2	Genotyping.....	42
2.2.2.1	Extraction of genomic DNA.....	42
2.2.2.2	Polymerase chain reaction (PCR).....	42
2.2.2.3	DNA gel electrophoresis.....	43
2.2.3	Sciatic nerve crush injury.....	43
2.2.4	Behavioral testing.....	44
2.2.4.1	Tail Suspension Test (TST).....	44
2.2.4.2	Open Field (OF).....	44
2.2.5	Nerve conduction studies.....	44
2.2.6	DBS and LFP recordings.....	45
2.2.6.1	Electrode implantation.....	45
2.2.6.2	DBS.....	45
2.2.6.3	LFP recordings and data analysis.....	45
2.2.6.4	Spectral power and imaginary coherence analysis.....	46
2.2.7	Autoradiography.....	47
2.2.8	Tissue dissection and processing.....	47
2.2.9	Histology.....	48
2.2.9.1	Nissl staining.....	48
2.2.9.2	Immunohistochemical staining of striatal interneurons.....	48
2.2.9.3	Unbiased stereology.....	49
2.2.9.4	Bright-field microscopy.....	49
2.2.10	Gene expression.....	49
2.2.10.1	RNA purification and quantification.....	50
2.2.10.2	Reverse transcriptase polymerase chain reaction (RT-PCR).....	50
2.2.10.3	Real-time PCR (qPCR).....	50

2.2.10.4	RNA-Sequencing (RNA-Seq).....	51
2.2.11	Microdialysis .....	52
2.2.11.1	Assembling microdialysis probes .....	52
2.2.11.2	Implantation of microdialysis probes .....	53
2.2.11.3	Microdialysis – Collection of microdialysis samples .....	53
2.2.12	High performance liquid chromatography (HPLC).....	54
2.2.12.1	HPLC analysis of monoamines of striatal tissue samples .....	54
2.2.12.2	HPLC analysis of striatal microdialysis samples .....	55
2.2.13	Western blot analysis.....	55
2.2.14	Statistical analysis .....	56
3	Results .....	57
3.1	Dystonia-like movements (DLM) triggered in $\Delta$ ETorA rats through a unilateral sciatic nerve crush .....	57
3.2	Alteration of theta and beta oscillations in the brain network of $\Delta$ ETorA rats .....	63
3.3	DBS improves clinical phenotype and modulates the brain network oscillations in $\Delta$ ETorA rats .....	64
3.4	Increased glucose metabolism depending on genetic background and environmental trigger .....	67
3.5	Striatal neurons are unaltered in cell number and in gene expression levels of neuronal markers .....	69
3.6	Striatal monoamine metabolism is altered in sciatic nerve-injured $\Delta$ ETorA rats .....	73
3.7	Transcriptome analysis by RNA-Seq of the striatum .....	84
4	Discussion .....	90
4.1	Nerve-injured $\Delta$ ETorA rats as a new DYT-TOR1A rodent model with DLM on a DYT-TOR1A genetic background .....	90
4.2	DBS as a beneficial therapeutic approach in nerve-injured $\Delta$ ETorA rats.....	92

4.3	Peripheral trauma has an impact on brain glucose metabolism in the central motor network .....	94
4.4	$\Delta$ ETorA rats display no alterations in striatal neuron cell number and striatal glutamatergic and cholinergic gene expression profiles.....	95
4.5	$\Delta$ ETorA rats exhibit abnormalities in catecholamine metabolism after peripheral trauma.....	98
4.6	Evidence of new potential pathways in DYT-TOR1A dystonia by whole-transcriptome analysis .....	101
4.7	Synopsis.....	106
5	References .....	108
6	Appendix .....	123
6.1	Supplementary data .....	123
6.2	List of Figures.....	129
6.3	List of Tables .....	131
6.4	Abbreviations.....	132
7	Curriculum vitae .....	137
8	Publications.....	139
9	Danksagung .....	143

## Abstract

Early-onset torsion dystonia (DYT-TOR1A, DYT1) is an inherited hyperkinetic movement disorder caused by a mutation of the *TOR1A* gene encoding the torsinA protein. DYT-TOR1A is characterized as a network disorder of the central nervous system (CNS), including predominantly the cortico-basal ganglia-thalamo-cortical loop resulting in a severe generalized dystonic phenotype. The pathophysiology of DYT-TOR1A is not fully understood. Molecular levels up to large-scale network levels of the CNS are suggested to be affected in the pathophysiology of DYT-TOR1A. The reduced penetrance of 30% - 40% indicates a gene-environmental interaction, hypothesized as “second hit”. The lack of appropriate and phenotypic DYT-TOR1A animal models encouraged us to verify the “second hit” hypothesis through a unilateral peripheral nerve trauma of the sciatic nerve in a transgenic asymptomatic DYT-TOR1A rat model ( $\Delta$ ETorA), overexpressing the human mutated torsinA protein. In a multiscale approach, this animal model was characterized phenotypically and pathophysiologically.

Nerve-injured  $\Delta$ ETorA rats revealed dystonia-like movements (DLM) with a partially generalized phenotype. A physiomarker of human dystonia, describing increased theta oscillation in the globus pallidus internus (GPi), was found in the entopeduncular nucleus (EP), the rodent equivalent to the human GPi, of nerve-injured  $\Delta$ ETorA rats. Altered oscillation patterns were also observed in the primary motor cortex. High-frequency stimulation (HFS) of the EP reduced DLM and modulated altered oscillatory activity in the EP and primary motor cortex in nerve-injured  $\Delta$ ETorA rats. Moreover, the dopaminergic system in  $\Delta$ ETorA rats demonstrated a significant increased striatal dopamine release and dopamine turnover. Whole transcriptome analysis revealed differentially expressed genes of the circadian clock and the energy metabolism, thereby pointing towards novel, putative pathways in the pathophysiology of DYT-TOR1A dystonia.

In summary, peripheral nerve trauma can trigger DLM in genetically predisposed asymptomatic  $\Delta$ ETorA rats leading to neurobiological alteration in the central motor network on multiple levels and thereby supporting the “second hit” hypothesis. This novel symptomatic DYT-TOR1A rat model, based on a DYT-TOR1A genetic background, may prove as a valuable chance for DYT-TOR1A dystonia, to further investigate the pathomechanism in more detail and to establish new treatment strategies.

## Zusammenfassung

Früh beginnende Torsionsdystonie (DYT-TOR1A, DYT1) ist eine genetisch bedingte hyperkinetische Bewegungsstörung, die aufgrund einer Mutation im *TOR1A* Gen verursacht wird, welches für das TorsinA-Protein codiert. DYT-TOR1A wird als zentrale Netzwerkstörung bezeichnet und betrifft hauptsächlich die kortiko-striato-thalamo-kortikale Funktionsschleife, welches schließlich zu einem schweren generalisierten dystonen Phänotyp führt. Die Pathophysiologie von DYT-TOR1A ist nicht vollständig verstanden, man geht jedoch davon aus, dass Ebenen im Zentralnervensystem von molekularer Basis bis hin zu ganzen Netzwerken betroffen sind. Die reduzierte Penetranz von nur 30% bis 40% deutet auf eine Gen-Umwelt-Interaktion hin, im Sinne einer „2-Treffer-Hypothese“. Auch das Fehlen eines adäquaten DYT-TOR1A Tiermodelles hat uns dazu veranlasst, die „2-Treffer-Hypothese“ zu verifizieren, indem eine unilaterale periphere Quetschläsion des Nervus ischiadicus in einem transgenen, asymptomatischen DYT-TOR1A Rattenmodell ( $\Delta$ ETorA) durchgeführt wurde, welches das humane mutierte TorsinA-Protein überexprimiert. Das Tiermodell wurde phänotypisch und pathophysiologisch auf verschiedenen Analyseebenen charakterisiert.

$\Delta$ ETorA Ratten mit Quetschläsion entwickelten Dystonie-ähnliche Bewegungen (DLM) mit teilweise generalisiertem Phänotyp. Erhöhte Theta-Oszillationen im Globus pallidus internus (GPi) sind bezeichnend für die humane Dystonie, welche auch im Nucleus entopeduncularis (EP), dem Äquivalent zum humanen GPi, von  $\Delta$ ETorA Ratten mit Quetschläsion nachgewiesen wurden. Veränderte oszillatorische Muster wurden auch im primären Motorkortex gefunden. Hochfrequenz-Stimulation (HFS) des EP konnte das klinische Erscheinungsbild verbessern und hatte zudem auch einen modulatorischen Effekt auf die veränderte oszillatorische Aktivität des EP und des primären Motorcortex von  $\Delta$ ETorA Ratten mit Quetschläsion. Auch das veränderte dopaminerge System erwies sich als ein pathologisches Merkmal in  $\Delta$ ETorA Ratten. Es fand sich eine erhöhte striatale Ausschüttung von Dopamin und ein erhöhter Dopaminumsatz. In der Transkriptomanalyse kamen die zirkadiane Uhr und der Energiemetabolismus als weitere potentielle Signalwege in der Pathophysiologie der DYT-TOR1A Dystonie zum Vorschein.

Zusammengefasst konnten DLM in genetisch prädisponierten, asymptomatischen  $\Delta$ ETorA Ratten mittels peripheren Nerventraumas ausgelöst werden, welches zu neurobiologischen Veränderungen in verschiedenen Ebenen des zentralen

motorischen Netzwerk führte. Somit konnte die „2-Treffer-Hypothese“ bestätigt werden. Dieses neue symptomatische DYT-TOR1A Rattenmodell, fundiert auf der genetischen Grundlage von DYT-TOR1A, kann sich als wertvolle Möglichkeit für die DYT-TOR1A Dystonie erweisen, um Pathomechanismen genauer zu untersuchen und neue Behandlungsstrategien zu entwickeln.

## 1 Introduction

### 1.1 Dystonia

*“Dystonia is a movement disorder characterized by sustained or intermittent muscle contractions causing abnormal, often repetitive, movements, postures, or both. Dystonic movements are typically patterned, twisting, and may be tremulous. Dystonia is often initiated or worsened by voluntary action and associated with overflow muscle activation”*, is the current generally valid definition for dystonia described by Alberto Albanese in 2013.<sup>1</sup>

Dystonia is the third most common movement disorder after essential tremor and Parkinson's disease (PD). It is described as a disease as well as a syndrome or a symptom and is considered a central network disorder. Dystonic movements can present as single or repetitive, short- or long-lasting abnormal movements. The dystonic phenotype is very diverse due to variability in movement intensity, frequency, speed, amplitude, and duration. It also shows a broad range of different types of movements from twisting, turning, jerks, fixed postures to dystonic storm, which is a rare life-threatening episode of severe generalized dystonia. Dystonic movements are based on excessive involuntary muscle co-contractions of agonist and antagonist. In dystonia, any voluntary muscles can be affected, and the involvement of affected muscles can spread over time. Dystonia can occur spontaneously, or it can be inherited.

Dystonia was described for the first time as “dystonia musculorum deformans” by Hermann Oppenheim in 1911.<sup>2</sup> Definition and classification of dystonia changed over time because of increased knowledge about this movement disorder. The latest dystonia definition was published in 2013 by Alberto Albanese and an international consensus committee and thereby replaced the first consensus definition of dystonia from 1984.<sup>1,3</sup> The new two axes classification focuses on clinical characteristics (Axis I) and etiology (Axis II). The new classification of dystonia is presented in Table 1 and is described more in detail in the following passage.<sup>1</sup>

**Table 1: Classification of dystonia by Albanese et al. 2013<sup>1</sup>**

Axis I. Clinical characteristics	Axis II. Etiology
<p><b>Age at onset</b></p> <ul style="list-style-type: none"> <li>• Infancy (neonatal to 2 years)</li> <li>• Childhood (3–12 years)</li> <li>• Adolescence (13–20 years)</li> <li>• Early adulthood (21–40 years)</li> <li>• Late adulthood (&gt;40 years)</li> </ul> <p><b>Body distribution</b></p> <ul style="list-style-type: none"> <li>• Focal</li> <li>• Segmental</li> <li>• Multifocal</li> <li>• Hemidystonia</li> <li>• Generalized</li> </ul> <p><b>Temporal pattern</b></p> <ul style="list-style-type: none"> <li>• Persistent</li> <li>• Action-specific</li> <li>• Diurnal fluctuations</li> <li>• Paroxysmal</li> </ul> <p><b>Classification of dystonias by associated features</b></p> <ul style="list-style-type: none"> <li>• Isolated dystonia</li> <li>• Combined dystonia</li> </ul>	<p><b>Nervous system pathology</b></p> <p><i>Evidence of degeneration</i></p> <p><i>Evidence of structural (often static) lesions</i></p> <p><i>No evidence of degeneration or structural lesion</i></p> <p><b>Inherited or acquired</b></p> <p><i>Inherited</i></p> <ul style="list-style-type: none"> <li>• Autosomal dominant</li> <li>• Autosomal recessive</li> <li>• X-linked recessive</li> <li>• Mitochondrial</li> </ul> <p><i>Acquired</i></p> <ul style="list-style-type: none"> <li>• Perinatal brain injury</li> <li>• Infection</li> <li>• Drug</li> <li>• Toxic</li> <li>• Vascular</li> <li>• Neoplastic</li> <li>• Brain injury</li> <li>• Psychogenic</li> </ul> <p><i>Idiopathic</i></p> <ul style="list-style-type: none"> <li>• Sporadic</li> <li>• Familial</li> </ul>

This new dystonia classification by clinical characteristics includes the age of onset, body distribution, temporal pattern, and associated features as well as by etiology according to nervous system pathology and inheritance. It is supposed to improve diagnosis and treatment with the aim of a better outcome for dystonia patients.<sup>1</sup>

Age of onset is a relevant feature for diagnosis and prognosis, and it is subdivided in infancy, childhood, adolescence, early adulthood, and late adulthood. Dystonias with an early-onset are more likely to be rare, with a genetic background and a progression from focal to generalized such as DYT-TOR1A (DYT1). Dystonias with a late-onset, which most often present with a focal pattern such as writer's cramp, torticollis, and blepharospasm are more frequent.<sup>1,4</sup>

The distribution of affected body regions is a meaningful clinical characteristic for diagnosis and therapy. Body distribution can be focal, segmental, multifocal, generalized. In addition, hemidystonia is described for this part. Affected body regions do not remain constant. Dystonic symptoms can spread over time to different body

regions. In writer's cramp only one body part is affected as an example for focal dystonia. In segmental dystonia two or more contiguous body parts are involved. Meige syndrome is an example of segmental dystonia in which blepharospasm is combined with mouth, tongue or jaw dystonia. Two or more noncontiguous body parts are involved in multifocal dystonia, like in blepharospasm, together with a writer's cramp. The meaning of "generalized" is that the trunk and at least two other sites are affected. DYT-TOR1A is a typical example of generalized dystonia. In hemidystonia two or more body parts of one body side are involved. Possible causes for hemidystonia are cerebral insults such as ischemia or a tumor, along with many other reasons.<sup>1,5</sup>

Temporal pattern is structured in persistent, action-specific, diurnal fluctuations, and paroxysmal. Temporal pattern is a useful indicator for diagnosis and treatment. Dystonia can persist almost constantly throughout the day (persistent), appear only during specific activities or tasks (action-specific), fluctuate during the day (diurnal fluctuations), or be self-limited during sudden episodes, usually elicited by a trigger (paroxysmal).<sup>1</sup>

Associated features distinguish between isolated and combined dystonia. Isolated dystonia shows only dystonic motor features, apart from tremor. If dystonia is combined with another movement disorder, such as PD, the term combined dystonia is used.<sup>1</sup>

In the second axis of the classification, the nervous system pathology is divided into subgroups of dystonia with degeneration, static lesion, and no evidence of degeneration or structural lesion.<sup>1</sup>

Furthermore, dystonia can be classified as inherited, acquired and idiopathic. Modes of inheritance in dystonia with proven genetic background can be autosomal dominant, such as DYT-TOR1A, DYT-THAP1 (DYT6), DYT-SGCE (DYT11), DYT-ATP1A3 (DYT12); autosomal recessive like Wilson's disease; X-linked recessive in DYT-TAF1 (DYT3); mitochondrial in Leigh syndrome. Dystonia can also be acquired through perinatal brain injury; infection via viral encephalitis, HIV, tuberculosis, syphilis and others; drug intake like levodopa, neuroleptics etc.; toxic explosion with methanol, cobalt, carbon disulfide, cyanide and many more; vascular events like ischemia, hemorrhage etc.; neoplasticity because of brain tumor or paraneoplastic encephalitis; brain injury including head trauma, brain surgery and others; psychogenic cause. Idiopathic dystonia can have a familiar background or can be sporadic.<sup>1</sup>

Because of the heterogeneity in dystonia it is still complicated to find a consensus and satisfactory classification for dystonia.<sup>6,7</sup> Therefore, a modified dystonia classification was generated by adding the term “complex dystonia” to the subgroup associated features of Axis I. Complex dystonia describes dystonia together with other neurologic or systemic diseases. Dystonia doesn't have to be the most prominent disease and can also be an inconsistent phenotype in complex dystonia.<sup>8</sup> This modified version is currently used in clinical practice in Germany.

## 1.2 DYT nomenclature

In the dystonia nomenclature, dystonias were designated with the prefix DYT, followed by a number. The numeric DYT locus symbol was assigned chronologically to the first description in the literature of the dystonic phenotype and/or the genetic loci. Currently, 29 different DYT loci are defined with the DYT nomenclature system, designated as DYT1-DYT29.<sup>8</sup> A new dystonia nomenclature was recommended and provided by the International Parkinson and Movement Disorder Society Task Force.<sup>9</sup> In this new and more informative nomenclature the gene name of the identified mutation is added to the symbol prefix DYT. As an example, DYT1 was suggested to be replaced by DYT-TOR1A.<sup>9,10</sup> However, it is complicated to find a generally satisfying nomenclature because of the diversity and complexity of dystonia and the difficulties in the nomenclature itself. An ongoing discussion exists between dystonia experts regarding the most useful dystonia nomenclature.<sup>6,7,11</sup>

## 1.3 Pathophysiology of Dystonia

Dystonia is a very diverse disorder with a pathophysiology that is still not fully understood. Traditionally, dystonia was linked to basal ganglia pathology. Further investigations proved the involvement of different brain areas structurally or functionally. Dystonia was suggested to rather be a functional network disorder involving basal ganglia, cerebellum, and cerebral cortex and many other brain areas that are part of the central motor network. There is clear evidence for anatomical and structural changes in patients with secondary dystonia.<sup>12,13</sup> Various studies pointed out the basal ganglia, especially the putamen are involved in dystonia. In a study with 28 patients with hemidystonia or isolated limb dystonia, lesions were detected in the putamen, caudate nucleus, thalamus, or a combination of these structures<sup>14</sup>, which

was also confirmed by further studies.<sup>15,16</sup> Dystonia was found in 36% of the cases in a cohort of 240 patients with basal ganglia lesions.<sup>17</sup> Cortex, cerebellum, brainstem, spinal cord, thalamus are additional structures involved in dystonia.<sup>18-21</sup> However, it has to be considered that not all described structural defects cause dystonia in every individual consistently and not all dystonia patients show the same anatomical basis. Also, structural defects can have a late onset (weeks or years) of dystonia, indicating that the lesion itself is not directly responsible for dystonia. Instead, reorganization of brain structures and compensatory mechanism could be putative explanations for dystonia.<sup>16,22,23</sup> Changes in the grey-matter volume were also detected. The grey-matter volume was increased in the putamina of patients with blepharospasm as well as in sensorimotor areas of patients with secondary cervical dystonia and focal hand dystonia. A decreased grey-matter volume was detected in the sensorimotor cortex, cerebellum and thalamus of patients with writer's cramp.<sup>24-27</sup> Furthermore, abnormal brain function regarding the glucose metabolism under movement free condition was described in the brain regions of the lentiform nuclei, cerebellum and supplementary motor areas in manifesting and non-manifesting DYT-TOR1A gene carriers compared to healthy subjects.<sup>28</sup>

Characteristic features of dystonia are abnormalities in the pallidal activity. In the globus pallidus internus (GPi) of human dystonia patients as well as in the entopeduncular nucleus (EP) of *dt<sup>sz</sup>* hamsters, a reduced discharge rate and an abnormal bursting activity were described.<sup>29,30</sup> An additional element in the pathophysiology of dystonia is the altered theta oscillation activity in the GPi. In dystonia patients the theta frequency band (4-12 Hz) in local field potential (LFP) recordings was increased, reflecting an abnormal neuronal synchronization.<sup>31-33</sup> The prokinetic oscillatory activity of the theta band correlated with the electromyography (EMG) activity of affected dystonic muscles as well as dystonic symptom severity.<sup>34,35</sup> Additionally, coherence exists between theta oscillation patterns and electroencephalography (EEG) activity of cortical motor areas.<sup>34,36</sup> The exact role of the altered oscillation patterns in the theta band as a causal factor for the dystonic phenotype is still unclear. However, the involvement of the altered pallidal frequency patterns in dystonia pathology is supported by high-frequency stimulation (HFS) of the GPi, which is improving dystonic symptom severity by reducing oscillatory pallidal theta activity.<sup>34,35</sup> The influence of the GPi in dystonia can be emphasized by the

improvement of dystonic symptoms, especially in DYT-TOR1A patients, by HFS of the GPi.<sup>37</sup>

Moreover, the influence of different neurotransmitter systems in the pathophysiology of dystonia is discussed. The involvement of the dopaminergic system in the pathophysiology of dystonia can easily be confirmed. Dopa-responsive dystonia (DRD) patients respond effectively to L-3,4-dihydroxyphenylalanine (levodopa, L-DOPA).<sup>38</sup> On the other hand, a dystonic phenotype can be triggered through a dopamine (DA) receptor blocker, seen in patients with a psychiatric disorder.<sup>39</sup> An analysis of the dopaminergic system showed a decreased expression of DA receptors D2 (D<sub>2</sub>R) and an increased expression of DA receptors D1 (D<sub>1</sub>R) in the striatum of different types of dystonia.<sup>40-43</sup> Conflicting data exist about the striatal expression patterns of DA, and its metabolites. Decreased or equivalent DA and DA metabolites expression levels as well as increased DA turnover rates were detected in DYT-TOR1A patients and DYT-TOR1A mouse models.<sup>44-49</sup> A decreased DA reuptake indicates a reduced DA transporter (DAT) activity in a transgenic DYT-TOR1A mouse model.<sup>50</sup> Based on neuroimaging and neurophysiological studies, additional physiological concepts for dystonia are discussed, namely loss of inhibition, disturbed sensorimotor integration and maladaptive plasticity.<sup>12,51</sup> Voluntary movements are target-oriented and precisely mediated through “surround inhibition”.<sup>52</sup> This loss of inhibition can evoke dystonic movements, characterized through co-contractions of agonistic and antagonistic muscles and an overflow activity of non-involved muscles. Loss of inhibition was evaluated within the cortex, brainstem, and spinal cord for different types of dystonia such as focal hand dystonia and blepharospasm.<sup>53-56</sup> Deficits in separating sensory stimuli in location (spatial discrimination) and time (temporal discrimination) in patients with focal dystonia indicate alterations of sensorimotor integration, which was detected in unaffected body parts.<sup>57,58</sup> Dystonic symptoms can also be alleviated by so-called sensory tricks such as a slight touch of the cheek in patients with cervical dystonia.<sup>51</sup> In a physiological state, sensorimotor integration transforms sensory input into a controlled motor output and all sensory information is filtered beforehand by specific brain areas, referred to “sensory gating”.<sup>59</sup> Basal ganglia and cerebellum seem to be the structures involved in abnormal sensorimotor integration relating to the function of “sensory gating”. “Sensory gating” is the process of filtering all environmental sensory input by the central nervous system (CNS), while altering the somatosensory threshold in the cortex. Sensory input reaches cerebellum directly from the spinal cord and

indirectly from the basal ganglia via the cerebro-pontine-cerebellar pathway.<sup>60-62</sup> Furthermore, maladaptive plasticity is described as another important element in the pathophysiology of dystonia. Indicative of this concept is the impaired sequence learning of DYT-TOR1A patients.<sup>63</sup> General neuronal plasticity is an important mechanism for learning and memory by modifying and adapting neuronal connections in the brain in response to the environment. A model for synaptic plasticity is long-term potentiation (LTP) and long-term depression (LTD).<sup>64</sup> An abnormal plasticity was detected in striatal, brainstem and cortical areas in dystonia patients as well as in dystonia animal models.<sup>65</sup> DYT-TOR1A patients and patients with writer's cramp and blepharospasm showed an increase in LTP-like plasticity compared to healthy subjects.<sup>66-68</sup> Moreover, abnormal plasticity was detected in cortical areas of unaffected body parts of patients with focal dystonia.<sup>69</sup> In a dystonia monkey model, focal dystonia was induced by a specific overuse motor task, which resulted in a less well organized somatosensory cortex with larger receptive and overlapping fields.<sup>70</sup> An asymptomatic DYT-TOR1A mouse model showed increased striatal LTP-like plasticity and decreased LTD-like plasticity.<sup>71</sup> It can be assumed that maladaptive plasticity evolves dystonic symptoms by forming abnormal motor engrams.<sup>72</sup> Despite all these findings, it has still to be clarified what is cause and what is effect in the pathophysiology of dystonia, and whether there is a common pathophysiologic finding for all types of dystonia. A potential concept of the pathophysiology of dystonia is illustrated in Figure 1.

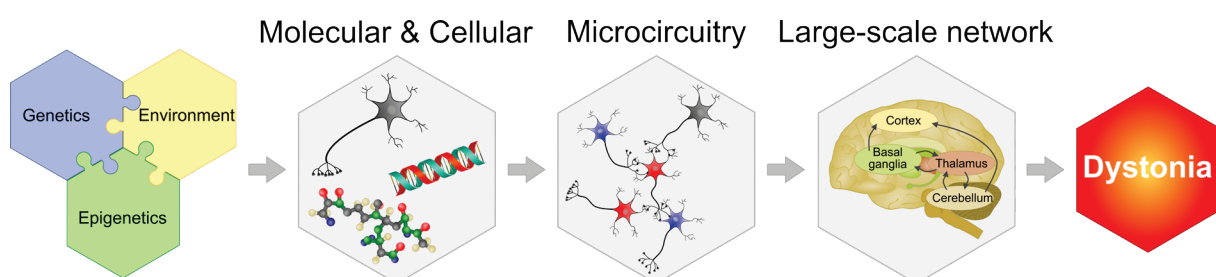


**Figure 1: Potential concept of the pathophysiology of dystonia**

The pathophysiological concept of dystonia includes different biological levels, involving genetic alterations together with epigenetic factors and environmental triggers, which can influence molecular structures and gene expression profiles as well as cellular components. Cellular networks can be affected through maladaptive plasticity, loss of inhibition, aberrant neuronal firing, and neurotransmission, which leads to a disturbance of the large-scale brain network, predominantly affecting the cortico-basal ganglia-thalamo-cortical loop. Potential changes of the brain activity through alterations in signal transduction, metabolic processes and local field oscillation patterns can finally be a putative source for the development of dystonia.

### 1.3.1 Basal ganglia

The basal ganglia comprise a group of interconnected nuclei in the CNS involved in multiple processes, including motor control, motor learning, cognitive functions, and emotions.<sup>73</sup> The basal ganglia are subdivided into a dorsal part, which is associated with motor functions and into a ventral part, which is associated with limbic functions. The ventral division of the basal ganglia includes the ventral striatum (nucleus accumbens), ventral pallidum and ventral tegmental area. The dorsal division of the basal ganglia comprises the dorsolateral part of the striatum (subdivided into caudate nucleus and putamen), the pallidum (globus pallidus (GP)); subdivided into external segment (GPe) and internal segment (GPi); and the rodent GPi equivalent, the EP, subthalamic nucleus (STN) and the substantia nigra (SN); subdivided into the dorsal part, the pars compacta (SNc), and the ventral part, the pars reticulata (SNr)).<sup>74</sup> These structures are involved in motor control, which is a part of the cortico-basal ganglia-thalamo-cortical loop (Figure 2). The primary input structure of the basal ganglia, the striatum, receives excitatory input from cortex and thalamus through the neurotransmitter glutamate on inhibitory gamma-aminobutyric acid (GABA)-ergic medium-sized densely spiny neurons (MSNs). MSNs represent about 95% of all striatal neurons and can be subdivided into two main classes according to their projection output targets. MSNs expressing DA class-1 receptors (includes D<sub>1</sub>R and D<sub>5</sub>R) and the muscarinic acetylcholine receptor M4 belong to the direct pathway, which is monosynaptic and an excitatory pathway. Activated GABAergic MSNs project directly to GABAergic neurons of the output structures, the GPi and SNr. The inhibition of GPi and SNr neurons lead to a disinhibition of excitatory glutamatergic neurons of the thalamus, projecting into the cortex and thereby promoting movement initiation. MSNs expressing DA class-2 receptors (includes D<sub>2</sub>R, D<sub>3</sub>R, and D<sub>4</sub>R) and the adenosine A<sub>2a</sub> receptor belong to the indirect pathway, which is polysynaptic and an inhibitory pathway. GABAergic projections from the MSNs inhibit the GABAergic neurons of the GPe, leading to a disinhibition excitatory glutamatergic of STN neurons. Disinhibition of the STN activates the inhibitory effect on the GABAergic basal ganglia output structures GPi and SNr and results in an inhibition of excitatory glutamatergic thalamic neurons, leading to movement inhibition. Further interactions and modulations of striatal circuits influence the motor output, like synaptic connections between direct and indirect pathway MSNs, different types of striatal cholinergic and GABAergic interneurons, thalamostriatal projections and the neuromodulators DA and

serotonin (5-hydroxytryptamine, 5-HT). The nigrostriatal pathway is the central part of the important neuromodulator DA from the SNc to the striatum. Depending on the class of DA receptors, DA can have an excitatory effect (interaction with D<sub>1</sub>R) or an inhibitory effect (interaction with D<sub>2</sub>R). DA has a modulatory effect on GABAergic and cholinergic interneurons on the excitability of striatal MSNs and the synaptic transmission in the cortex. Thalamostriatal projections influence striatal circuits mainly through glutamatergic transmission on cholinergic interneurons.<sup>73-79</sup>

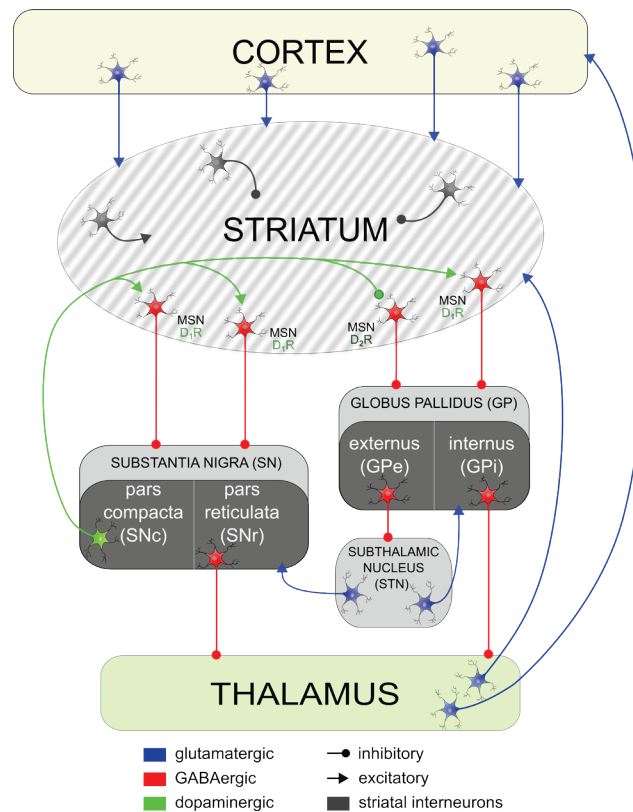


**Figure 2: Basal ganglia network**

The scheme shows the main pathways of the basal ganglia, including the various types of neurons and their inhibitory and excitatory connections.

Basal ganglia pathology contributes to many movement disorders such as PD and Huntington's disease (HD).<sup>73</sup> The involvement of the basal ganglia in the pathophysiology of dystonia could also be shown in patients with secondary dystonia and dystonia animal models.<sup>17,80</sup> Moreover, the successful treatment of DYT-TOR1A patients by deep brain stimulation (DBS) of the GPi confirms the assumption that the basal ganglia play a role in dystonia.<sup>81</sup> An imbalance between the direct and indirect pathway led to thalamo-motor-cortical hyperexcitability in patients with focal dystonia.<sup>82</sup>

### 1.3.2 Striatal interneurons

Striatal interneurons have a strong modulatory effect especially on the activity of MSNs in striatal circuits, even though the striatal interneurons comprise only ~3% - 5% of all striatal neurons.<sup>83-85</sup> Striatal interneurons are diverse and specified in two main types of cells; the medium-sized GABAergic interneurons and the large cholinergic interneurons (CINs).<sup>83,84</sup> CINs receive excitatory glutamatergic input from the cortex (weaker) and thalamus (stronger), from inhibitory GABAergic MSNs, and dopaminergic neurons of the SN.<sup>77,86-88</sup> CINs implement inhibitory and excitatory output depending on the acetylcholine receptor (AChR) types and projecting targets, which are MSNs and different types of GABAergic interneurons.<sup>76,77</sup> Nicotinic AChR (nAChR) are predominantly expressed on presynaptic DA terminals and parvalbumin-expressing fast-spiking interneuron (FSI) terminals.<sup>89,90</sup> MSNs and GABAergic interneurons express muscarinic AChR (mAChR).<sup>77,89,91</sup> CINs themselves express D<sub>2</sub>R and D<sub>5</sub>R and M<sub>2</sub> and M<sub>4</sub> mAChRs. The characteristics of CINs are the tonic low-frequency firing pattern (<10 Hz) and the corelease of glutamate and acetylcholine (ACh).<sup>92-93</sup> The second group of striatal interneurons, the GABAergic interneurons, can be subdivided according to their electrophysiological characteristic and protein expression profile in fast-spiking parvalbumin (PV) interneurons (FSI), calretinin (CR) expressing interneurons, tyrosine hydroxylase (TH) positive interneurons and the low-threshold spiking interneuron (LTS) population coexpressing the neuromodulators neuropeptide Y (NPY), somatostatin (SOM), and nitric oxide synthase (NOS) or the enzyme nicotinamide adenine dinucleotide phosphate-diaphorase (NADPH-d). Afferent connections receive GABAergic interneurons from the cortex, the thalamus, CIAs, and GABAergic interneurons and dopaminergic neurons of the SN. GABAergic interneurons provide feed-forward inhibition over inhibitory synaptic connections on both types of MSNs, GABAergic interneurons, and CINs.<sup>76,77,84,89,94</sup> Primarily, striatal interneurons regulate striatal output through modulating the timing and firing patterns of MSNs and forming striatal microcircuits.<sup>84</sup> CINs in particular can regulate the DA release in the striatum through nAChR on presynaptic DA terminals.<sup>90</sup> The regulation of corticostriatal synaptic plasticity and the induction of long-term striatal plasticity can also be influenced by LTS interneurons, especially through NOS.<sup>95,96</sup> FSIs are described as being a potential mediator in sensorimotor integration.<sup>97</sup> The influence of striatal interneurons on dystonia was described in different studies, while a striatal GABAergic dysfunction has been linked to hyperkinetic movements.<sup>98</sup> Dystonia-like

impairments were also described in a mouse model after selective inhibition of FSIs.<sup>99</sup> Data about the numbers of striatal interneurons in different dystonia animal models are not confirmed. A loss of striatal PV-positive GABAergic interneurons was detected in an idiopathic dystonia hamster model.<sup>100</sup> A DYT-TOR1A mouse model showed a specific cell loss of striatal CINs, but the cell number of GABAergic interneurons in the striatum was unaltered.<sup>101</sup> Enlarged cell bodies of striatal ACh- and PV-positive interneurons were found in a DYT-TOR1A knock-in mouse model without showing any cell loss of striatal interneurons.<sup>102</sup>

### 1.3.3 Dopaminergic and serotonergic neurotransmitters

DA is a major neuromodulator in the CNS and the peripheral nervous system (PNS). The nigrostriatal pathway plays an important role in movements where dopaminergic cell bodies reside in the SNc and send efferent fibers to neurons of the striatum.<sup>103</sup> DA belongs to the neurotransmitter family of catecholamines, next to norepinephrine and epinephrine. All catecholamines are synthesized from the amino acid tyrosine in a stepwise pathway. Tyrosine, synthesized through hydroxylation of phenylalanine by phenylalanine hydroxylase in the liver, is actively transported to catecholaminergic neurons of the CNS. In the classical pathway of the DA synthesis, L-tyrosine is getting hydroxylated via TH to L-DOPA, and L-DOPA is converted to DA by aromatic amino acid decarboxylase (AADC). The cytosolic DA is transported into synaptic vesicles by the vesicular monoamine transporter 2 (VMAT2) and stored in synaptic vesicles until DA is released into the synaptic cleft through exocytosis, depending on action potentials. Dopaminergic signaling takes place on DA receptors. D<sub>1</sub>-like receptors (D<sub>1</sub>R and D<sub>5</sub>R) are mostly involved in postsynaptic signaling, D<sub>2</sub>-like receptors in pre- and postsynaptic inhibition. The most abundant DA receptor is D<sub>1</sub>R, followed by D<sub>2</sub>R and only low expression of D<sub>3</sub>R, D<sub>4</sub>R, and D<sub>5</sub>R. DA has to be removed from the synaptic cleft by reuptake or degradation to stop DA signaling. DAT is the important transporter for DA reuptake into dopaminergic neurons. DA, leaked from vesicles in dopaminergic neurons, is degraded by monoamine oxidase (MAO). After DA is taken up by glial cells from the synaptic cleft, DA is gradually degraded in 3-methoxytyramine (3-MT) by catechol-O-methyl transferase (COMT) and further metabolized to homovanilic acid (HVA) via MAO. In an additional degradation pathway, MAO breaks down DA in 3,4-dihydroxyphenylacetic acid (DOPAC), which is finally degraded by COMT to HVA (for review see Meiser et al. 2013 and Ayano et al. 2016) (Figure 3).<sup>103,104</sup>

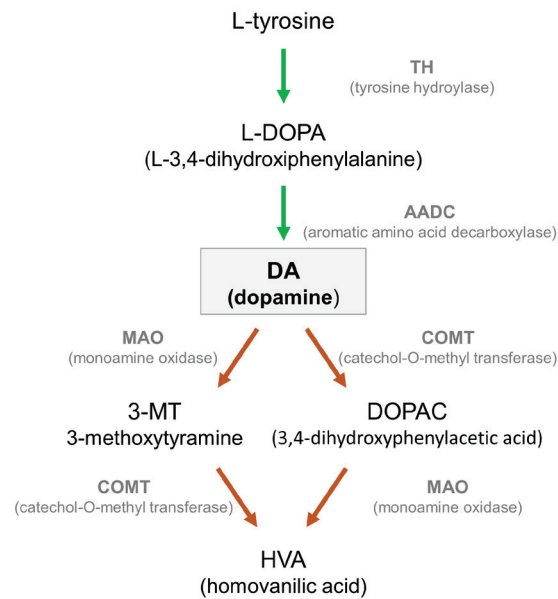


**Figure 3: Biosynthesis and metabolism of DA in the brain**

Schematic overview shows the biosynthesis of DA starting from L-tyrosin and the DA metabolism.

The dopaminergic influence on MSNs as well as on the interneurons FSI, CIN, and LTS in the striatum has already been described (1.3.1 and 1.3.2).<sup>88,105,106</sup> Multiple data connect the dopaminergic system to the DYT-TOR1A pathogenesis in various ways. Different DYT-TOR1A mouse models showed alterations in DA levels and/or its metabolites.<sup>45-47,49,107,108</sup> In human DYT-TOR1A studies, an increase of striatal DOPAC/DA turnover as well as enlarged dopaminergic cell bodies of the SN have been observed.<sup>44,109</sup> It could be shown that torsinA influences the DAT expression on the cell surface<sup>110</sup>, keeping in mind that torsinA mRNA is synthesized in cell bodies of dopaminergic neurons of the SN and torsinA protein is expressed in axons and nerve terminals in the striatum.<sup>111,112</sup> However, the missing response of DYT-TOR1A patients to dopaminergic treatments indicates that the dopaminergic system is not a unique characteristic in the pathogenesis of DYT-TOR1A dystonia.<sup>48</sup>

A further monoamine neurotransmitter next to DA is 5-HT. Only about 1% - 2% of the total amount of 5-HT is produced in the CNS.<sup>113</sup> Serotonergic neurons are mainly located in the raphe nuclei and project to many different brain areas and the brainstem.<sup>114</sup> The basal ganglia receive serotonergic input from the dorsal raphe nucleus.<sup>115</sup> For synthesis of 5-HT, the amino acid L-tryptophan is converted by tryptophan hydroxylase (TPH) into 5-hydroxytryptophan (5-HTP) and further decarboxylated to 5-HT via AADC (Figure 4). 5-HT is transported by VMAT2 into synaptic vesicles and released into the synaptic cleft.<sup>114,116</sup> Serotonergic signaling occurs through 5-HT receptors, which comprises 18 different 5-HT receptors of seven

families (5-HT<sub>1</sub> to 5-HT<sub>7</sub>).<sup>117,118</sup> 5-HT reuptake transporter (SERT) regulates metabolic homeostasis of 5-HT by transporting 5-HT back to the presynaptic neuron where 5-HT is metabolized by MAO in combination with aldehyde dehydrogenase (ALDH) to 5-hydroxyindole acetic acid (5-HIAA) (Figure 4).<sup>119</sup>

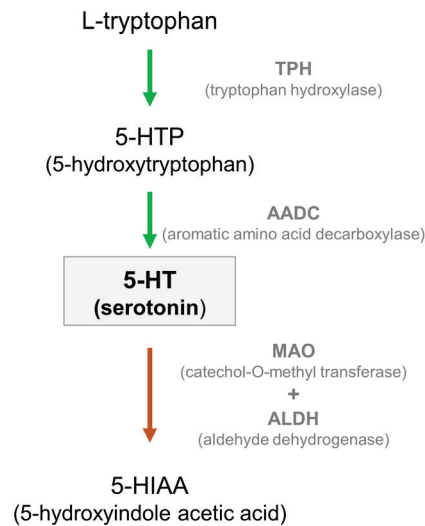


**Figure 4: Biosynthesis and metabolism of 5-HT**

Schematic overview shows the biosynthesis of 5-HT starting from L-tryptophan and the 5HT metabolism.

A putative role in the modulation of motor behavior and the pathophysiology of involuntary movement disorders is described for the serotonergic system, which is supported by the serotonergic innervation of the basal ganglia network. Serotonergic terminals project to basal ganglia nuclei, including the striatum, GPi, SN and STN.<sup>115,120,121</sup> Alterations of the serotonergic system in different types of dystonia were reviewed by M. Smit.<sup>122</sup> Demonstrating the connection between 5-HT and dystonia, two patients with dystonia musculorum deformans had decreased level of 5-HT in the dorsal raphe nuclei and increased levels of 5-HT and 5-HIAA in the GPi and GPe as well as increased levels of 5-HIAA in raphe nuclei obscurus.<sup>123</sup> In a mouse model, overexpressing the human wt torsinA (hWT), a reduction of 5-HT and elevated levels of 5-HIAA were detected in the striatum compared to wt and hΔGAG mice, which overexpress the human torsinA(ΔE). hΔGAG mice showed increased levels of 5-HT and 5-HIAA in the brainstem compared to wt and hWT mice.<sup>49</sup> Furthermore, 5-HT neurons were shown to influence the dopaminergic system mostly in an inhibitory manner.<sup>124</sup>

#### 1.4 Relevance of environmental factors in dystonia

Dystonias based on a genetic background often appear with reduced penetrance. A reduced penetrance is described for different types of dystonia, such as DYT-TOR1A (DYT1; reduced: 30% - 40%)<sup>125</sup>, DYT-THAP1 (DYT6; reduced: 60%)<sup>126</sup>, and DRD (reduced: 30%)<sup>127</sup>. Next to genetic modifiers, disease onset can be increased through certain environmental factors. Injuries, hypoxia and viral infection are already described in some case reports as triggers for dystonia.<sup>128-130</sup> In DYT-TOR1A gene carrier, a single-nucleotide polymorphism, D216H, explains a small proportion of the clinical penetrance of DYT-TOR1A.<sup>131</sup> In an exploratory study a significant association between the environmental factor, perinatal adversities, and the clinical penetrance of DYT-TOR1A was described.<sup>132</sup> Peripheral trauma also seems to be a crucial risk factor for developing dystonia.<sup>130,133-135</sup> Additionally, a bite of a moray into the right heel of a DYT-TOR1A gene carrier elicited dystonia. Based on this data, the “second hit” hypothesis arose by evaluating the interaction of a peripheral trauma in a DYT-TOR1A gene carrier.

#### 1.5 Treatment of dystonia

More than three million people suffer from dystonia worldwide, and the phenotype of all types of dystonia is very diverse.<sup>136</sup> For a proper treatment strategy, a comprehensive diagnosis is necessary. Treatment differs depending on the dystonic phenotype and has to be adjusted for every single dystonia patient. Dystonia is not yet curable. The aim of the available treatment strategies is to improve life quality by relieving pain and ameliorating abnormal movements and postures.<sup>136</sup> Dystonic movements can be improved in some cases by a sensory trick (*geste antagoniste*).<sup>23</sup> Physical and occupational therapy have shown a clinical benefit by specialized exercises. A broad spectrum of oral medications is used for the treatment of dystonia by influencing different neurotransmitter systems, such as anticholinergic drugs, DA-related drugs like L-DOPA, and GABA-related drugs like baclofen and benzodiazepines.<sup>137</sup> The botulinum neurotoxin injection is the preferred treatment strategy for patients with focal dystonia.<sup>136</sup> The treatment of choice in isolated and generalized dystonias is DBS of the GPi, which results in neuromodulation with an as yet unclear mechanism.<sup>81</sup> DBS is used for different types of dystonia by a continuous HFS of the GPi as a safe and successful treatment.<sup>138,139</sup> The highest benefit in disease

outcome by DBS is seen in less severely affected dystonia patients with a shorter disease duration and in DYT-TOR1A patients.<sup>37,140,141</sup> A clinical improvement up to 85% on average was reported for dystonia.<sup>142</sup> Disease duration seems to have a negative influence on disease outcome for DBS treatment. In patients with generalized dystonia, a 15-year disease duration anticipates a slower and worse improvement.<sup>142</sup> An initial improvement of dystonic movements in response to DBS varies between minutes to hours for mobile dystonia, and weeks to months for tonic dystonia by reaching a maximal effect generally after several weeks to months.<sup>81,143</sup> It was shown that patients with primary generalized dystonia improved up to three years through chronic pallidal DBS and benefited up to ten years by sustained improvement.<sup>139,144-148</sup> Nevertheless, clinical symptoms returned within 48 hours to one week after turning the stimulation off in primary generalized dystonia patients treated with HFS for three months to five years. The severity of dystonic symptoms reached a similar level compared to the situation before DBS surgery, but dystonic symptoms disappeared faster when stimulation was turned on again.<sup>139,147,149,150</sup> The GPi as a major output structure of the basal ganglia became an established DBS target for dystonia. Overactivity of the direct pathway results in a net reduction of the GPi activity in dystonia. The reduced GPi output to the thalamus finally leads to an enhanced thalamocortical activation with consecutive clinical manifestation of dystonia.<sup>151</sup> An increased theta frequency band (4-12 Hz) of the GPi is described as a pallidal physiomaer for dystonia.<sup>33,35</sup> The abnormal firing and synchrony of discharge patterns can be modulated by HFS. In dystonia, HFS suppresses the theta activity in the GPi and causes desynchronization of neurons in the theta frequency band with simultaneous improvement of the motor symptoms.<sup>35</sup> Changes of the neuronal activity patterns, induced by HFS, are not limited to the stimulation target. HFS also effects targets, which are functionally connected to the cortex–basal ganglia network, which finally drives the motor output. It could be seen that HFS is decreasing the coupling of cortical EEG and the LFP recorded theta power.<sup>34</sup> DBS also has effect on the neuronal plasticity. The increased LTP-like plasticity in dystonia patients could be reduced by long-term DBS, even below the level of plasticity of healthy controls.<sup>66-68,149</sup> A potential explanation could be the desynchronization of the excessive synchronized pallidal activity by restoring a normal plasticity in the sensorimotor loop.<sup>51,152</sup> Dystonia patients often require individualized treatments comprising combinations of several therapeutic options.

## 1.6 DYT-TOR1A dystonia

Early-onset torsion dystonia (DYT-TOR1A) is an autosomal dominantly inherited disease with a severe generalized phenotype primarily caused by a trinucleotide GAG in-frame deletion ( $\Delta$ GAG, “ $\Delta$ E”) in the coding region (exon 5) of the *TOR1A* gene on chromosome 9q34 encoding the torsinA protein. This mutation of the *TOR1A* gene results in a loss of a glutamic acid residue at position 302 or 303 in the carboxy-terminal region of torsinA.<sup>153,154</sup> As the most common form of inherited dystonia it is characterized by a disease onset during childhood or adolescence typically in a lower limb (mean age nine years), yet less common in upper limbs (mean age 15 years), which frequently generalizes over months and years with a final involvement of the trunk, other limbs and body parts.<sup>4,155</sup> If dystonia does not develop before the age of 28, non-manifesting carriers usually stay symptom-free their whole life.<sup>156</sup> A critical clinical feature of dystonia is the reduced penetrance of 30% - 40%. This reduced penetrance indicates that an additional trigger for DYT-TOR1A dystonia is required, next to the  $\Delta$ E mutation of the *TOR1A* gene.<sup>125</sup> DYT-TOR1A dystonia is more common among Ashkenazi Jews compared to other ethnic groups. The prevalence in the non-Jewish population is 1 to 200,000.<sup>157</sup> It is estimated that the Ashkenazi Jewish population has a five to ten times higher prevalence for DYT-TOR1A dystonia.<sup>158</sup> Dystonic movements of DYT-TOR1A patients persist for a lifetime and need to be treated. DYT-TOR1A patients generally respond to pharmaceuticals insufficiently; however, they can improve dramatically by DBS of the GPi.<sup>37,159</sup>

## 1.7 TorsinA

TorsinA is a 332-amino acid intracellular membrane protein and belongs to the AAA+ (ATPases associated with various cellular activities) protein family, which is a large and diverse family of enzymes with an ATP-binding domain.<sup>160,161</sup> AAA+ proteins act as oligomers, usually hexamers, by using energy of adenosine triphosphate (ATP) hydrolysis to induce conformational changes. This class of proteins is involved in diverse cellular functions, such as protein degradation, membrane trafficking, and transcriptional regulation.<sup>161,162</sup> TorsinA is ubiquitously expressed in all tissues and localized to the endoplasmic reticulum (ER) and the nuclear envelope (NE), an ER subdomain which surrounds the nucleus.<sup>153,163</sup> The synthesis of torsinA messenger ribonucleic acid (mRNA) takes place in the cell body, followed by a fast export to the

terminals of the axons and dendrites.<sup>111,112</sup> The expression levels of torsinA depend on developmental and localization patterns.<sup>164</sup> A high torsinA mRNA expression pattern was observed in dopaminergic neurons of SNc. TorsinA mRNA and protein are expressed in different levels in the striatum, cerebral cortex, hippocampus, SN, GP, brainstem, thalamus, cerebellum, and spinal cord.<sup>111,112,163,165</sup>

For the functionality of torsinA, activation by a binding partner is needed. TorsinA has to interact with one of the major co-activating factors lamina-associated protein1 (LAP1; TOR1AIP1) or luminal domain like LAP1 (LULL1; TOR1AIP2), which belong to ER transmembrane AAA+-like proteins.<sup>166,167</sup> The function of torsinA is not fully understood. Potential torsinA functions were investigated through mammalian cells and torsinA model organisms. TorsinA has different functions by interaction or co-localization with further proteins. Known functions of torsinA include intracellular trafficking by interaction with the cytoplasmic kinesin light chain 1 (KLC1)<sup>168</sup>; organization of the ER and NE structure through binding the ER transmembrane protein LULL1 and the NE protein LAP1<sup>166,169,170</sup>; and synaptic vesicle (SV) exocytosis through snapin, a SNAP25 (synaptosomal associated protein of 25 kDa)-binding protein, co-localization in secretory granules.<sup>171</sup> TorsinA is suggested to influence the dynamics of the cytoskeleton through the connection to the type III intermediate filament protein vimentin and the microtubule-associated protein tau, which influences the nuclear shape, neurite outgrowth, cell migration, and adhesion.<sup>172-174</sup> TorsinA also has an effect on secretory pathways based on chaperone functionality, such as protein quality control and protein degradation and alters the cell-surface expression of the DAT.<sup>110,171,175,176</sup> A stress-associated function is attributed to torsinA. It could be shown that torsinA has a neuroprotective role in response to oxidative stress on cellular stress in dopaminergic neurons and by preventing the onset of the ER stress response.<sup>177-180</sup> In summary, torsinA has many cellular functions and is involved in different pathways. Through the  $\Delta E$  mutation of the *TOR1A* gene, characteristics and functions of the mutated torsinA (torsinA( $\Delta E$ )) change. It is still unclear how torsinA( $\Delta E$ ) mutation results in DYT-TOR1A. The loss of the glutamic acid residue of the torsinA( $\Delta E$ ) leads to an impaired interaction between torsinA( $\Delta E$ ) and LAP1 or LULL1, resulting in defective torsinA( $\Delta E$ ) activation and finally to a reduced ATPase activity of torsinA( $\Delta E$ ), which can be a hint for a loss of torsinA function.<sup>181-183</sup> TorsinA( $\Delta E$ ) has a dominant-negative effect on the torsinA(wt) by suppressing its activity and can also shift the torsinA(wt) from the ER to NE.<sup>110,169,181</sup> Furthermore, the functionality of torsinA( $\Delta E$ ) is

not affected because of a misfolded protein structure.<sup>184</sup> However, abnormal intracellular disulfide links and a reduced half-life of the torsinA( $\Delta$ E) could be determined, leading to different degradation processes; while wild-type torsinA is degraded through autophagy, mutated torsinA( $\Delta$ E) is degraded by the ubiquitin-proteasome system.<sup>185,186</sup> In addition, the  $\Delta$ E mutation seems to influence intracellular trafficking since torsinA( $\Delta$ E) does not bind KLC1.<sup>168,187</sup> Experimental overexpression of torsinA( $\Delta$ E) inhibits neurite outgrowth and cell-surface distribution of DAT in mammalian cells.<sup>110,168,174</sup> Ultrastructural alterations in the NE as well as formations of NE derived cytoplasmic membranous inclusions could be detected in some of the DYT-TOR1A animals and cell models that either (over)express torsinA( $\Delta$ E), lack or demonstrate a reduced level of torsinA.<sup>107,181,188-190</sup> In human DYT-TOR1A brains the NE pathology was described only once as perinuclear inclusion bodies in specific regions of the brainstem and midbrain<sup>191</sup>, but this could not be confirmed.<sup>192,193</sup> The inconsistent data of structural changes in the NE need to be verified because of difficulties in processing human post mortem tissue and the fact that overexpression of torsinA( $\Delta$ E) is not a physiological condition of DYT-TOR1A. Even with the incomplete knowledge about the functionality of torsinA and torsinA( $\Delta$ E), published data indicate the relevance of torsinA for the DYT-TOR1A phenotype and the restriction to the CNS.

## 1.8 DYT-TOR1A animal models

Animal models can provide a huge benefit in proofing causation and testing hypotheses. In dystonia research, invertebrates, rodents, and primates are used as model organisms, but there is not a single model that can mimic every aspect of dystonia. Animal models of dystonia can be separated into symptomatic and etiologic models. Symptomatic animal models show clinical features comparable to dystonia in humans. So far, symptomatic animal models of dystonia either result from spontaneous mutations or are induced through pharmaceuticals. These symptomatic animal models are useful for determining anatomical and physiological processes in dystonia. However, the molecular pathophysiology based on a known genetic mutation, such as in hereditary forms of dystonia, cannot be analyzed by these models.<sup>194</sup> An example of symptomatic animal models of generalized dystonia through spontaneous mutations is the *dt<sup>sz</sup>* hamster.<sup>195,196</sup> An injection of kainic acid, an AMPA receptor agonist, into the cerebellum of mice is an example of a pharmaceutical animal

model for dystonia.<sup>197</sup> Etiologic animal models are generated through genetic manipulation and are effective tools to further analyze the pathophysiology of dystonia. However, an often missing dystonic phenotype is a disadvantage of etiological dystonia animal models.<sup>194</sup> Etiologic DYT-TOR1A rodent models are useful for analyzing the pathophysiology of dystonia and for the identification of new treatments because of the high homogeneity between the rodent *Tor1a* gene and the human *TOR1A* gene. However, the differences between humans and rodents regarding lifespan, physiology, and genetic background should always be kept in mind.<sup>4,198</sup> The genetic DYT-TOR1A rodent models include heterozygous *Dyt1*  $\Delta$ GAG knock-in (KI) mice (Dang et al., Goodchild et al.), where one normal and one mutated ( $\Delta$ GAG) *Tor1a* gene is expressed.<sup>46,181</sup> *Dyt1* knockdown (KD) mice (Dang et al.) show a reduced level of normal torsinA.<sup>46,47</sup> Only 50% of normal torsinA is produced in *Dyt1* knockout (KO) mice (*Tor1a*<sup>+/-</sup> mouse; Goodchild et al.).<sup>181</sup> Different types of brain region-specific or cell-specific *Dyt1* conditional KO mice were generated like cerebral cortex-specific *Dyt1* conditional KO mice (*Dyt1* cKO; Yokoi et al.), striatum-specific *Dyt1* conditional KO mice (*Dyt1* sKO; Dang et al.) and cholinergic neuron-specific *Dyt1* conditional KO animals (*Dyt1* ChKO, Rossi et al.).<sup>199-201</sup> Transgenic DYT-TOR1A rodent models overexpress the human transgene, encoding human wild-type torsinA or mutated torsinA ( $\Delta$ EtorsinA) protein by using different promotor regions. Examples are  $\Delta$ E-torsinA (TG) mice (Shashidharan et al.), TH- $\Delta$ E-TorsinA and TH-hTorsinA mice (Page et al.), hWT and hMT torsinA transgenic mice (Sharma et al.), hWT and h $\Delta$ GAG torsinA transgenic mice (Grundmann et al.), and WtTorA and  $\Delta$ ETorA rats (Grundmann et al.). However, none of the genetic DYT-TOR1A rodent models show an overt dystonic phenotype. Some of the genetic DYT-TOR1A rodent models have common features in motor learning, motor skills, activity level, morphology, brain and neurotransmitter metabolism, and especially DA metabolism; some features are inconsistent between the different animal models and some features are comparable to human DYT-TOR1A dystonia.<sup>49,107,188,190,202</sup>

### 1.8.1 Transgenic $\Delta$ ETorA DYT-TOR1A rat model

$\Delta$ ETorA rats harbor the full-length human mutant *TOR1A* gene ( $\Delta$ E), including promotor, intronic, and regulatory regions. This is the only DYT-TOR1A animal model harboring the whole human *TOR1A* gene expressing the human mutant torsinA ( $\Delta$ EtorsinA) protein under the control of the endogenous human promotor and its regulatory elements. The same protein expression patterns of the human  $\Delta$ EtorsinA

observed in the human brain were also seen in  $\Delta$ ETorA rats. High and intermediate expression levels of human  $\Delta$ EtorsinA protein were detected in the cortex, striatum, hippocampus, and cerebellum and low expression in the brainstem, SN, and olfactory bulbs. NE abnormalities, normal level of activity as well as normal levels of DA and its metabolites could be demonstrated, which is inconsistent with other genetic DYT-TOR1A rodent models or human DYT-TOR1A patients. Severe alterations in synaptic plasticity in the striatum could be shown.  $\Delta$ ETorA rats also demonstrated a motor phenotype through impaired motor learning, hind limb clasping and decreased limb grasping, without showing dystonia-like movements.<sup>188</sup>

## 1.9 Aim of the study

The pathophysiology of dystonia is still unknown. In addition, the reduced penetrance in dystonia is an important clinical feature in which a gene-environment interaction is assumed. Based on the “second hit” hypothesis that an environmental factor can trigger a dystonic phenotype in genetically predisposed subjects, this study aimed to elicit a similar human dystonia endophenotype in a transgenic asymptomatic DYT-TOR1A rat model ( $\Delta$ ETorA), which overexpresses the human mutant torsinA protein by a unilateral sciatic nerve crush injury. Via multiscale characterization in relation to genotype and phenotype, the following questions about the pathophysiology of DYT-TOR1A should be addressed in this DYT-TOR1A rat model (Figure 5):

- Phenotype level:
  - Do  $\Delta$ ETorA rats develop a dystonic phenotype after sciatic nerve crush injury?
- Large-scale network level:
  - Are there alterations in the theta and beta frequencies in  $\Delta$ ETorA rats, seen in DYT-TOR1A patients?
  - Does DBS improve dystonia in nerve-injured  $\Delta$ ETorA rats by modulation of pathologically altered oscillations?
  - Do dystonic  $\Delta$ ETorA rats present alterations in the glucose metabolism in the brain?
- Microcircuitry level:
  - Is striatal DA transmission affected in dystonic  $\Delta$ ETorA rats?
- Molecular and cellular level:
  - Are striatal targets of neurotransmitter systems differently expressed in dystonic  $\Delta$ ETorA rats?
  - Does peripheral trauma have an influence on the cell numbers of striatal neurons in  $\Delta$ ETorA rats?
  - Can we detect novel pathophysiological pathways through whole-transcriptome analysis in dystonic  $\Delta$ ETorA rats?

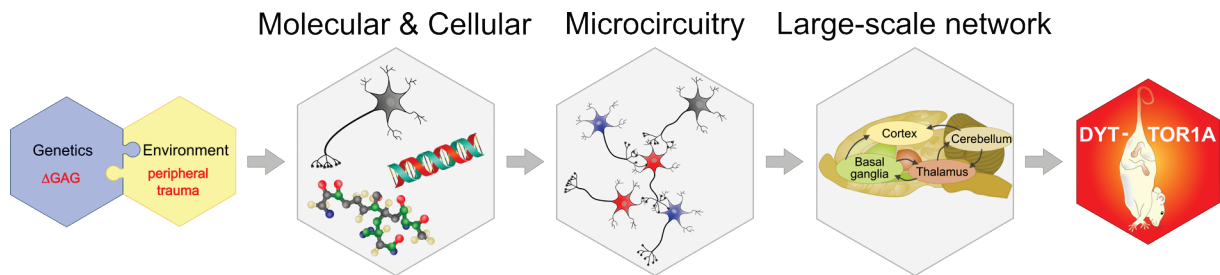


**Figure 5: Schematic illustration of the multiscale characterization in a DYT-TOR1A rat model ( $\Delta ETorA$ )**

The pathophysiology of dystonia in a  $\Delta ETorA$  rat model with a unilateral sciatic nerve crush injury was characterized in a multiscale approach on the level of molecular biology, cellularity, microcircuitry, and large-scale network.

## 2 Material and Methods

### 2.1 Material

#### 2.1.1 Devices

2100 Bioanalyzer	Agilent Technologies, Santa Clara, CA, USA
AC amplifier DAM80	WPI Instruments, Sarasota, FL, USA
Analytical balance AB204-S/PH	Mettler-Toledo, Gießen, Germany
Camcorder GC-PX100	JVC, Bad Vilbel, Germany
Centrifuge 5427 R	Eppendorf, Hamburg, Germany
Centrifuge Megafuge 1.0 R	Heraeus, Hanau, Germany
ChemiDoc Touch	Bio-Rad, Munich, Germany
Cryostat CM1950	Leica, Wetzlar, Germany
DC Temperature Control System	FHC, Bowdoin, ME, USA
DECADE Elite	Antec Scientific, Zoeterwoude, Netherlands
Dräger Vapor 19.3 Isoflurane system	Dr. Wilfried Müller GmbH, Prittriching, Germany
ELISA Reader Infinite 200 PRO	Tecan, Männedorf, Switzerland
Gel iX20 Imager	Intas, Göttingen, Germany
Heating plate	MEDAX, Neumünster, Germany
High-speed scanner CR 35 Bio	Raytest, Straubenhardt, Germany
Hotplate magnetic stirrer	Labinco, Breda, Netherlands
HPLC 1260 Infinity	Agilent Technologies, Santa Clara, CA, USA
Laboratory tube pump 323S/RL	Watson-Marlow, Rommerskirchen, Germany
Mastercycler nexus	Eppendorf, Hamburg, Germany
Micro1401-3	CED, Cambridge, UK
Microcentrifuge	VWR, Darmstadt, Germany
Microdialysis setup	AgnTho's AB, Lidingö, Sweden
Micromotor drill	Stoelting Co., Wood Dale, IL, USA
Microscope Axio Imager.M2	Zeiss, Oberkochen, Germany
Microscope BX53	Olympus, Hamburg, Germany
Mini-PROTEAN Tetra System	Bio-Rad, Munich, Germany
Multichannel systems stimulus generator (Type STG 4004)	MultichannelSystems, Reutlingen, Germany
NanoDrop One	Thermo Fisher, Darmstadt, Germany
Neurosoft-Evidence 3102 electromyograph	Schreiber & Tholen, Stade, Germany

NextSeq 550 System	Illumina, San Diego, CA, USA
Open field EthoVision XT	Noldus, Wageningen, Netherlands
PerfectBlue gel system	PEQLAB, Erlangen, Germany
pH meter peqMETER 1.14	PEQLAB, Erlangen, Germany
Pipettes	Eppendorf, Hamburg, Germany
Platform shaker Polymax 1040	Heidolph Instruments, Schwabach, Germany
Power Source power supply	VWR, Darmstadt, Germany
PowerPac Basic	Bio-Rad, Munich, Germany
PowerPac HC	Bio-Rad, Munich, Germany
Precision balance PFB 6000-1M	KERN & SOHN, Balingen, Germany
QuantStudio 3 Real-Time PCR System	Thermo Fisher, Darmstadt, Germany
Rodent Brain Matrix, adult rat, coronal	Ted Pella, Redding, CA, USA
SenCell (ISAAC)	Antec Scientific, Zoeterwoude, Netherlands
Stemi 2000 Stereo microscope	Zeiss, Oberkochen, Germany
Stereo Investigator hardware	MBF Bioscience, Williston, VT, USA
Stereotaxic instrument	Stoelting Co., Wood Dale, IL, USA.
Stereotaxic probe holders	Stoelting Co., Wood Dale, IL, USA
Stereotaxic robot	Neurostar, Tübingen, Germany
ThermoMixer C	Eppendorf, Hamburg, Germany
Tissue Lyser LT	Qiagen, Hilden, Germany
Transmitted light microscope OBL 127	KERN & SOHN, Balingen, Germany
Ultra Fine Hemostat (13020-12)	Fine Science Tools, Heidelberg, Germany
Ultrasonic homogenizer SONOPULS mini20	BANDELIN, Berlin, Germany
Vortex mixer	Labinco, Breda, Netherlands

### 2.1.2 Consumables

AN69 membrane	Hospal, Meyzieu, France
Anchor screws, MCS1x2	AgnTho's AB, Lidingö, Sweden
Appose ULC skin stapler 35W	Covidien, Minneapolis, MN, USA
Column shield filter	ERC, Riemerling, Germany
Coverslips	R. Langenbrinck, Emmendingen, Germany
Custom-made plug	GT-Laborteknik, Arnstein, Germany
	Dr. Maisch GmbH, Ammerbuch, Germany
Fused silica capillary tubing, 75 µm ID, 150 µm OD	
	BGB Analytik, Boeckten, Switzerland

Kraft-Mix Extrem Schnell (two components)	Pattex, Düsseldorf, Germany
MicroAmp Optical 96-Well reaction plate	Thermo Fisher, Darmstadt, Germany
MicroAmp Optical adhesive film	Thermo Fisher, Darmstadt, Germany
MultiSensitive phosphor screens	PerkinElmer, Waltham, MA, USA
NeuroSep 115 (150 x 1 mm, 3 µm, C18-3)	ERC, Riemerling, Germany
Nitrocellulose blotting membrane	GE Healthcare, Boston, MA, USA
NUCLEOSIL® 120-5 C <sub>18</sub> , 5 µm particles, 120 Å pores	MACHEREY-NAGEL, Düren, Germany
Object slides superfrost	R. Langenbrinck, Emmendingen, Germany
PE tubing, 0,38 x 1,09 mm	Hartenstein, Würzburg, Germany
Peel-A-Way disposable embedding molds	Polysciences, Warrington, PA, USA
Precolumn Reprosil Universal-RP, 5 µm, 10 x 4 mm	
PT/IR Microelectrode	FHC Inc., Bowdoin, ME, USA
Pump tubings 2 clips/152mm black-white, 950 µm ID	AHF Analysentechnik, Tübingen, Germany
Pump tubings 2 clips/152mm orange-green, 380 µm ID	AHF Analysentechnik, Tübingen, Germany
Stainless steel beads, 5 mm	Qiagen, Hilden, Germany
Stainless steel needle 25 G 5/8 0,5 x 16 mm	BD Microlance, Heidelberg, Germany
Stainless steel needle 26 G 3/8 0,45 x 10 mm	BD Microlance, Heidelberg, Germany
Suture Silkam 4/0 DS19	B. Braun, Melsungen, Germany
Tissue-Tek cryomold	Sakura, Staufen, Germany
Ultrafree-MC centrifugal filter 0.22 µm	Merck, Darmstadt, Germany
Whatman paper	Hartenstein, Wuerzburg, Germany

### 2.1.3 Chemicals, reagents and pharmaceuticals

2-Methylbutane	Carl Roth, Karlsruhe, Germany
3,4-Dihydroxyphenylacetic acid (DOPAC)	Sigma-Aldrich, Taufkirchen, Germany
30% Acrylamide/Bis-acrylamide solution	Bio-Rad, Munich, Germany
5-Hydroxyindole-3-acetic acid (5-HIAA)	Sigma-Aldrich, Taufkirchen, Germany
A/C Flüssigkeit	Speiko, Bielefeld, Germany
Acetic acid, ≥99.8%	Sigma-Aldrich, Taufkirchen, Germany
Acetonitril	Sigma-Aldrich, Taufkirchen, Germany
Agarose	Carl Roth, Karlsruhe, Germany
Ammonium peroxodisulfate (APS)	Sigma-Aldrich, Taufkirchen, Germany

Aquatex	Merck, Darmstadt, Germany
Bepanthen Augen- und Nasensalbe	Bayer Vital GmbH, Leverkusen, Germany
Boric acid	AppliChem, Darmstadt, Germany
Bovine serum albumin (BSA)	Sigma-Aldrich, Taufkirchen, Germany
Bromophenol Blue sodium salt	Sigma-Aldrich, Taufkirchen, Germany
Bupivacain 0,25%	Jenapharm, Jena, Germany
Calcium chloride dihydrate ( $\text{CaCl}_2 \cdot 2\text{H}_2\text{O}$ )	Sigma-Aldrich, Taufkirchen, Germany
Citric acid	Sigma-Aldrich, Taufkirchen, Germany
Cresyl violet (acetate)	Merck, Darmstadt, Germany
Cutasept F	BODE Chemie, Hamburg, Germany
D(+)-Saccharose	Carl Roth, Karlsruhe, Germany
Diethylene triamine pentaacetic acid (DTPA)	Carl Roth, Karlsruhe, Germany
di-Sodium hydrogen phosphate dihydrate ( $\text{Na}_2\text{HPO}_4 \cdot 2\text{H}_2\text{O}$ )	Merck, Darmstadt, Germany
DL-Dithiothreitol (DTT)	Sigma-Aldrich, Taufkirchen, Germany
Dopamine hydrochloride	Sigma-Aldrich, Taufkirchen, Germany
DreamTaq Hot Start Green PCR Master Mix	Thermo Fisher, Darmstadt, Germany
EDTA $\cdot 2\text{H}_2\text{O}$	Carl Roth, Karlsruhe, Germany
Ethanol absolute for molecular biology	AppliChem, Darmstadt, Germany
Ethanol	Sigma-Aldrich, Taufkirchen, Germany
GelStar Nucleic Acid Gel Stain, 10,000X	Lonza, Basel, Switzerland
Glycerol	Merck, Darmstadt, Germany
Glycine	Sigma-Aldrich, Taufkirchen, Germany
Heparin-Natrium 25.000 I.E. Inj.-Lösung	Ratiopharm, Ulm, Germany
Homovanillic acid (HVA)	Sigma-Aldrich, Taufkirchen, Germany
Isofluran CP	CP-Pharma, Burgdorf, Germany
Kalocryl CPGM red	Speiko, Bielefeld, Germany
LiChrosolv water	Merck, Darmstadt, Germany
Lowry assay	Sigma-Aldrich, Taufkirchen, Germany
Magnesium chloride ( $\text{MgCl}_2$ )	Sigma-Aldrich, Taufkirchen, Germany
Methanol	CHEMSOLUTE, Renningen, Germany
Nonfat dry milk	Cell Signaling, Danvers, MA, USA
Normal goat serum (NGS)	Dako, Santa Clara, CA, USA
Normal rabbit serum (NRS)	Vector Laboratories, Burlingame, CA, USA

Nuclease-free water	Ambion, Darmstadt, Germany
O'RangeRuler 100 bp DNA Ladder	Thermo Fisher, Darmstadt, Germany
Octane-1-sulphonic acid (OSA)	Carl Roth, Karlsruhe, Germany
ortho-Phosphoric acid (H <sub>3</sub> PO <sub>4</sub> )	Carl Roth, Karlsruhe, Germany
PageRuler Plus Prestained Protein Ladder	Thermo Fisher, Darmstadt, Germany
Paraformaldehyde (PFA)	Merck, Darmstadt, Germany
Ponceau S solution	Sigma-Aldrich, Taufkirchen, Germany
Potassium dihydrogen phosphate (KH <sub>2</sub> PO <sub>4</sub> )	Merck, Darmstadt, Germany
Precision Plus Protein WesternC Blotting Standards	Bio-Rad, Munich, Germany
Rimadyl solution (50 mg/mL)	Zoetis, Berlin, Germany
RNA <sup>later</sup> RNA Stabilization Reagent	Qiagen, Hilden, Germany
Serotonin hydrochloride (5-HT)	Sigma-Aldrich, Taufkirchen, Germany
Sodium chloride (NaCl)	Sigma-Aldrich, Taufkirchen, Germany
Potassium chloride (KCl)	Merck, Darmstadt, Germany
Sodium dihydrogen phosphate dihydrate (NaH <sub>2</sub> PO <sub>4</sub> · 2H <sub>2</sub> O)	Carl Roth, Karlsruhe, Germany
Sodium dodecyl sulphate (SDS)	Carl Roth, Karlsruhe, Germany
β-Mercaptoethanol	Sigma-Aldrich, Taufkirchen, Germany
SuperScript IV VILO Master Mix	Thermo Fisher, Darmstadt, Germany
TaqMan Gene Expression Assay (FAM)	Thermo Fisher, Darmstadt, Germany
TaqMan Gene Expression Master Mix	Thermo Fisher, Darmstadt, Germany
Tetramethylethylenediamine (TEMED)	Carl Roth, Karlsruhe, Germany
Tissue-Tek O.C.T. Compound	Sakura, Staufen, Germany
Tramadol AL Tropfen (100 mg/mL)	ALIUD Pharma, Laichingen, Germany
Triethylamine (TEA)	Carl Roth, Karlsruhe, Germany
Tris(hydroxymethyl)aminomethane (TRIS)	Serva, Heidelberg, Germany
Triton X-100	Sigma-Aldrich, Taufkirchen, Germany
TWEEN 20	Sigma-Aldrich, Taufkirchen, Germany
Vitro-Clud	R. Langenbrinck, Emmendingen, Germany
Western Lightning Plus-ECL	PerkinElmer, Waltham, MA, USA
Xylene	Sigma-Aldrich, Taufkirchen, Germany

### 2.1.4 Buffers and solutions

<b>Acetic acid (0.02 M)</b>	114.7 $\mu$ l acetic acid ad 100 ml ddH <sub>2</sub> O sterile filtration (0.2 $\mu$ m)
<b>Artificial cerebrospinal fluid (aCSF)</b>	2.0 mM Na <sub>2</sub> HPO <sub>4</sub> · 2H <sub>2</sub> O 1.0 mM MgCl <sub>2</sub> 1.2 mM CaCl <sub>2</sub> · 2H <sub>2</sub> O 145 mM NaCl 2.7 mM KCl pH 7.4 sterile filtration (0.2 $\mu$ m)
<b>Artificial cerebrospinal fluid with high KCl (aCSF<sup>K+</sup>)</b>	2.0 mM Na <sub>2</sub> HPO <sub>4</sub> · 2H <sub>2</sub> O 1.0 mM MgCl <sub>2</sub> 1.2 mM CaCl <sub>2</sub> · 2H <sub>2</sub> O 145 mM NaCl 50 mM KCl pH 7.4 sterile filtration (0.2 $\mu$ m)
<b>Cresyl violet solution</b>	0.1% cresyl violet 1% acetic acid
<b>DTT (2 M)</b>	5 g DTT 16.21 ml Nuclease-free water
<b>HPLC sample buffer</b>	150 mM H <sub>3</sub> PO <sub>4</sub> 500 $\mu$ M DTPA

**HPLC mobile phase – tissue**

9% NaH<sub>2</sub>PO<sub>4</sub> x 2H<sub>2</sub>O  
0.975 mM OSA  
0.1 mM EDTA  
2.0 mM KCl  
0.5 mM TEA  
14% Methanol  
pH 3.88  
sterile filtration (0.2 µm)

**HPLC mobile phase – microdialysis sample (DA)**

100 mM H<sub>3</sub>PO<sub>4</sub>  
100 mM citric acid  
2 mM KCl  
pH 6.0  
0.1 mM EDTA  
950 mg/L OSA  
8% Acetonitrile  
sterile filtration (0.2 µm)

**HPLC mobile phase – microdialysis sample (monoamine metabolites)**

100 mM H<sub>3</sub>PO<sub>4</sub>  
100 mM citric acid  
2 mM KCl  
0.1 mM EDTA  
pH 3.0  
5% Acetonitrile  
sterile filtration (0.2 µm)

**Laemmli sample buffer (4x)**

250 mM TRIS, pH 6.8  
20% β-Mercaptoethanol  
40% Glycerol  
0.1 % Bromophenol Blue  
10% SDS

<b>PBS (1x)</b>	137 mM NaCl 2.7 mM KCl 2.0 mM $\text{KH}_2\text{PO}_4$ 10 mM $\text{Na}_2\text{HPO}_4 \cdot 2\text{H}_2\text{O}$ pH 7.4
<b>PFA solution (4%)</b>	4 g PFA 100 ml PBS (1x) pH 7.4
<b>RLT/DTT buffer</b>	980 $\mu\text{l}$ RLT buffer 20 $\mu\text{l}$ DTT (2 M)
<b>SDS PAGE buffer</b>	25 mM TRIS, pH 8.3 200 mM Glycine 0.05% SDS
<b>Separating gel (10%)</b>	3.30 ml Acrylamide/Bis-acrylamide (30%) 2.50 ml TRIS (1M), pH 8.8 0.10 ml SDS (10%) 0.10 ml APS (10%) 0.004 ml TEMED 4.00 ml ddH <sub>2</sub> O
<b>Stacking gel 5%</b>	1.70 ml Acrylamide/Bis-acrylamide (30%) 1.25 ml TRIS (1M), pH 6.8 0.10 ml SDS (10%) 0.10 ml APS (10%) 0.01 ml TEMED 6.80 ml ddH <sub>2</sub> O

<b>TBE (1x)</b>	89 mM TRIS 89 mM Boric acid 2 mM EDTA · 2H <sub>2</sub> O pH 8.0
<b>TBST (1x)</b>	10 mM TRIS 150 mM NaCl 0.05% v/v TWEEN 20 pH 8.0
<b>Transfer buffer</b>	25 mM TRIS, pH 8.3 192 mM Glycine 20% methanol
<b>TRIS (1 M), pH 6.8</b>	36.3 g TRIS ad 300 ml ddH <sub>2</sub> O pH 6.8
<b>TRIS (1.5 M), pH 8.8</b>	54.5 g TRIS ad 300 ml ddH <sub>2</sub> O pH 8.8

### 2.1.5 Antibodies

**Table 2: Primary antibodies used in immunohistochemistry**

Reactivity	Host	Clone	Dilution	Reference
Calretinin	Mouse	6B8.2	1:300	MAB1568, Millipore
Choline acetyltransferase	Goat	Polyclonal	1:300	AB144P, Millipore
Neuronal nitric oxide synthase	Rabbit	Polyclonal	1:300	24431, ImmunoStar
Parvalbumin	Rabbit	Polyclonal	1:1,000	Ab11427, Abcam

**Table 3: Primary antibodies used for western blot**

Reactivity	Host	Clone	Dilution	Reference
Dopamine transporter	Rabbit	Polyclonal	1:5,000	AB2231, Merck
GAPDH	Mouse	6C5	1:15,000	CB1001, Merck

**Table 4: Secondary antibodies used in immunohistochemistry**

Reactivity	Host	Conjugation	Dilution	Reference
Mouse IgG	Goat	Biotin	1:100	BA-9200, Vector
Goat IgG	Rabbit	Biotin	1:100	BA-5000, Vector
Rabbit IgG	Goat	Biotin	1:100	BA-1000, Vector

**Table 5: Secondary antibodies used for western blot**

Reactivity	Host	Conjugation	Dilution	Reference
Rabbit IgG	Donkey	HRP	1:10,000	711-035-152, Jackson ImmunoResearch
Mouse IgG	Donkey	HRP	1:10,000	715-035-150, Jackson ImmunoResearch

### 2.1.6 Commercial kits

DAB Peroxidase (HRP) Substrate Kit	Vector Laboratories, Burlingame, CA, USA
DNeasy Blood & Tissue Kit	Qiagen, Hilden, Germany
RNeasy Micro Kit	Qiagen, Hilden, Germany
VECTASTAIN ABC HRP Kit	Vector Laboratories, Burlingame, CA, USA

### 2.1.7 Primer sequences

Primer sequences for genotyping of the company Sigma-Aldrich (Taufkirchen, Germany)

DYT1 fwd. 5' TAA AAA TGT GTA TCC GAG TGG AAA T 3'

DYT1 rev. 5' G AAG GAC TGA GTG TTG TTT CTT TTC 3'

### 2.1.8 TaqMan Gene Expression Assays

TaqMan Gene Expression Assays of the company Applied Biosystems (Darmstadt, Germany) with gene name and assay ID.

Acacb	acetyl-CoA carboxylase beta	Rn00588290_m1
Acadm	acyl-CoA dehydrogenase medium chain	Rn00566390_m1
Acat1	acetyl-CoA acetyltransferase 1	Rn00567139_m1
Ache	acetylcholinesterase	Rn00596883_m1
Atf6	activating transcription factor 6	Rn01490844_m1
Bdh1	3-hydroxybutyrate dehydrogenase 1	Rn00588855_m1
Calb2	calbindin 2 (calretinin)	Rn00588816_m1
Chat	choline O-acetyltransferase	Rn01453446_m1
Chrm1	cholinergic receptor muscarinic 1	Rn01454631_m1
Chrm2	cholinergic receptor muscarinic 2	Rn02532311_s1
Chrm4	cholinergic receptor muscarinic 4	Rn01512605_s1
Chrn2	cholinergic receptor nicotinic beta 2 subunit	Rn00570733_m1
Cpt1a	carnitine palmitoyltransferase 1A	Rn00580702_m1
Darpp32	protein phosphatase 1 regulatory inhibitor subunit 1B	Rn01452984_m1
Drd1	dopamine receptor D1	Rn03062203_s1
Drd2	dopamine receptor D2	Rn00561126_m1
Drd3	dopamine receptor D3	Rn00567568_m1
Drd4	dopamine receptor D4	Rn00681263_g1
Drd5	dopamine receptor D5	Rn00562768_s1
Gapdh	glyceraldehyde-3-phosphate dehydrogenase	Rn99999916_s1
Gria4	glutamate ionotropic receptor AMPA type subunit 4	Rn00568544_m1
Grin2b	glutamate ionotropic receptor NMDA type subunit 2b	Rn00680474_m1
Hk2	hexokinase 2	Rn00562457_m1
Htr1a	5-hydroxytryptamine receptor 1A	Rn00561409_s1
Htr2a	5-hydroxytryptamine receptor 2A	Rn00568473_m1
Kirrel3	kirre like nephrin family adhesion molecule 3	Rn01524778_m1
Mct12	solute carrier family 16, member 12	Rn02046868_s1
nNOS	nitric oxide synthase 1	Rn00583793_m1
Pex11a	peroxisomal biogenesis factor 11 alpha	Rn00585152_m1
Pvalb	parvalbumin	Rn00574541_m1
VACHT	vesicular acetylcholine transporter	Rn01450312_s1

### 2.1.9 Software

Agilent OpenLAB Control Panel

EthoVision XT

Evidence

Fiji

GraphPad Prism (version 6 and 8)

Image Lab (version 6.0.1)

Inkscape

Kinovea

MATLAB (release 2016b)

Microsoft Office

QuantStudio™

Spike2

Stereo Investigator (version 11.07)

StereoDrive

ZEN blue edition

Agilent Technologies, Santa Clara, CA, USA

Noldus, Wageningen, Netherlands

Schreiber & Tholen, Stade, Germany

[www.fiji.sc](http://www.fiji.sc)

GraphPad Software, San Diego, CA, USA

Bio-Rad, Hercules, CA, USA

[www.inkscape.org](http://www.inkscape.org)

[www.kinovea.org](http://www.kinovea.org)

The MathWorks, Inc, Natick, MA, USA

Microsoft, Redmond, USA

Thermo Fisher, Darmstadt, Germany

CED, Cambridge, UK

MBF Bioscience, Williston, VT, USA

Neurostar, Tübingen, Germany

Zeiss, Oberkochen, Germany

## 2.2 Methods

### 2.2.1 Animal model

$\Delta$ ETorA (line 8) rats were generated on a Sprague Dawley genetic background by Kathrin Grundmann-Hauser, University of Tübingen, Germany.<sup>188</sup> Male  $\Delta$ ETorA (line 8) and male nontransgenic (wildtype, wt) littermates were used. The animal age at experiment onset was  $10 \pm 2$  weeks. Breeding was implemented by the animal facility of the University of Tübingen. At least one week before experiment onset, the animals were housed in the animal facilities of the University of Würzburg (Department of Neurology, Zentrum für Experimentelle Molekulare Medizin). The animals were kept under standard conditions in an artificial 12 h/12 h light-dark-cycle, at a temperature of  $22 \pm 2$  °C and 45 - 65% humidity with free access to food and water. All animal experiments were approved by the Government of Lower Franconia, Würzburg, Germany.

### 2.2.2 Genotyping

The determination of a genotype is based on the polymerase chain reaction (PCR) of genomic deoxyribonucleic acid (DNA) by using specific primers and followed by a DNA gel electrophoresis.

#### 2.2.2.1 Extraction of genomic DNA

Genomic DNA was isolated from rat ear biopsies by using the DNeasy Blood & Tissue kit according to the manufacturer's instructions "Purification of Total DNA from Animal Tissues (Spin-Column Protocol)".

#### 2.2.2.2 Polymerase chain reaction (PCR)

The DreamTaq Hot Start Green PCR Master Mix was used for the PCR. This mix already includes an optimized buffer, deoxynucleotides (dNTPs), a Hot Start Taq DNA polymerase, two tracking dyes, and a density reagent. The sequences of the specific primers for the human mutated *TOR1A* gene ( $\Delta$ ETorA) are listed in 2.1.7. The following PCR reaction mix and thermocycler program were used for the  $\Delta$ ETorA genotyping PCR:

PCR reaction mix:

1.0 $\mu$ l	Genomic DNA template (10 – 500 $\mu$ g)
12.5 $\mu$ l	DreamTaq Hot Start Green PCR Master Mix (2X)
2.5 $\mu$ l	DYT1 fwd. Primer (10 $\mu$ M)
2.5 $\mu$ l	DYT1 rev. Primer (10 $\mu$ M)
6.5 $\mu$ l	Nuclease-free water

Thermocycler program:

Temperature	Duration	
94 °C	2 min	
94 °C	30 sec	} 32 cycles
60 °C	30 sec	
72 °C	30 sec	
72 °C	5 min	
10 °C	$\infty$	

The expected size of the PCR product for  $\Delta$ ETorA transgenic animals is 230 base pairs (bp). For wt animals, no PCR product amplification will occur.

**2.2.2.3 DNA gel electrophoresis**

For separating DNA fragments by their molecular weight, the DNA gel electrophoresis was run with a 2% agarose gel in TBE (1x) buffer at 140 V for 30 minutes (min). 25  $\mu$ l of the PCR sample, which already includes tracking dyes and a density reagent, was used for the DNA gel electrophoresis. O'RangeRuler 100 bp DNA Ladder was used as a molecular weight marker. By adding the fluorescent stain GelStar Nucleic Acid Gel Stain into the agarose gel, PCR products could be made visible using a UV light source.

**2.2.3 Sciatic nerve crush injury**

Rats were deeply anesthetized by an inhalational anesthesia of 2% isoflurane in 100% oxygen. The right hind limb was shaved. After skin incision and right sciatic nerve exposure, the right sciatic nerve was crushed at the region of the sciatic notch with a non-serrated clamp (Ultra Fine Hemostat) with a constant and reproducible pressure for three times 10 seconds (sec). Incisions were closed by using skin sutures and skin

staples. Sterile conditions were complied. Skin staples were removed four to six days after surgery. According to the guidelines of GV-SOLAS, the rats were treated after the surgery with Rimadyl (5 mg/kg body weight, subcutaneous injection). In sham-operated animals, the same surgery was performed but without crushing the sciatic nerve.

#### **2.2.4 Behavioral testing**

The assessment of the phenotype was conducted through different tests. All behavioral tests were performed before nerve crush injury (pre OP) until twelve weeks after nerve crush injury (post OP) at regular intervals. Experimental procedure and data analysis were carried out blinded to experimental groups.

##### **2.2.4.1 Tail Suspension Test (TST)**

For the TST the rats were lifted carefully by their tail for the video recording of three sequences of 10 sec each. During these sequences, the rat was not allowed to climb up, rotate or move strongly. Furthermore, the video recording should capture the whole body including both front and hind limbs. The video recordings were analyzed by using the video player Kinovea.

##### **2.2.4.2 Open Field (OF)**

In an arena of 58.5 x 58.5 x 45 cm and a dark and quiet environment, the spontaneous exploration behavior of rats was recorded and analyzed with the automated video tracking system EthoVision XT. Rats could acclimatize in this dark and quiet environment for at least 30 min before the recordings started. Recordings of freely moving rats for a 5 min period started 3 sec after the rat was placed into the middle of the arena.

#### **2.2.5 Nerve conduction studies**

During an inhalational anesthesia of 1.5% isoflurane in 100% oxygen, compound muscle action potentials (CMAP) and latencies were recorded with a steel needle electrode in the flexor digitorum brevis muscle after supramaximal stimulation of the tibial nerve above the ankle (distal) and of the sciatic nerve at the sciatic notch (proximal) by using a digital Neurosoft-Evidence 3102 electromyograph. Nerve

conduction velocities (NCV) were calculated using latencies and distance measurements of the distal and proximal stimulation positions.

## **2.2.6 DBS and LFP recordings**

### **2.2.6.1 Electrode implantation**

Rats were anesthetized with 2% isoflurane in 100% oxygen, and electrodes were implanted into the EP as well as two different regions of the primary motor cortex (MC) contralateral to the crushed sciatic nerve nine weeks after injury. After shaving, disinfecting and fixing the head of the rat into a stereotaxic frame, a midline incision was made and holes were drilled into the skull for electrodes, fixation screws and a reference screw. For the EP, a monopolar platinum/iridium electrode with an impedance between 0.8 and 1.1 MOhm was implanted according to the following coordinates:  $-2.28$  mm anterior-posterior (AP),  $-2.7$  mm medial-lateral (ML), and  $-7.3$  mm dorsal-ventral (DV). The following coordinates were used for implanting self-made monopolar platinum/iridium electrodes into MC:  $0.96$  mm AP,  $-2.0$  mm ML, and  $-1.0$  mm DV (MC1) and  $3.72$  mm AP,  $-3.0$  mm ML, and  $-1.2$  mm DV (MC2). The electrodes were fixed together with screws to the skull by dental cement. A custom-made plug was connected to the electrode of the EP, and the ground wire of the plug was fixed with a screw on the lateral part of the skull. The incision was closed by skin sutures.

### **2.2.6.2 DBS**

The animals were connected to a cable-bound multichannel stimulation system. For HFS of the EP, a rectangular pulse shape of  $200$   $\mu$ s pulse length and  $130$  Hz frequency was used. The amplitude was set specifically to every single rat by increasing this parameter until side effects were detected with a subsequent reduction of 10%. The stimulation was performed for a maximum of 21 days (stim-ON) and compared to sham stimulation (stim-OFF). Figure 6 shows a schematic illustration of the setup for DBS and LFP recordings.

### **2.2.6.3 LFP recordings and data analysis**

In lightly anesthetized (isoflurane) animals, all LFP recordings were performed while the stimulator was switched off. The recordings took place with a delay of about 10 min after discontinuing from the stimulator. LFP signals were amplified  $\times 1000$ , analog-filtered between  $0.1$  Hz and  $1000$  Hz by using an AC differential amplifier, recorded

digitally at 20 kHz and down-sampled at 1–2 kHz with a recording time of 120 sec. The pin connector of the assembled electrode was connected to the silver screw on the contralateral nasal bone. Experiments were performed in cooperation with Flora Vitale.

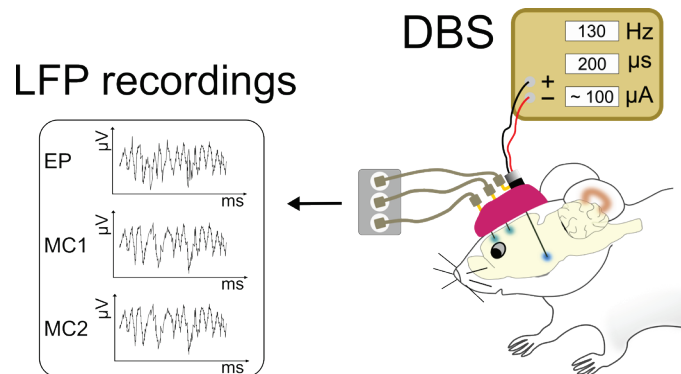


**Figure 6: Schematic illustration of the setup for DBS and LFP recordings in rats**

Electrodes are implanted into the EP, MC1 and MC2 contralateral to the crushed sciatic nerve and fixed to the skull by dental cement. HFS is performed by connecting the implanted electrode of the EP to the cable-bound DBS setup. LFP signals are recorded from the EP, MC1 and MC2 while the stimulator is switched off.

#### 2.2.6.4 Spectral power and imaginary coherence analysis

The analysis of the LFP recordings was performed by using MATLAB. The preparation of signals for spectral analysis was implemented with the Fieldtrip Toolbox (<http://www.ru.nl/neuroimaging/fieldtrip>).<sup>203</sup> Recordings with artifacts were visually identified and rejected. Visually identified segments with electrical artefacts were rejected. Infinite impulse response Butterworth filter of fourth-order with forward and reverse pass was used for processing signals for down-sampling to 256 Hz, bandpass-filtering (cutoff frequencies 0.5 and 100 Hz) and notch-filtering of 49-51 Hz. An artifact-free segment was pseudorandomly selected for analysis.

For spectral power calculation, discrete prolate spheroidal sequences as tapers were used followed by a Fourier transformation.<sup>203</sup> Over  $\pm 2$  Hz spectral smoothing was achieved. The frequency range of interest was 1-100 Hz with a resolution of 0.5 Hz. Power was expressed as relative power after normalization by the mean standard deviation of power within 5-45 Hz and 55-95 Hz and distributed in the theta (4–7 Hz) and beta (14–35 Hz) ranges. For imaginary coherence analysis, the coherence estimates between the EP and MC1 as well as EP and MC2 in the theta power was computed by using the Fieldtrip Toolbox.<sup>204</sup> Coherence analysis depends on the function of phase consistency and amplitude covariation. The magnitude of imaginary

coherence ranges from 0 (no linear relationship) to 1 (complete correlation). Analysis was performed in cooperation with Uri Eduardo Ramirez Pasos.

### 2.2.7 Autoradiography

$^{18}\text{F}$ -fluorodeoxyglucose ( $^{18}\text{F}$ -FDG) (37 MBq) was injected intraperitoneally into rats after a fasting period of at least 17 hours (h). Rats were anesthetized by isoflurane and sacrificed by cervical dislocation 60 min after  $^{18}\text{F}$ -FDG distribution. The brain was dissected, embedded in Tissue-Tek O.C.T., frozen and cut into 20  $\mu\text{m}$  coronal sections. Sections were exposed for 60 min on autoradiography plates and afterwards visualized with a digital autoradiography system.

The quantification of  $^{18}\text{F}$ -FDG uptake distribution was analyzed with the software Fiji, based on intensity measurements of triplicates for each region of interest (ROI). Striatum, MC, somatosensory cortex (SC), thalamus, SN and cerebellar lobule are the regions of interest and were drawn manually, guided by the rat stereotaxic atlas.<sup>205</sup> Background subtracted data of the ROIs were normalized to the reference. Reference was corpus callosum (CC) for all ROIs, except for the cerebellar lobule. The reference of the cerebellar lobule was the gigantocellular reticular.

The experiments were performed in cooperation with Prof. Dr. Dr. Takahiro Higuchi and colleagues of the Department of Nuclear Medicine (University Hospital Würzburg, Germany).

### 2.2.8 Tissue dissection and processing

Rats were sacrificed by the use of  $\text{CO}_2$  inhalation. After transcardial perfusion of the rats with 0.4% heparin in PBS (1x) solution, the striatum of the left and right hemispheres was dissected. Tissue for protein isolation was snap-frozen in liquid nitrogen. In 500  $\mu\text{l}$  RNA stabilization solution *RNA/later*, tissue for RNA isolation was incubated for 24 h at 4 °C. After removing the supernatant, the tissue was snap-frozen in liquid nitrogen. All tissues were stored at -80 °C. For histology, the rats were transcardially perfused first with 300 ml of 0.4% heparin in PBS (1x) solution followed by 350 ml of 4% paraformaldehyde (PFA) solution. The brain was dissected, post-fixed in 4% PFA solution overnight at 4 °C and transferred into 30% sucrose in PBS (1x). After the tissue had sunk in a 30% sucrose in PBS (1x) solution at 4 °C, it was

embedded in Tissue-Tek O.C.T., frozen in liquid nitrogen-cooled in 2-methylbutane and stored at -20 °C.

## **2.2.9 Histology**

PFA fixed, and in Tissue-Tek O.C.T. embedded brain tissue was serially cut by a cryostat in 40 µm coronal sections through the rat striatum for histological analysis. According to the rat brain atlas, twelve series of the whole striatum were generated from about 2.7 mm to -4.1 mm relative to the bregma.<sup>205</sup>

### **2.2.9.1 Nissl staining**

Sections on object slides were dried for at least 2 h at room temperature (RT), incubated in 0.1% cresyl violet solution for 30 min, rinsed three times for 5 min in aqua bidest, and dehydrated in a graded series of ethanol (three times 70%, two times 90%, two times 100%, for 1 min each). Finally, the sections were incubated two times for 5 min in xylene and mounted with Vitro-Clud.

### **2.2.9.2 Immunohistochemical staining of striatal interneurons**

One striatal free-floating series was stained for each cell type: CR, PV, choline acetyltransferase (ChAT) and neuronal nitric oxide synthase (nNOS) specific striatal interneurons.

Sections for immunohistochemical staining against CR were blocked in 10% bovine serum albumin (BSA), 0.5% Triton X-100 in PBS (1x) for 3 h at RT, incubated for three days at 4 °C with mouse anti-calretinin in 5% BSA, 0.1% Triton X-100 in PBS (1x) and for 2 h at RT with biotinylated goat anti-mouse IgG in 1% BSA in PBS (1x).

For immunohistochemical staining of ChAT, sections were preincubated in 20% normal rabbit serum (NRS) in PBS (1x) for 3 h at RT, applied with goat anti-choline acetyltransferase in 1% NRS in PBS (1x) for three days at 4 °C and with biotinylated rabbit anti-goat IgG in 1% NRS in PBS (1x) for 2 h at RT.

Immunohistochemical staining against nNOS was performed with an incubation step for 3 h at RT with a blocking solution of 15% normal goat serum (NGS), 5% BSA, 0.5% Triton X-100 in PBS (1x). The primary rabbit anti-neuronal nitric oxide synthase antibody incubation was carried out in a 5% NGS, 0.1% Triton X-100 in PBS (1x) solution for three days at 4 °C and the secondary biotinylated goat anti-rabbit IgG antibody in a 1% NGS in PBS (1x) solution for 2 h at RT.

Sections for PV specific immunohistochemical staining were incubated with 5% NGS, 2% BSA, 0.5% Triton X-100 in PBS (1x) for 3 h at RT. In 5% NGS, 0.1% Triton X-100 in PBS (1x) diluted rabbit anti-parvalbumin was incubated overnight at RT. Incubation of biotinylated goat anti-rabbit IgG in 1% NGS in PBS (1x) was accomplished for 2 h at RT.

All sections were incubated for 2 h at RT with the VECTASTAIN ABC HRP Kit and subsequently with the DAB Peroxidase (HRP) Substrate Kit according to the manufacturer's protocols. The sections were mounted in Aquatex.

### **2.2.9.3 Unbiased stereology**

Stereological experiments were implemented for the determination of the total number of cells by the optical fractionator method with the StereoInvestigator software and the BX53 light microscope using an objective with a magnification of 100x and a 1.25 numerical aperture. Unbiased analysis for each target was performed randomly on one striatal series out of twelve with a section interval range of approximately 480  $\mu\text{m}$ . For all interneuron quantifications a counting frame of 60 x 60  $\mu\text{m}$  in a sampling grid of 100 x 100  $\mu\text{m}$  for ChAT<sup>+</sup> cells and nNOS<sup>+</sup> cells, 120 x 120  $\mu\text{m}$  for CR<sup>+</sup> cells, 160 x 160  $\mu\text{m}$  for PV<sup>+</sup> cells was used to accomplish a Gundersen coefficient of errorless or equal to 0.1 for each section. The counting frame for Nissl<sup>+</sup> cells was 20 x 20  $\mu\text{m}$  in a sampling grid of 600 x 600  $\mu\text{m}$ . The optical fractionator was set to a 16  $\mu\text{m}$  disector height and 2  $\mu\text{m}$  guard zone. The mounted thickness was measured at every counting site.

### **2.2.9.4 Bright-field microscopy**

Images were acquired on the Axio Imager.M2 microscope by using objectives with a 20x and 100x magnifications and the ZEN blue edition software.

### **2.2.10 Gene expression**

Real-time PCR (qPCR) and ribonucleic acid (RNA) sequencing (RNA-Seq) are techniques used to monitor gene expression changes across different experimental conditions.<sup>206</sup> For analyzing a set of selected genes, qPCR was performed while RNA-Seq provides a genome-wide overview of the expression of all genes at once. Here, the gene expression analysis of the striatum was performed.

### 2.2.10.1 RNA purification and quantification

Snap frozen tissues were homogenized with 350  $\mu$ l RLT/DTT buffer by the Tissue Lyser LT with one 5 mm stainless steel bead at a frequency of 50 Hz for 2 min. Total RNA was isolated by using the RNeasy Micro Kit according to the manufacturer protocol "Purification of Total RNA from Animal Tissues". RNA concentration and purity were measured by the NanoDrop One. Purified RNA was directly processed with the reverse transcription or stored at -80 °C for further processing.

### 2.2.10.2 Reverse transcriptase polymerase chain reaction (RT-PCR)

SuperScrip IV VILO™ Master Mix was used for the complementary DNA (cDNA) synthesis. 20  $\mu$ l of the RT-PCR reactions mix contains RNA template (250 – 500 ng), 4  $\mu$ l of SuperScrip IV VILO Master Mix and nuclease-free water. cDNA was synthesized at 25 °C for 10 min, 50 °C for 10 min and 85 °C for 5 min in a thermocycler. The cDNA sample was diluted 1:10 with nuclease-free water. Short term storage for cDNA was at -20 °C and long-term storage at -80 °C.

### 2.2.10.3 Real-time PCR (qPCR)

TaqMan Gene Expression Assays and TaqMan Gene Expression Master Mix were used for quantitative qPCR. Every TaqMan Gene Expression Assay consists of target-specific primers, a sequence-specific probe with dye label (6-carboxyfluorescein, FAM) on 5' end and a nonfluorescent quencher on the 3' end. All used TaqMan Gene Expression Assays are listed in 2.1.8. TaqMan Gene Expression Master Mix contains DNA polymerase, dNTPs and buffer. A 12  $\mu$ l qPCR reaction mix and a two-Step-qPCR cyclor program were used for the gene expression analysis. Triplicates were performed for each sample and all conditions.

#### qPCR reaction mix:

- 5.0  $\mu$ l cDNA template (1:10 dilution)
- 6.0  $\mu$ l TaqMan Gene Expression Master Mix (2X)
- 0.6  $\mu$ l TaqMan Gene Expression Assay (20X)
- 0.4  $\mu$ l Nuclease-free water

qPCR cyclor program:

Temperature	Duration	
50 °C	2 min	
95 °C	10 min	
95 °C	15 sec	} 40 cycles
60 °C	1 min	

Relative quantification of the gene expression level was analyzed with the  $2^{-\Delta\Delta CT}$  method; therefore, the results were normalized to the endogenous control *glyceraldehyde 3-phosphate dehydrogenase (Gapdh)* and the calibrator wt control.

**2.2.10.4 RNA-Sequencing (RNA-Seq)**

The experiment was performed by the Core Unit Systems Medicine (Dr. Sascha Dietrich/ Dr. Tobias Heckel, Medical Faculty, University of Würzburg, Germany). RNA concentration and purity of the samples were assessed by the bioanalyzer. Libraries were prepared according to the Illumina TruSeq stranded mRNA Sample Preparation Guide by a total RNA input of 80 ng and 14 PCR cycles. This protocol allows the sequencing of poly(A)<sup>+</sup> messenger RNAs (mRNAs) by priming the reverse transcription with an oligo(dT) and generating barcoded cDNA ready for sequencing. Two times 14 libraries (28 samples) were pooled and sequenced as single-end on an Illumina NextSeq 500 system with a read length of 75 nt in two runs. Reads were processed using cutadapt (version 2.1). The reference genome retrieved from the NCBI RefSeq Rattus norvegicus Genome Rnor\_6.0 (<https://www.ncbi.nlm.nih.gov/genome/?term=txid10116>) was completed with the sequence for the mutated human *TOR1A* gene (OMIM: 605204.0001). The reads were mapped using STAR (STAR\_2.6.1a\_08-27) and counted with the featureCounts from Subread package (version 1.6.3).<sup>207,208</sup> Differential gene expression (DEG) analysis was performed by using DESeq2 (version 1.22.2).<sup>209</sup> Genes with a Benjamin-Hochberg corrected p-value below 0.05 were classified as DEGs. Finally, gene expression was quantified using the normalized metric “Reads per kilobase million” (RPKM) calculated according to Wagner et al. 2012.<sup>210</sup>

Downstream analysis with RPKM values and DEGs were performed by myself. Pathway analyses, based on DEGs, were further conducted with Enrichr, a comprehensive gene set enrichment analysis (GSEA) web server.<sup>211,212</sup>

## 2.2.11 Microdialysis

Microdialysis is a technique for sampling proteins and other molecules in living animals. During brain microdialysis, samples were collected from the extracellular fluid of the brain tissue in real-time.

### 2.2.11.1 Assembling microdialysis probes

For assembling the microdialysis probes, the polyethylene (PE) tubing and silica capillary tubing were cut into 3 cm long pieces. To build the metal tubing, the plastic part of the 25 G needle was removed, and the tip of the needle was bent. A hole was pierced through the pre-cut PE tubing by using a 26 G needle, and the pre-cut silica capillary tubing was pushed through. The metal tubing was slid onto one end of the silica capillary tubing. The joint of the three components was fixed with glue. The other end of the silica capillary tubing was cut to the required length of 7.5 mm. One end of a 1 cm long semi-permeable membrane was sealed with a drop of glue. The sealed membrane was slid onto the 7.5 mm silica capillary tubing and fixed with glue. The active membrane part has a length of 3 mm from the tip of the microdialysis probe. The rest of the membrane is the inactive part, which was sealed with a thin layer of glue. A self-assembled microdialysis probe is presented in Figure 7.



**Figure 7: Self-assembled microdialysis probe for rats**

The microdialysis buffer enters the microdialysis probe through the stainless-steel tubing by a constant flow rate steered by a syringe pump. The inlet tubing contains the fused silica capillary tubing to enable the microdialysis buffer to flow down to the tip of the microdialysis probe, which is covered with a semi-permeable membrane. The exchange of molecules by diffusion takes place on the 3 mm long active part of the semi-permeable membrane. The dialysate is transported out of the microdialysis probe through the PE outlet tubing and collected via a microsampler.

### 2.2.11.2 Implantation of microdialysis probes

Microdialysis probes were implanted 24 h before microdialysis into the striatum of the left and right hemisphere of the rats during inhalation-anesthesia with 2% isoflurane in 100% oxygen. The head of the rats was shaved and fixed in a stereotaxic frame. After disinfection and local anesthesia, a midline incision was made. Two holes were drilled according to the coordinates for the position of the microdialysis probe 0.7 mm AP, at either -3.0 mm (left hemisphere) or 3.0 mm (right hemisphere) ML. Two additional holes around the microdialysis probe holes were drilled, and screws were inserted into the holes. Before the implantation of the microdialysis probe, the microdialysis probe was tested, filled with aCSF and attached to the probe holder in a straight position. The microdialysis probe was inserted slowly into the target region with the coordinates probe 0.7 mm AP, at either -3.0 mm (left hemisphere) or 3.0 mm (right hemisphere) ML, -7.0 mm DV and directly fixed to the dry skull by dental cement. For fixation stability, the screws were also covered by dental cement in one layer with the microdialysis probes. A hook was added and fixed with dental cement to the skull. Parts of the incision were closed by skin sutures. The microdialysis probe was flushed with aCSF, and the inlet and outlet were covered with caps.

### 2.2.11.3 Microdialysis – Collection of microdialysis samples

Necessary components for the collection of microdialysis samples are the microdialysis setup from AgnTho's AB and a self-made box with a size of 35 x 35 x 35 cm. The syringes were filled with aCSF or aCSF<sup>K+</sup> and attached to the syringe pump. All tubings were connected to the system and prefilled with aCSF. One day after the implantation of the microdialysis probes, the rat was placed into the box of the microdialysis setup, and the tubings of the microdialysis system were connected to the inlet and outlet parts of the microdialysis probe. The perfusion rate was 1.5 µl/min. After connecting the rats to the microdialysis setup, a 60 min stabilization period followed, and the perfusate was discarded. For the experiment, 22 samples were collected for 15 min each. 7.5 µl of 0.02 M acetic acid was added into the tubes of each sample. The system was running first with aCSF followed by collection of six baseline samples (sample 1 – 6). 90 min after the experiment was started (beginning of sample 7) the buffer was switched to aCSF<sup>K+</sup>, which contains a high potassium concentration and stimulates the transmitter release at the synapses. aCSF<sup>K+</sup> was infused for 30 min through the microdialysis probes; afterwards, additional 14 perfusate samples were

collected (sample 9 – 22) by the perfusion of aCSF. All samples were collected in a refrigerated microsampler and finally stored at -80 °C. Figure 8 shows a schematic illustration of the *in vivo* microdialysis perfusion.

### 2.2.12 High performance liquid chromatography (HPLC)

HPLC is an analytical technique to separate, identify, and quantify different components of substance mixtures based on their molecular structure. Monoamines in brain tissue and brain microdialysis samples were analyzed with the HPLC system 1260 Infinity and the electrochemical detector DECADE Elite. The HPLC system consisted of the following components: 1260 Infinity High Performance Degasser Module, 1260 Infinity Binary Pump, 1260 Infinity Standard Autosampler, 1290 Infinity Thermostat, 1260 Infinity Thermostatted Column Compartment. The electrochemical flow cell (SenCell) of the detector consists of a 2 mm glassy carbon working electrode (WE), an in-situ Ag/AgCl (ISAAC) reference electrode, and a stainless steel L316 auxiliary electrode (AUX). The reversed-phase chromatography (RPC) was used as the separation mechanism.

#### 2.2.12.1 HPLC analysis of monoamines of striatal tissue samples

Frozen tissue was transferred into the 55 µl ice-cold HPLC sample buffer, fumigated with argon for 20 sec and homogenized by sonication on ice (50 % amplitude, 20 sec). After centrifugation for 15 min at 14,000 rpm at 4 °C, the supernatant was transferred to the Ultrafree-MC centrifugal filter and centrifuged for 10 min at 10,000 rpm at 4 °C. Monoamines were determined from the flow-through. The total protein concentration was measured by a Lowry assay by using BSA standards.<sup>213</sup> The rest of the sample was stored at -80 °C.

5 µl of the sample was loaded onto a NUCLEOSIL 120-5 C<sub>18</sub> column (250 mm x 4 mm; 5 µm, 120 Å) using an autosampler. Separation was accomplished by the use of an isocratic mode with a flow rate of 1 ml/min at 30 °C. Detection was based on oxidation at the WE with a potential of +770 mV versus ISAAC reference electrode, a range of 5 nA and 50 nA, filter setting of 0.05 Hz and a temperature of 37 °C. External standard calibration was used for identification by retention times and quantification by total peak areas. Concentrations of 5-HT and its metabolite 5-HIAA as wells as DA and its metabolites DOPAC and HVA were calculated as ng/mg total protein of the striatum and normalized to wt ctrl animals.

### 2.2.12.2 HPLC analysis of striatal microdialysis samples

DA of striatal microdialysis samples were analyzed by loading 10  $\mu\text{l}$  of the microdialysis sample on a NeuroSep 115  $\text{C}_{18}$  column (150 mm x 1 mm; 3  $\mu\text{m}$ ), via an autosampler, separated with a flow rate of 75  $\mu\text{l}/\text{min}$  at 42  $^{\circ}\text{C}$  and detected with a working potential of 460 mV, a range of 1 nA, filter settings of 0.5 Hz at a temperature of 42  $^{\circ}\text{C}$ . For the quantification of the metabolites of DA, 5  $\mu\text{l}$  of the microdialysis sample was separated on a NeuroSep 115  $\text{C}_{18}$  column (150 mm x 1 mm; 3  $\mu\text{m}$ ) with a flow rate of 150  $\mu\text{l}/\text{min}$  at 37  $^{\circ}\text{C}$  and detected by a 570 mV potential, a 20 nA range, and a temperature of 37  $^{\circ}\text{C}$ . DA and the metabolites DOPAC and HVA were identified by retention time and quantified by peak area as nM per sample by using external standards.

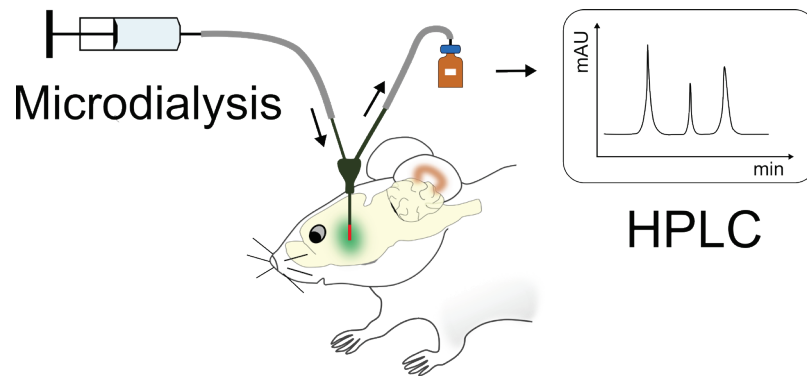


**Figure 8: Schematic illustration of *in vivo* microdialysis perfusion coupled to HPLC**

Microdialysis probes are implanted into the striatum of the rats. Microdialysis samples are collected by perfusing the probe with a constant flow rate of aCSF or aCSF<sup>K+</sup>. The exchange of molecules takes place on the active membrane, which is marked in red. The perfusates are collected into tubes within a refrigerated microsampler. Finally, monoamines of the perfusate samples are analyzed by HPLC.

### 2.2.13 Western blot analysis

For protein analysis through western blot, snap-frozen striatal tissue samples were prepared as already described in 2.2.12.1. For total protein amount analysis, the Lowry assay was performed. Laemmli sample buffer (4x) was added to the protein samples and heated for 5 min at 95  $^{\circ}\text{C}$ . The protein samples were separated through a sodium dodecyl sulfate polyacrylamide gel electrophoresis (SDS-PAGE) by the use of a 5% stacking gel and a 10% separating gel under denaturing conditions. Afterward, proteins were transferred for 1 h at 0.4 A from the gel to a nitrocellulose membrane using a wet/tank blotting system. The membrane was blocked with 5% milk in TBST for 2 h at RT and probed with the primary antibody in 5% milk in TBST overnight at 4  $^{\circ}\text{C}$ . The

membrane was washed three times for 10 min in TBST and afterward incubated with the corresponding horseradish peroxidase (HRP)-coupled secondary antibody diluted in 5% milk in TBST for 1 h at RT. Membrane was washed again three times for 10 min, and the protein immunodetection by an ECL substrate was accomplished according to the manufacturer's protocol. ChemiDoc Touch was used for the visualization of the chemiluminescent signals. Densitometric analysis was performed with the Image Lab software. Data were normalized to the corresponding GAPDH signal and finally normalized to wt ctrl animals.

#### 2.2.14 Statistical analysis

Results are presented as mean  $\pm$  standard error of the mean (SEM). Graph Pad Prism software was used for statistical analysis and for data illustrating. The normal distribution of each data set was verified by the Kolmogorov-Smirnov normality test and for data sets with an n-number less than four by Q-Q-plots. Non-normal distributed data were examined by the Mann-Whitney U test comparing two groups and the Kruskal-Wallis test with Dunn's multiple comparisons test comparing more than two groups. One-way ANOVA with Tukey's multiple comparisons test was accomplished for multiple groups of normally distributed data. Bonferroni-Holm correction was additionally applied for multiple paired comparisons. Statistical analysis of data from dystonia categories by body distribution was performed using the Chi-square test. The mixed-effects model with Dunn's multiple comparisons test was used for analyzing microdialysis data. P-value  $< 0.05$  was defined as statistically significant labeled as \* $p < 0.05$ , \*\* $p < 0.01$ , \*\*\* $p < 0.001$ , \*\*\*\* $p < 0.0001$ . Different labels were used to indicate statistical significance for microdialysis data ( $\Psi$   $p < 0.05$ ,  $\Psi\Psi$   $p < 0.01$ ,  $\Psi\Psi\Psi$   $p < 0.001$ ,  $\Psi\Psi\Psi\Psi$   $p < 0.0001$  wt ctrl vs  $\Delta$ ETorA crush; #  $p < 0.05$ , ##  $p < 0.01$ , ###  $p < 0.001$ , ####  $p < 0.0001$   $\Delta$ ETorA ctrl vs  $\Delta$ ETorA crush; \$  $p < 0.05$ , \$\$  $p < 0.01$ , \$\$\$  $p < 0.001$  wt ctrl vs wt crush; \*  $p < 0.05$ , \*\*\*\*  $p < 0.0001$  wt crush vs  $\Delta$ ETorA crush,  $\infty$   $p < 0.05$  wt ctrl vs  $\Delta$ ETorA ctrl). Statistical significance after Bonferroni-Holm correction of the p-values are indicated with §.

### 3 Results

#### 3.1 Dystonia-like movements (DLM) triggered in $\Delta$ ETorA rats through a unilateral sciatic nerve crush

The reduced penetrance of a dystonic phenotype in DYT-TOR1A gene carrier indicates an interaction between genetic background and an additional modifier such as an environmental factor. A DYT-TOR1A human gene carrier manifested a dystonic phenotype after a peripheral nerve trauma through a bite from a moray in the right heel.<sup>214</sup> Based on this case report and the clear evidence of peripheral trauma as a risk factor in different types of dystonia<sup>134</sup>, the influence of an environmental trigger through a unilateral sciatic nerve injury on DYT-TOR1A genetic background was investigated in a  $\Delta$ ETorA rat model, which overexpresses the human mutant TOR1A protein.

Video recordings of TST were used for the phenotype verification of naive and nerve-injured wt and  $\Delta$ ETorA rats. During TST DLM could be observed in nerve-injured rats (Figure 9 A-C). Retraction and clenching of the foot and leg of the nerve-injured side could be seen, which was interpreted as a focal dystonia-like phenotype (Figure 9 A-B). A bilateral involvement of the hindlimbs was characterized as beginning a generalization of a dystonia-like phenotype. DLM of the nerve-injured hindlimb spread to the non-nerve-injured hindlimb indicated by crossing the body midline during dystonia-like adduction (Figure 9 C). Normal postures of the hindlimbs could also be detected (Figure 9 D). Hindlimb clasping, which is not characterized as a dystonic phenotype, could be seen in all animals regardless of genotype and experimental settings during TST (Figure 9 E).

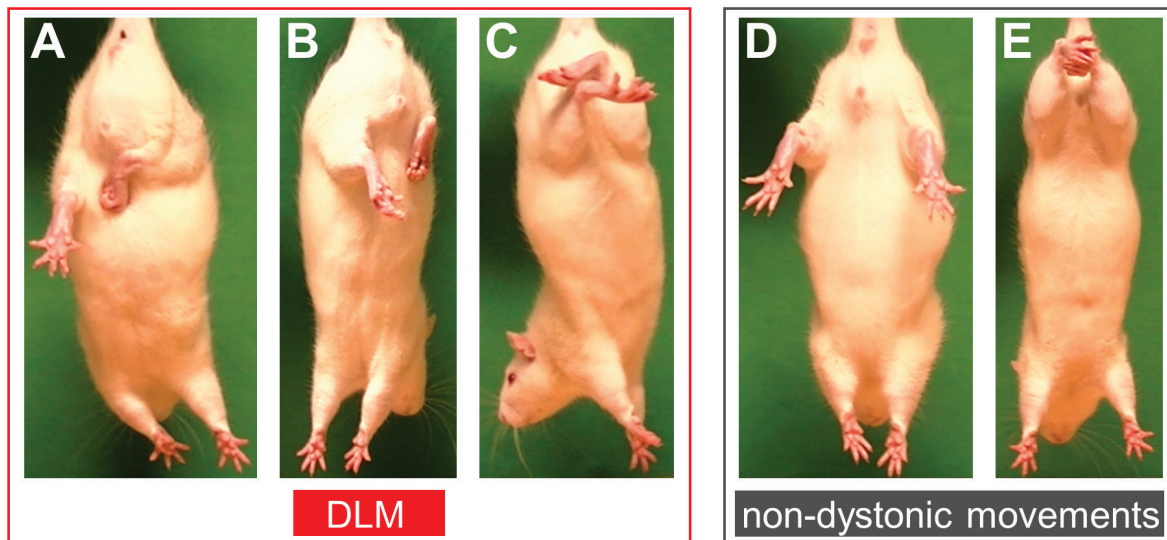


**Figure 9: DLM and non-dystonic postures during TST**

(A-E) Images of rats during TST show DLM after unilateral sciatic nerve crush injury and non-dystonic postures focused on the hindlimbs. (A) Focal DLM by a strong retraction and clenching of the right foot and leg. (B) Another example of focal DLM of the right hindlimb. (C) Simultaneous DLM of the right hindlimb and dystonia-like adduction of the left hindlimb crossing the body midline is interpreted as a sign for beginning a generalization. (D) Normal posture of hindlimbs. (E) Hindlimb clasping a non-dystonic phenotype.

To characterize the phenotype of nerve-injured rats, a new DLM scoring system was developed (Table 6). Only the hindlimbs were considered in the DLM scoring system. Recordings of three times 10 sec of the TST were rated with this new DLM scoring system from 0 to 4 points to assess duration and frequency of DLM: (0) no abnormal movements, (1) short hindlimb retraction and clenching seen in  $< 3$  sec of the evaluated time or  $\leq 2$  repetitions of DLM, (2) hindlimb retraction and clenching of  $\geq 3$  sec to  $< 10$  sec of the evaluated time or  $\geq 3$  repetitions of DLM, (3) hindlimb retraction and clenching of 10 sec to  $< 50\%$  of the evaluated time, (4) hindlimb retraction and clenching seen in  $\geq 50\%$  of the evaluated time.

**Table 6: Newly developed DLM scoring system**

<b>DLM score</b>	<b>0</b>	<b>1</b>	<b>2</b>	<b>3</b>	<b>4</b>
	no abnormal movements	short hindlimb retraction and clenching <b>&lt; 3 seconds</b> or <b>≤ 2 repetitions</b>	hindlimb retraction and clenching <b>≥ 3 seconds</b> to <b>&lt; 10 seconds</b> or <b>≥ 3 repetitions</b>	hindlimb retraction and clenching <b>10 seconds</b> to <b>&lt; 50% of the evaluated time</b>	hindlimb retraction and clenching <b>≥ 50% of the evaluated time</b>

During the whole experimental trial from pre OP until twelve weeks after sciatic nerve crush injury, a maximum DLM score of  $3.9 \pm 0.1$  in wt and  $4.0 \pm 0.0$   $\Delta$ ETorA rats was observed two weeks after nerve crush injury, followed by a slow decrease in both genotypes. DLM score of nerve-injured wt rats decreased to a minimum of  $0.4 \pm 0.3$  at week nine and stayed at a low DLM score level of  $0.6 \pm 0.3$  until week twelve. Nerve-injured  $\Delta$ ETorA rats revealed a significantly higher and constant DLM score from week nine ( $1.9 \pm 0.4$ ;  $p < 0.01$ ;  $H: 17.69$ ,  $p < 0.01$ ) to week twelve ( $1.9 \pm 0.4$ ;  $p < 0.05$ ;  $H: 16.61$ ,  $p < 0.01$ ) compared to nerve-injured wt rats. DLM score stayed  $< 1$  in all control groups over the whole experimental trial (Figure 10 A). The dystonia categories by body distribution during week nine to twelve after sciatic nerve crush injury (average) differed between nerve-injured wt and  $\Delta$ ETorA rats.  $\Delta$ ETorA rats were prone to generalization of DLM by showing 35% of beginning a generalization of DLM, 40% focal DLM and 25% without DLM. In wt rats, 70% did not show DLM while 30% developed focal DLM (Figure 10 B).

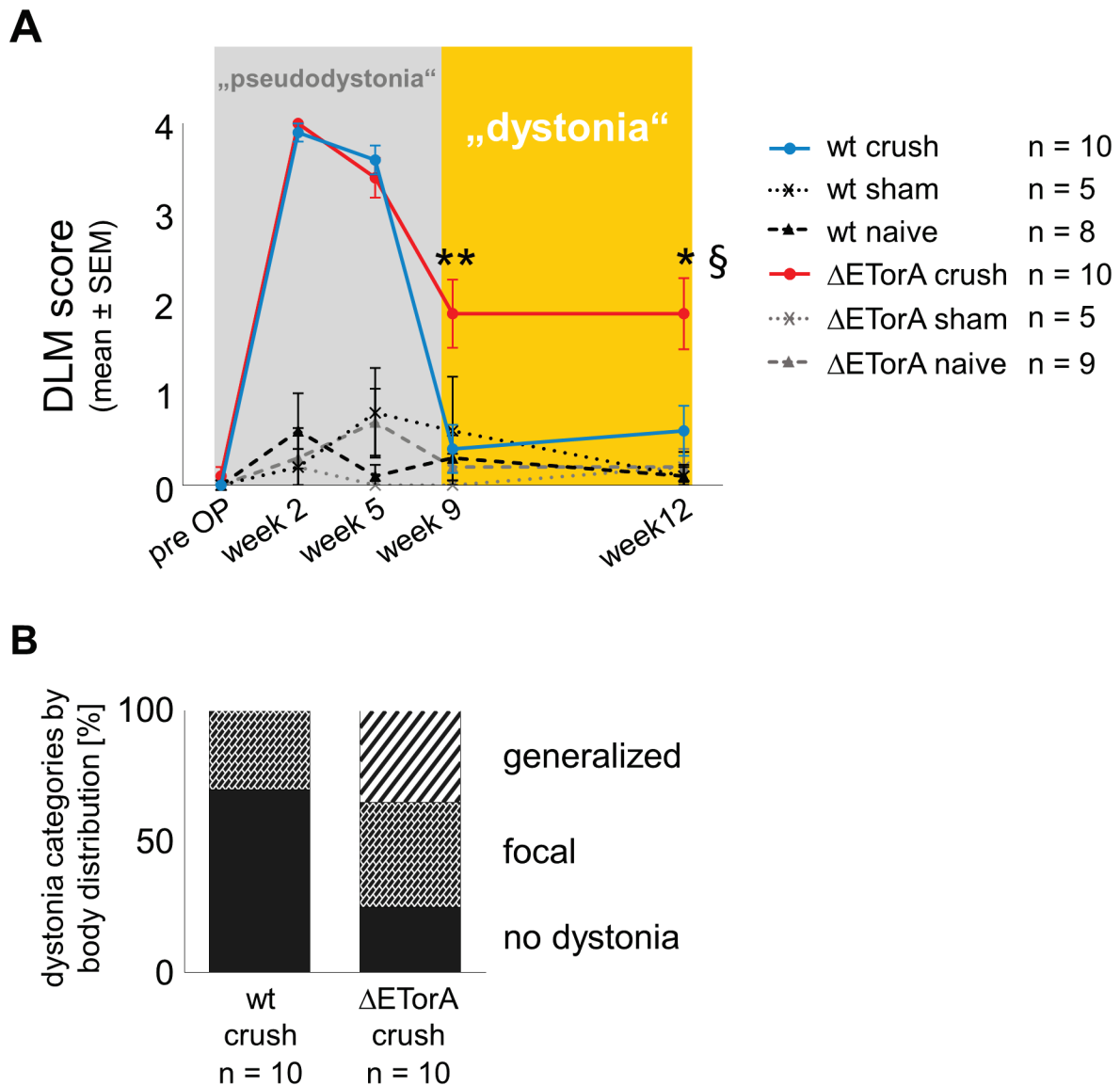


**Figure 10: Sciatic nerve crush triggers DLM in  $\Delta$ ETorA rats**

DLM analysis of TST recordings by using the newly developed DLM scoring system. (A)  $\Delta$ ETorA crush rats show a constant higher DLM score compared to wt crush rats starting at nine weeks after sciatic nerve crush injury (week 9:  $p < 0.01$ ; week 12:  $p < 0.05$ ). DLM score  $< 1$  is observed in all control groups during the whole examination period of twelve weeks. Mann-Whitney test comparing wt crush and  $\Delta$ ETorA crush rats for each time point followed by Bonferroni-Holm correction (§); \*  $p < 0.05$ , \*\*  $p < 0.01$ . (B) A distinction of dystonia categories by body distribution is made in focal, generalized and “no dystonia” according to the DLM scoring system of the hindlimbs. Chi-square test;  $\chi^2(2) = 57.74$ ,  $p < 0.0001$ .

The locomotor activity measurements were based on velocity measurements during a 5 min OF task. No differences between all experimental groups during the whole experimental trial from pre OP until twelve weeks after sciatic nerve crush injury were observed (Figure 11).

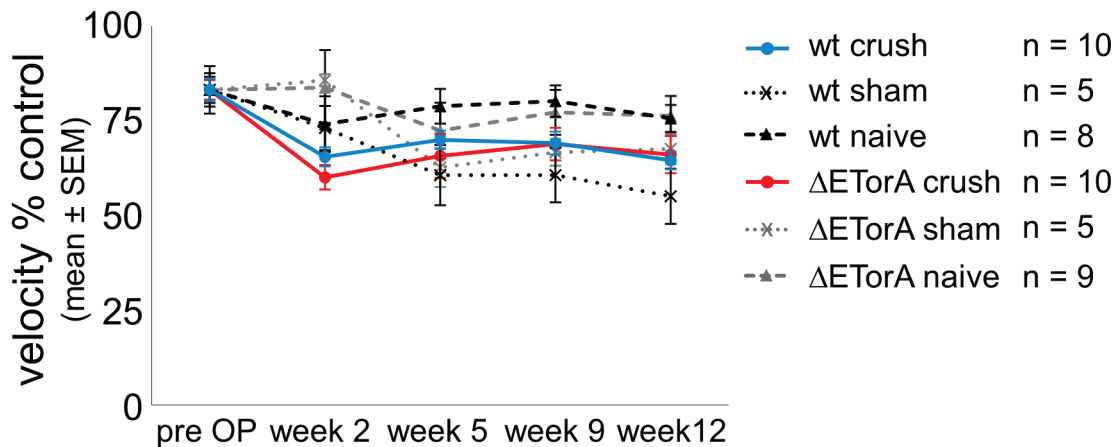


**Figure 11: Locomotor activity level is unaffected in  $\Delta$ ETorA rats**

In the OF test, the velocity during a 5 min recording does not differ between all analyzed groups.

Electrophysiological investigations of the sciatic nerves were performed to verify that an increase of DLM in  $\Delta$ ETorA rats did not result from an impaired sciatic nerve recovery after nerve injury. Electroneurography (ENG) recordings directly after sciatic nerve crush injury showed a complete conduction block of the proximal part of the sciatic nerve while the distal part of the sciatic nerve was unaffected in both wt and  $\Delta$ ETorA rats. After eleven weeks of sciatic nerve crush injury, a regeneration of the sciatic nerve was seen. However, recovery was not complete with a reduced amplitude and a prolonged latency (Figure 12 A). NCVs (contralateral:  $F_{3,27} = 0.6913$ ,  $p = 0.5653$ ; ipsilateral:  $F_{3,27} = 45.48$ ,  $p < 0.0001$ ; Figure 12 B) as well as distal (contralateral:  $F_{3,27} = 0.5846$ ,  $p = 0.6303$ ; ipsilateral:  $F_{3,27} = 35.57$ ,  $p < 0.0001$ ; Figure 12 C) and proximal (contralateral: contralateral:  $F_{3,27} = 0.7108$ ,  $p = 0.554$ ; ipsilateral:  $F_{3,27} = 50.93$ ,  $p < 0.0001$ ; Figure 12 D) CMAPs had recovered partially in the injured sciatic nerves of wt and  $\Delta$ ETorA rats eleven weeks after sciatic nerve crush injury. Significantly lower NCVs and CMAPs were seen in the injured sciatic nerves compared to the contralateral sciatic nerves or control animals in both genotypes. Significant differences in NCVs and CMAPs of the injured sciatic nerves comparing wt (NCV:  $25.14 \pm 1.69$  m/s, CMAP distal:  $7.98 \pm 0.71$  mV, CMAP proximal:  $4.50 \pm 0.59$  mV) and  $\Delta$ ETorA rats (NCV:  $25.41 \pm 1.08$  m/s, CMAP distal:  $8.18 \pm 1.03$  mV, CMAP proximal:  $5.21 \pm 0.94$  mV) were not observed. Therefore, the nerve regeneration was independent of the genetic background, and an increase of DLM in  $\Delta$ ETorA rats did not result from a higher vulnerability of the peripheral nerves to injury in  $\Delta$ ETorA rats compared to wt rats.

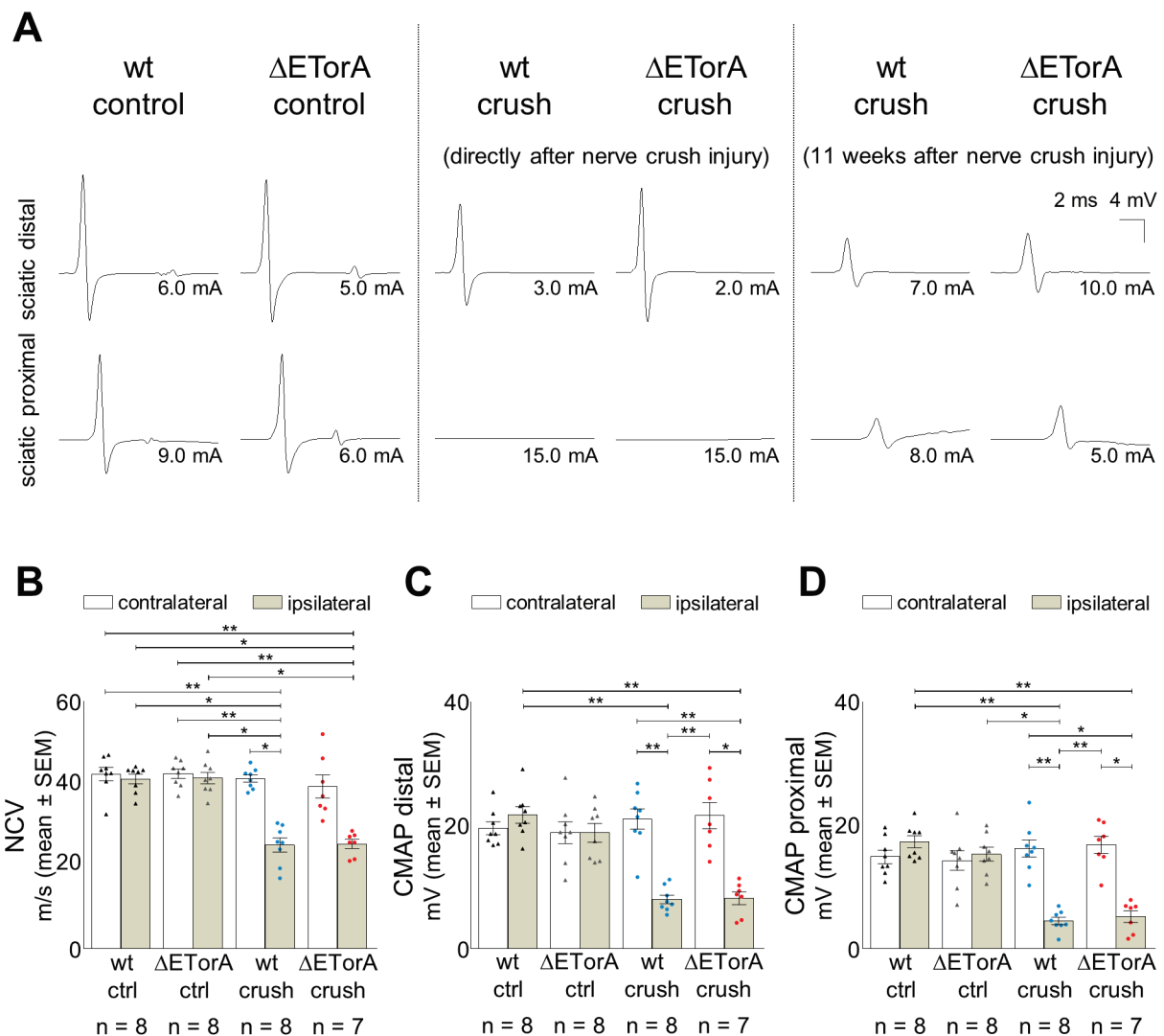


**Figure 12: Genetic background has no influence on peripheral nerve regeneration**

(A) Representative images from ENG recordings of the right sciatic nerve in ctrl animals (left), the unilateral sciatic nerve directly after crush injury (middle), and the unilateral sciatic nerve 11 weeks after crush injury (right). NCV (B), distal CMAP (C) and proximal CMAP (D) are significantly lower in the affected sciatic nerves of wt and  $\Delta$ ETorA rats 11 weeks after crush injury compared to the contralateral sciatic nerves and to sciatic nerves of control animals of the same genotype. Significant differences are not present when comparing the injured sciatic nerves of wt rats with  $\Delta$ ETorA rats. Kruskal-Wallis test with Dunn's multiple comparisons test; \*  $p < 0.05$ , \*\*  $p < 0.01$ .

### 3.2 Alteration of theta and beta oscillations in the brain network of $\Delta$ ETorA rats

A higher theta band in the GPi of dystonia patients was described in recorded LFPs.<sup>33,35</sup> Due to this finding, LFP recordings of the EP, the equivalent to the human GPi, and of the motor cortices were performed in nerve-injured wt and  $\Delta$ ETorA rats (Figure 13). Baseline recordings in  $\Delta$ ETorA rats showed a significantly higher theta power in EP and MC1 and a trend in MC2 compared to wt rats. The baseline beta power in  $\Delta$ ETorA rats was significantly lower in EP and non-significantly reduced in MC1 and MC2 compared to wt rats.

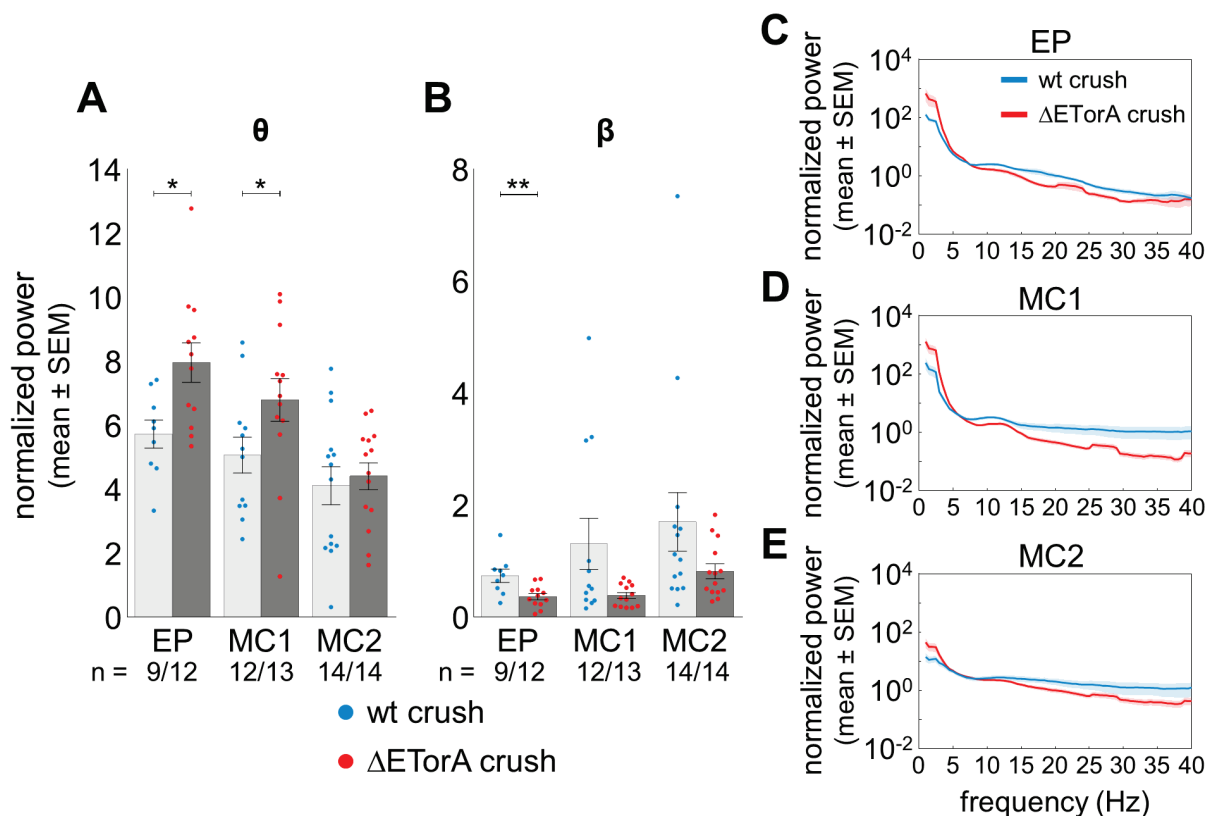


**Figure 13: Alterations in theta and beta oscillations in  $\Delta$ ETorA rats**

Theta and beta oscillations of LFP recordings on the contralateral targets of the CNS nine weeks after sciatic nerve crush injury. (A) Theta ( $\theta$ ) power of EP ( $p < 0.05$ ) and MC1 ( $p < 0.05$ ) is significantly higher in  $\Delta$ ETorA crush rats compared to wt crush rats. (B) Beta ( $\beta$ ) power is decreased in all targets of  $\Delta$ ETorA crush rats compared to wt crush rats, but only significantly in EP ( $p < 0.01$ ). Normalized power spectra of wt crush and  $\Delta$ ETorA crush rats in EP (C), MC1 (D), MC2 (E). Mann Whitney test; \*  $p < 0.05$ , \*\*  $p < 0.01$ .

### 3.3 DBS improves clinical phenotype and modulates the brain network oscillations in $\Delta$ ETorA rats

DBS of the GPI is a highly effective treatment option for DYT-TOR1A patients.<sup>37,139</sup> A DBS approach was implemented in the contralateral EP of nerve-injured  $\Delta$ ETorA rats with an HFS period of three weeks starting nine weeks after sciatic nerve crush injury. DBS stimulation over three weeks improved DLM in nerve-injured  $\Delta$ ETorA rats (stim ON) by a reduction of the DLM score of 68% when comparing baseline data with data three weeks post DBS (Figure 14 A).

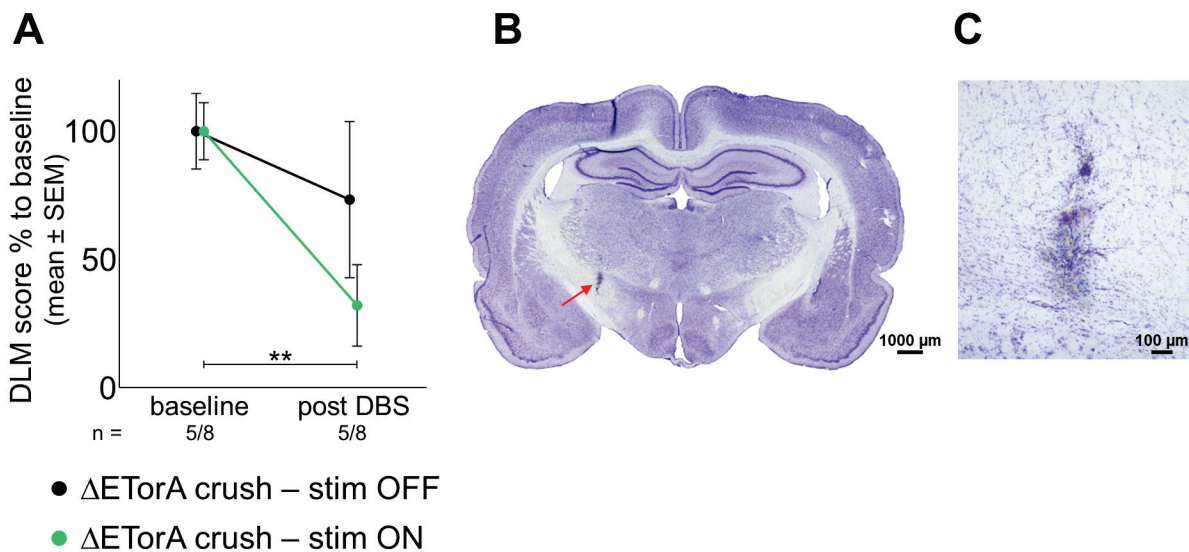


**Figure 14: DBS improves DLM in  $\Delta$ ETorA rats**

(A) DLM score decreases significantly after three weeks of EP-DBS in  $\Delta$ ETorA crush stim ON rats ( $p < 0.01$ ). DLM score in the non-stimulated group  $\Delta$ ETorA crush stim OFF persists on a constant level. Mann-Whitney test; \*\*  $p < 0.01$ . Representative image of Nissl stained coronal whole-brain section (B) and a higher magnification of the EP (C) showing the position of the unilateral EP-DBS microelectrode in the left hemisphere.

The theta oscillations were measured over three weeks of stimulation by LFP recordings comparing nerve-injured  $\Delta$ ETorA rats in on stimulation (stim ON) with off stimulation (stim OFF) (Figure 15 A-D). A significant effect of reduced theta activity was detected in MC2, whereas in MC1 and EP a non-significant decrease was found in nerve-injured  $\Delta$ ETorA rats under stim ON condition. The imaginary coherence was investigated in nerve-injured  $\Delta$ ETorA rats between the target group of EP-MC1 and EP-MC2 in stimulation on and off condition (Figure 15 E-G). There were no significant differences in the imaginary coherences of theta oscillations comparing the two groups EP-MC1 and EP-MC2 in stimulation off condition. In stimulation on condition imaginary

coherence analysis revealed a significantly higher interaction between EP and MC2 instead of EP and MC1 in theta activity. At the end of the experiment the position of the electrode of the EP was verified by Nissl staining (Figure 14 B-C). Two animals had to be excluded because of an off-target positioning. In 3.2, 3.3, Figure 13, Figure 14 and Figure 15 the animals were already excluded from the analysis.

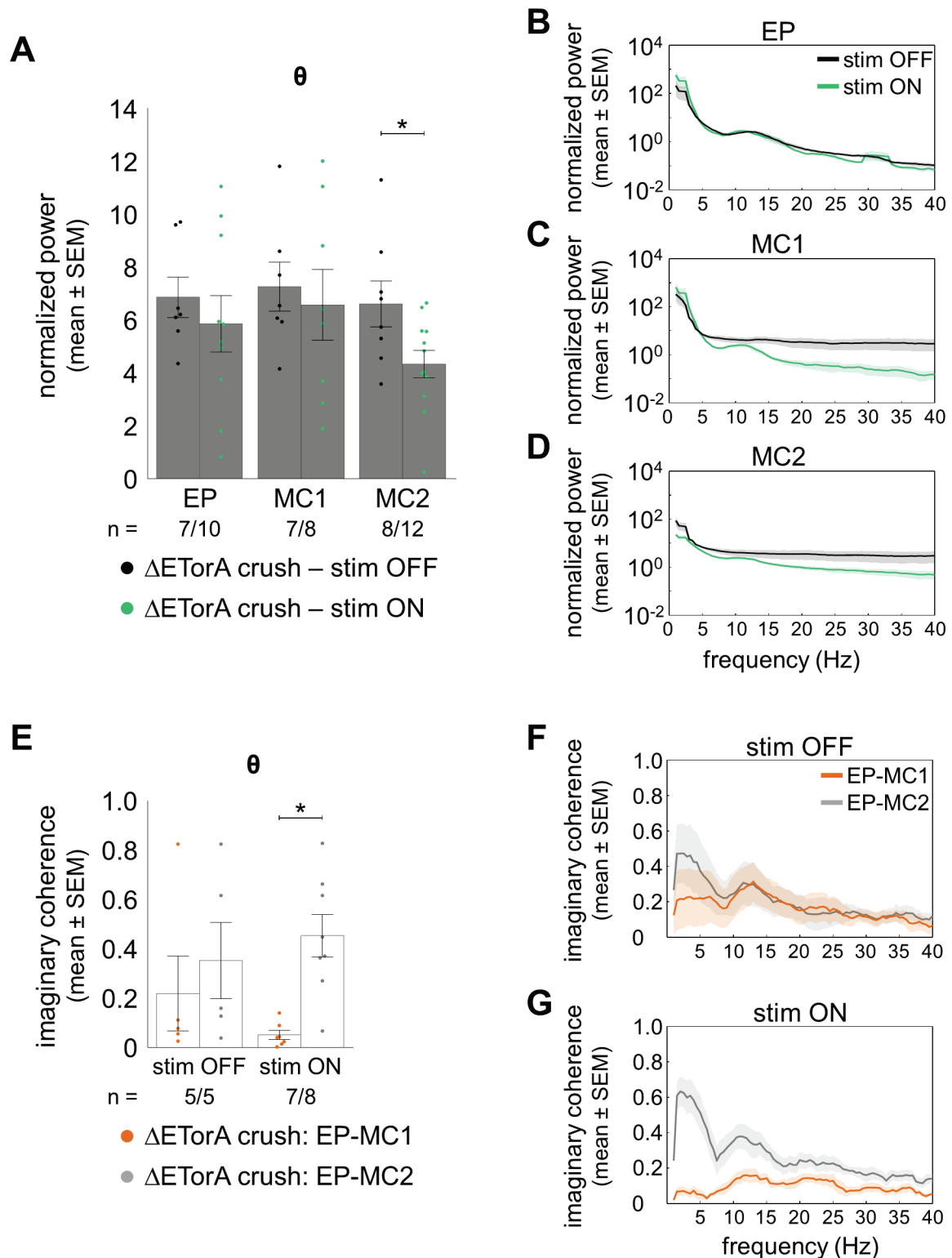


**Figure 15: Modulating effect of DBS on theta and beta oscillations**

(A) LFP recordings after three weeks of EP-DBS in  $\Delta$ ETorA crush rats indicate a significantly lower theta ( $\theta$ ) power of MC2 ( $p < 0.05$ ) and a non-significant lower theta power of MC1 an EP in on stimulation compared to off stimulation. Normalized power spectra of  $\Delta$ ETorA in off and on stimulation in EP (B), MC1 (D), MC2 (D). (E) A significantly higher imaginary coherence is observed in EP–MC2 compared to EP-MC1 ( $p < 0.05$ ) of theta ( $\theta$ ) power in on stimulation of  $\Delta$ ETorA crush rats. Imaginary coherence spectra of the EP-MC1 and EP-MC2 pairs in off stimulation (F) and on stimulation (G). Mann Whitney test; \*  $p < 0.05$ , \*\*  $p < 0.01$

### 3.4 Increased glucose metabolism depending on genetic background and environmental trigger

Dystonia is described as a functional network disease of the CNS.<sup>12</sup> Metabolic changes can influence signal transmission in these networks.<sup>215</sup> Through FDG autoradiography, regional metabolic patterns in different regions of the brain were analyzed twelve weeks after sciatic nerve crush injury (Figure 16). Peripheral trauma increased the glucose uptake in both genotypes analyzed in MC (contralateral:  $F_{3,31} = 5.82$ ,  $p < 0.01$ ; ipsilateral:  $F_{3,30} = 4.127$ ,  $p < 0.05$ ), SC (contralateral:  $F_{3,31} = 5.965$ ,  $p < 0.01$ ; ipsilateral:  $F_{3,31} = 4.893$ ,  $p < 0.01$ ) and striatum (contralateral:  $F_{3,31} = 3.744$ ,  $p < 0.05$ ; ipsilateral:  $F_{3,31} = 2.825$ ,  $p = 0.0548$ ). In nerve-injured wt rats, the glucose metabolism was significantly elevated in ipsilateral MC, SC and contralateral MC, SC, striatum as well as in nerve-injured  $\Delta$ ETorA rats, contralateral MC and SC compared to wt ctrl animals. A non-significant elevation of glucose uptake was observed in the ipsilateral and contralateral MC, SC and striatum of  $\Delta$ ETorA ctrl rats and additionally in the ipsilateral MC, SC, striatum and the contralateral striatum of nerve-injured  $\Delta$ ETorA rats compared to wt ctrl rats. There were no differences in the glucose metabolism in the thalamus, SN and cerebellar lobule (data not shown).

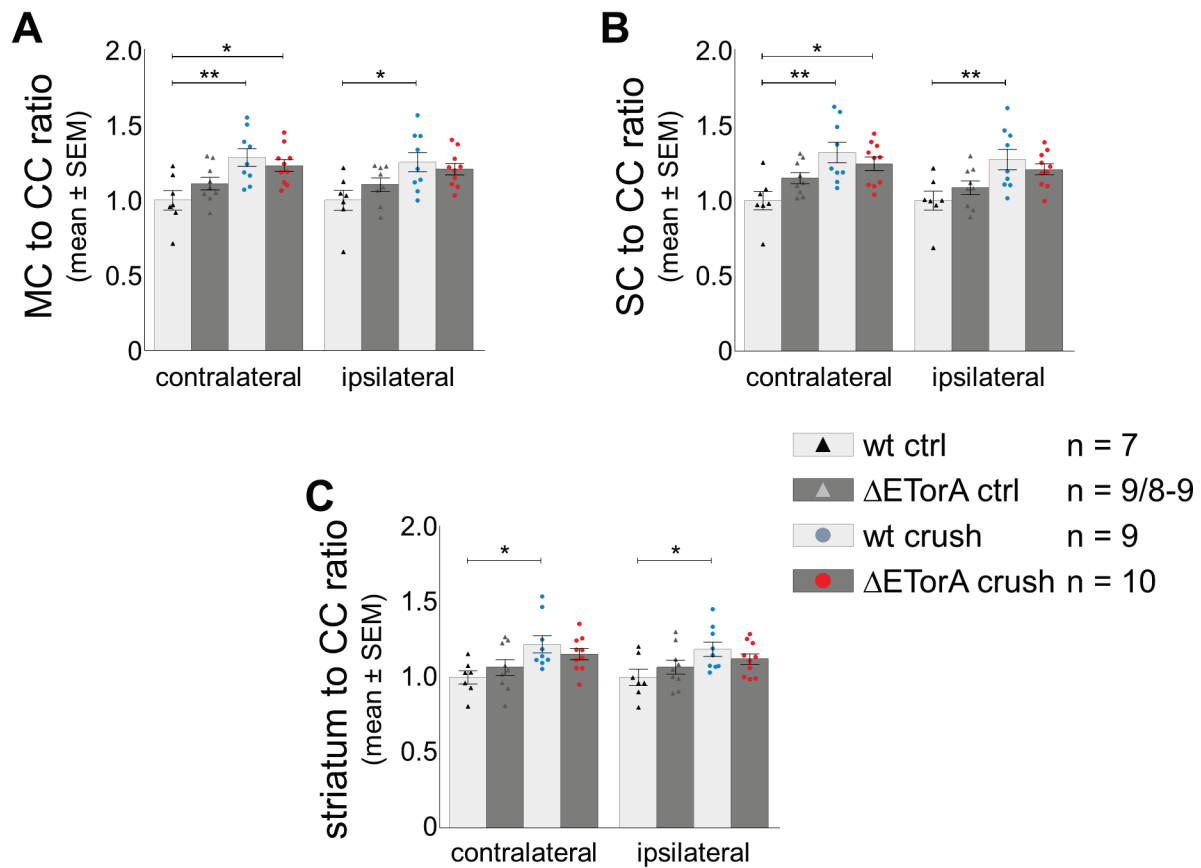


**Figure 16: Genetic and environmental factors have an impact on glucose metabolism**

*In vivo* FDG autoradiography reveals an increased glucose uptake twelve weeks after nerve crush injury in MC (A), SC (B), striatum (C). A significantly higher level of glucose uptake was detected in wt crush rats compared to wt ctrl rats in the contralateral MC ( $p < 0.01$ ), SC ( $p < 0.01$ ), striatum ( $p < 0.05$ ) and ipsilateral MC ( $p < 0.05$ ), SC ( $p < 0.01$ ), striatum ( $p < 0.05$ ). Glucose uptake is significantly increased in  $\Delta$ ETorA crush rats compared to wt ctrl rats in the contralateral MC ( $p < 0.05$ ) and SC ( $p < 0.05$ ). Data were normalized to CC and wt ctrl rats. One-way ANOVA with Tukey's multiple comparisons test; \*  $p < 0.05$ , \*\*  $p < 0.01$ .

### 3.5 Striatal neurons are unaltered in cell number and in gene expression levels of neuronal markers

Analysis of the cellular level of the basal ganglia was focused on the striatum. The striatum is the main input structure of the basal ganglia by glutamatergic input from the cortex and thalamus. Within the striatum, GABAergic MSNs are the main cell population that are modulated by different interneuron populations.<sup>73</sup> Stainings against the striatal interneuron markers PV<sup>+</sup> (Figure 17 A<sup>I</sup>-A<sup>IV</sup>), nNOS<sup>+</sup> (Figure 17 B<sup>I</sup>-B<sup>IV</sup>), CR<sup>+</sup> (Figure 17 C<sup>I</sup>-C<sup>IV</sup>), ChAT<sup>+</sup> (Figure 17 D<sup>I</sup>-D<sup>IV</sup>) and total striatal neurons, stained by Nissl<sup>+</sup> (Figure 17 E<sup>I</sup>-E<sup>IV</sup>) did not show any significant differences in the cell number, analyzed by a stereology approach comparing wt and  $\Delta$ ETorA rats twelve weeks after sciatic nerve crush injury and under control conditions in the striatum contralateral to the nerve crush (Figure 17 A<sup>V</sup>-E<sup>V</sup>). In addition, the mRNA gene expression levels of the interneuron markers PV, nNOS, CR, ChAT and the MSN marker DARPP32 did not demonstrate any differences in qPCR measurements (Figure 17 A<sup>VI</sup>-E<sup>VI</sup>).

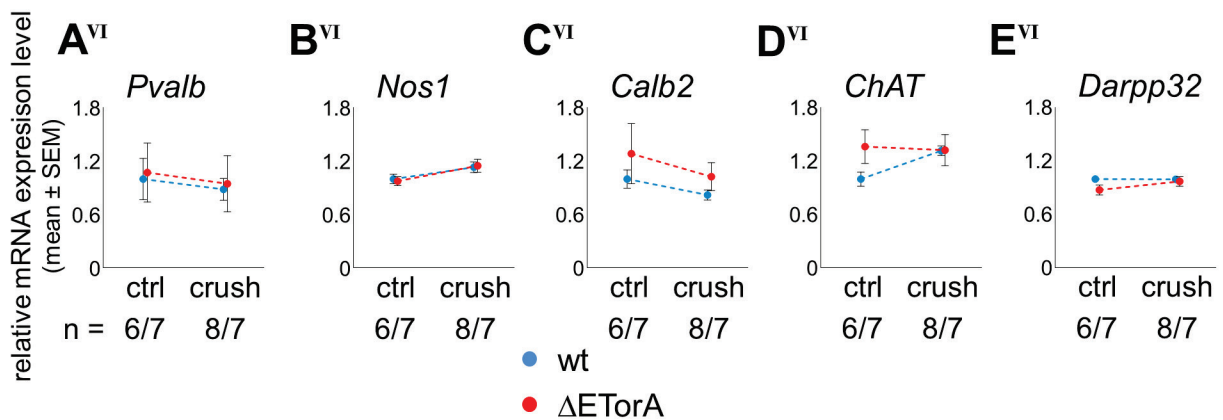
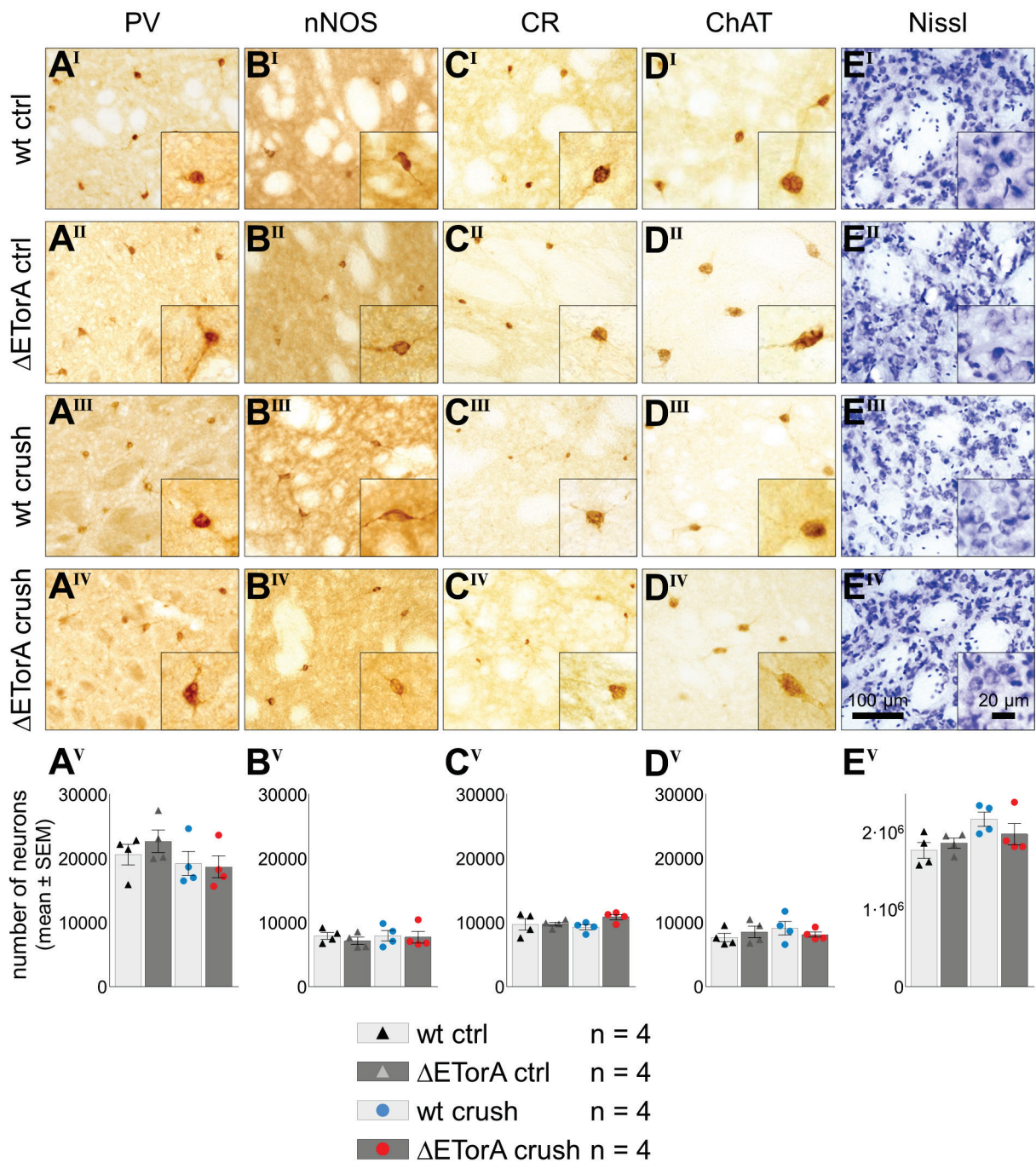


### Figure 17: Neuronal cell numbers and gene expression of neuronal marker in the striatum

Representative images of 40  $\mu\text{m}$  coronal sections of the striatum labeled by immunohistochemistry for the interneuronal makers PV (A<sup>I-IV</sup>), nNOS (B<sup>I-IV</sup>), CR (C<sup>I-IV</sup>), ChAT (D<sup>I-IV</sup>) and Nissl (E<sup>I-IV</sup>) in wt and  $\Delta\text{ETorA}$  rats with and without nerve crush. No differences are detected in the total striatal cell number of PV<sup>+</sup> (A<sup>V</sup>), nNOS<sup>+</sup> (B<sup>V</sup>), CR<sup>+</sup> (C<sup>V</sup>), ChAT<sup>+</sup> (D<sup>V</sup>) interneurons and Nissl<sup>+</sup> (E<sup>V</sup>) neurons investigated by stereology comparing wt and  $\Delta\text{ETorA}$  under ctrl and crush conditions twelve weeks after nerve crush injury. Relative mRNA gene expression levels of *Pvalb* (A<sup>VI</sup>), *Nos1* (B<sup>VI</sup>), *Calb2* (D<sup>VI</sup>), *ChAT* (E<sup>VI</sup>), *Darpp32* (F<sup>VI</sup>) are not differentially regulated in the contralateral striatum 12 weeks after sciatic nerve crush of wt and  $\Delta\text{ETorA}$  rats in ctrl and crush state. Data are normalized to *Gapdh* and wt ctrl rats.

Analysis of cholinergic markers on the transcript level did not show significant differences for the mAChR M1 (*Chrm1*), M2 (*Chrm2*) and M4 (*Chrm4*), the nicotinic acetylcholine receptor beta 2 subunit (*Chrn2*), acetylcholinesterase (*Ache*) and the vesicular acetylcholine transporter (*VACht*) comparing wt and  $\Delta\text{ETorA}$  rats twelve weeks after sciatic nerve crush injury and under control conditions in the striatum contralateral to the nerve crush (Figure 18).

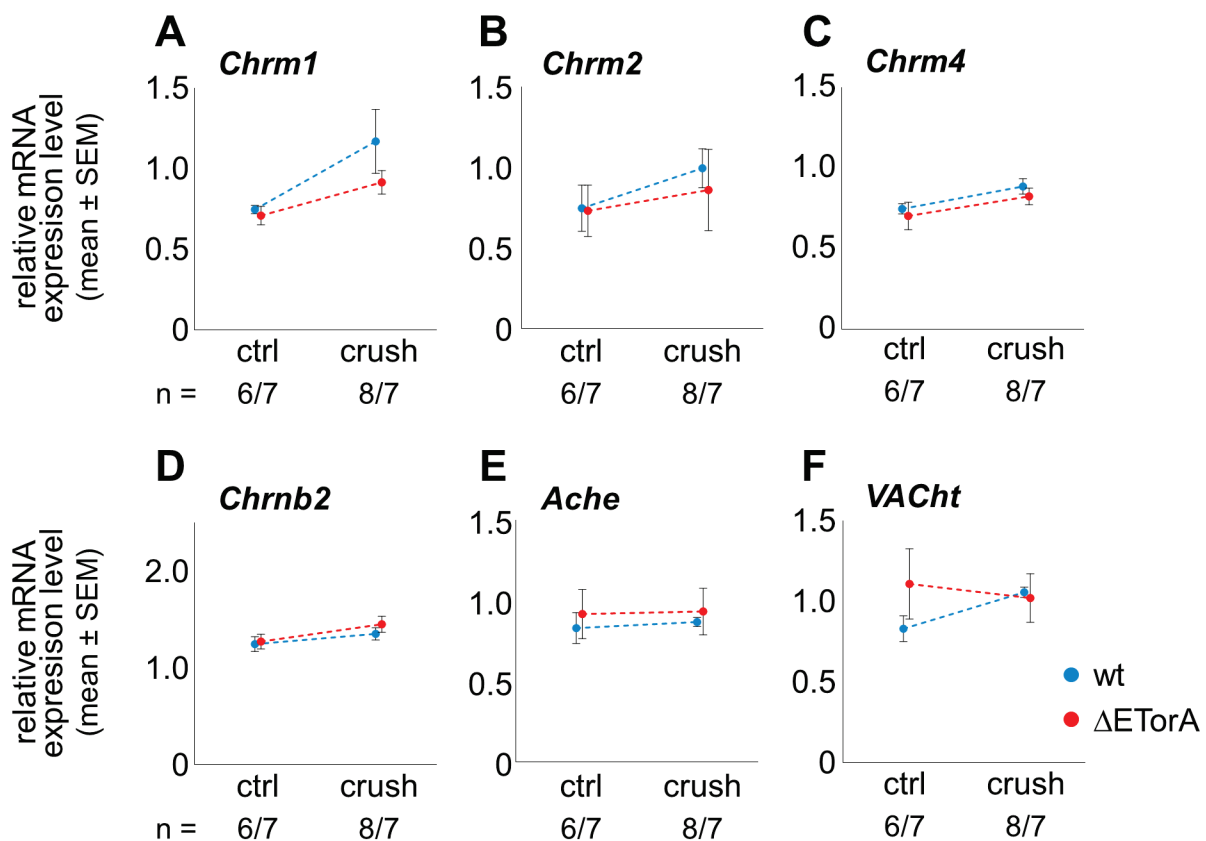


### Figure 18: Gene expression levels of cholinergic targets are unaffected

Relative mRNA gene expression levels of mAChRs (A-C), nicotinic acetylcholine receptor (D), acetylcholinesterase (E), vesicular acetylcholine transporter (F) in the contralateral striatum twelve weeks after sciatic nerve crush is determined by qPCR comparing wt and  $\Delta\text{ETorA}$  rats in ctrl and crush state. No differences are detected in all analyzed targets. Data are normalized to *Gapdh* and wt ctrl rats.

Due to the strong cortical glutamatergic transmission to striatal neurons of the cortico-basal ganglia-thalamo-cortical loop, striatal glutamate receptors were assessed by qPCR. mRNA expression levels of the striatal glutamate ionotropic receptor NMDA subunit 2B (*Grin2b*) and the glutamate ionotropic receptor AMPA subunit 4 (*Gria4*) did not show any differences when comparing ctrl and nerve-injured  $\Delta$ ETorA rats twelve weeks after sciatic nerve crush injury of both genotypes in the striatum contralateral to the nerve crush (Figure 19).

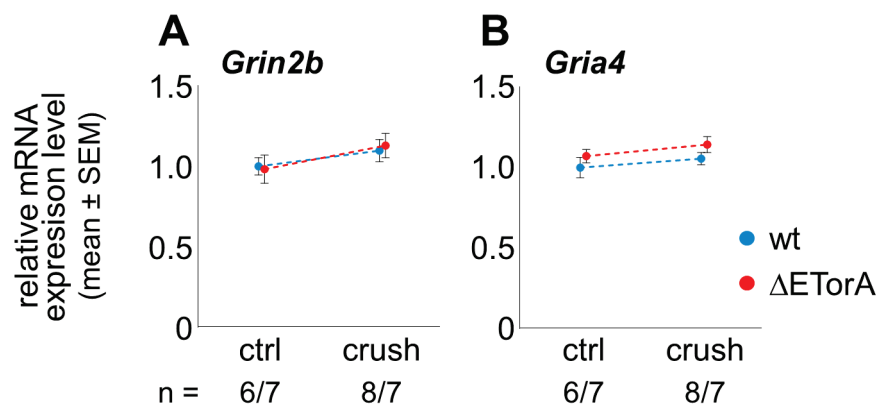


**Figure 19: Glutamate receptors are not differently expressed on mRNA levels**

(A-B) Differences in the relative mRNA gene expression levels of ionotropic glutamate receptors are not observed in the contralateral striatum twelve weeks after sciatic nerve crush when comparing wt and  $\Delta$ ETorA rats in ctrl and crush state. Data are generated by qPCR and normalized to *Gapdh* and wt ctrl rats.

### 3.6 Striatal monoamine metabolism is altered in sciatic nerve-injured $\Delta$ ETorA rats

DA is an essential neurotransmitter of the basal ganglia and has a strong influence on the direct and indirect pathway according to the interaction of the different types of DA receptors. DA neurons of the SN project to the main target structure of the midbrain, the striatum.<sup>103,104</sup> DA and DA metabolites were assessed on protein level by HPLC and DA receptors on mRNA expression level by qPCR in striatal tissue in naive state and twelve weeks after sciatic nerve crush injury in wt and  $\Delta$ ETorA rats.

The protein levels of DA and DA metabolites DOPAC and HVA of striatal tissue were analyzed by HPLC. The analysis showed a significant difference in the striatum contralateral to the nerve crush by an increase of DOPAC in nerve-injured  $\Delta$ ETorA rats compared to  $\Delta$ ETorA ctrl rats ( $H$ : 9.562,  $p < 0.05$ ; Figure 20 B). No additional significant dysregulations were found in DA or DA metabolites or the turnover ratio of DA and its metabolites in striatum contralateral (Figure 20 A, C-E) and ipsilateral (Figure 20 F-J) to the nerve crush.

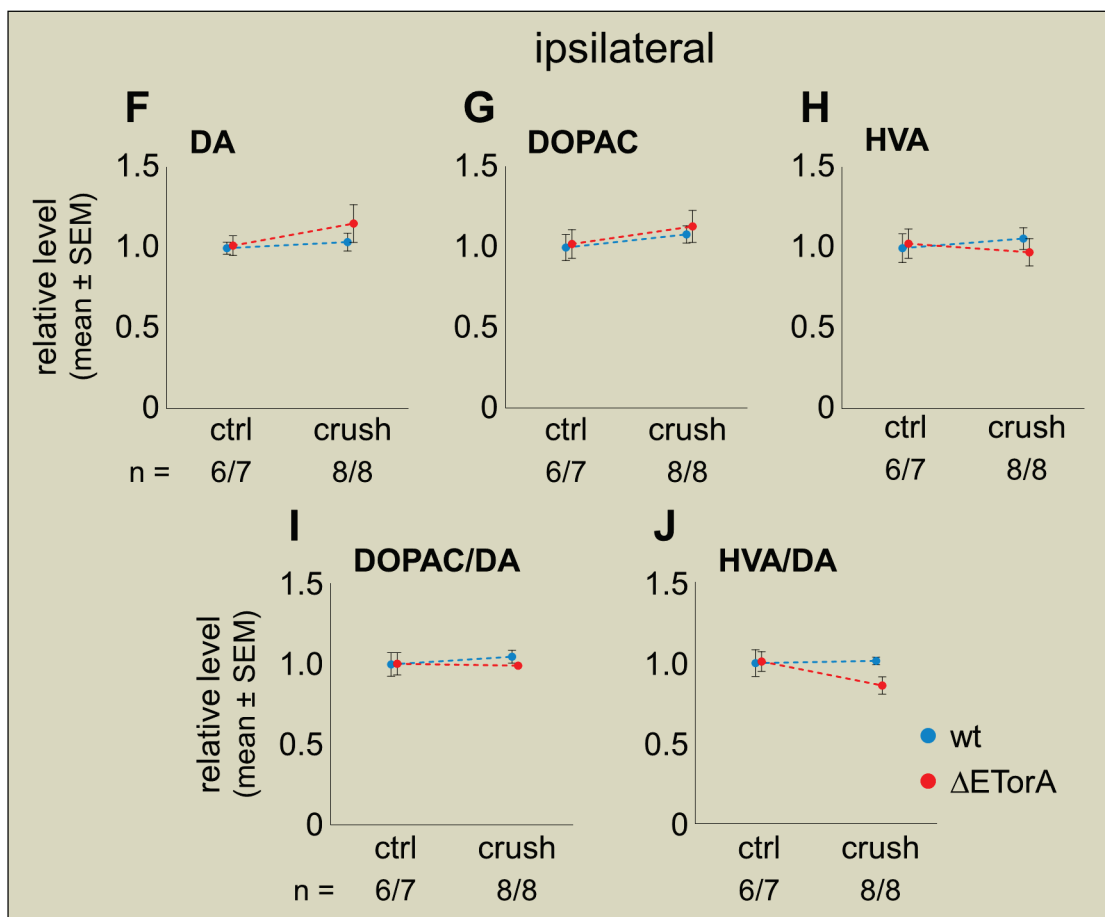
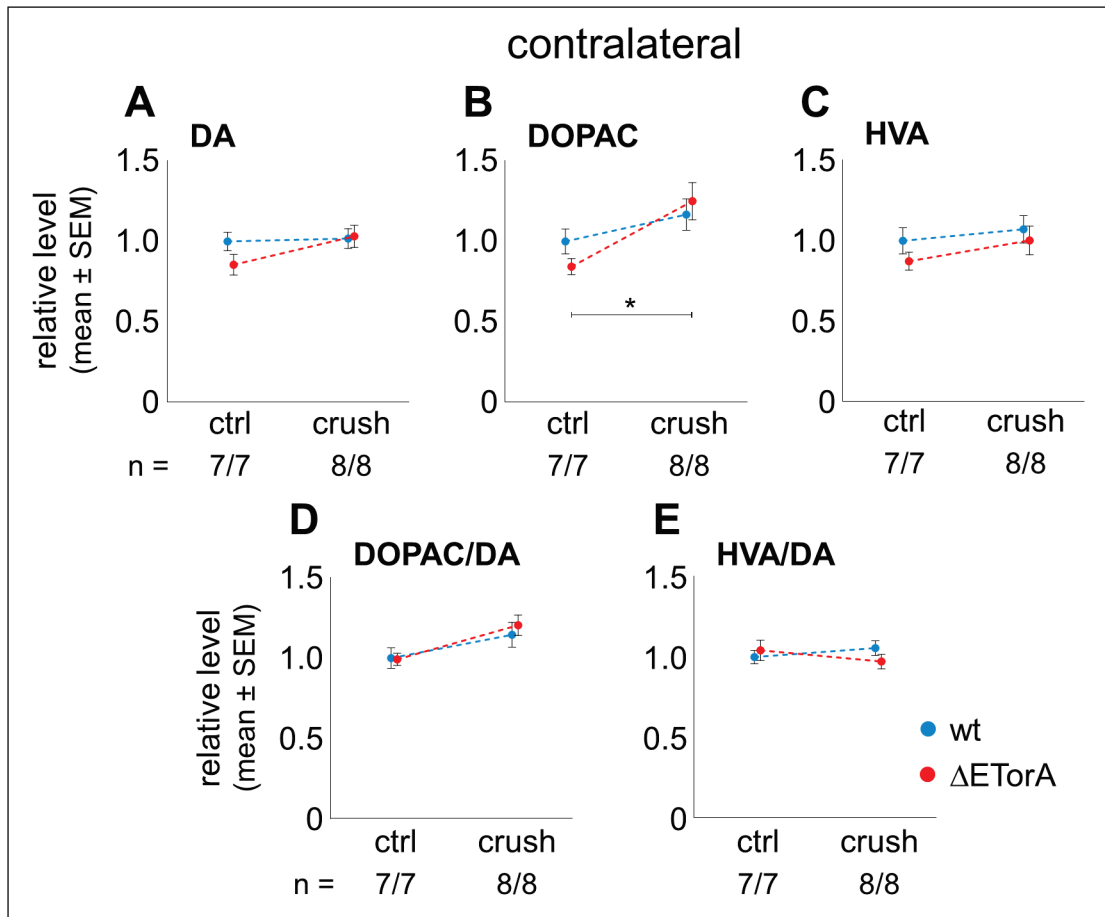


**Figure 20: Alterations in the striatal dopaminergic metabolism in  $\Delta$ ETorA rats**

HPLC analysis of DA and DA metabolites from striatal tissue twelve weeks after nerve crush injury contralateral (A-E) and ipsilateral to nerve crush (F-J). DOPAC is significantly increased in  $\Delta$ ETorA crush rats compared to  $\Delta$ ETorA ctrl rats ( $p < 0.05$ ) in the contralateral striatum. Normalized to wt ctrl rats. Kruskal-Wallis test with Dunn's multiple comparisons test; \*  $p < 0.05$ .

To analyze extracellular DA and DA metabolites specifically, microdialysis was performed on the contralateral striatum (Figure 21 A, Figure 22 A-B, Figure 23 A-B) and ipsilateral striatum (Figure 21 B, Figure 22 C-D, Figure 23 C-D) to the nerve crush twelve weeks after sciatic nerve crush injury. Baseline levels of vesicular DA release were assessed by perfusion of the microdialysis probe with aCSF. Additionally, the neuronal terminals of the striatum were stimulated by the perfusion of the microdialysis probes with aCSF<sup>K+</sup>, which contains a high concentration of potassium ( $K^+$  50 mM), and the vesicular DA release was investigated.

Baseline DA levels did not differ between ctrl and crush, wt and  $\Delta$ ETorA rats in the striatum of both hemispheres (Figure 21). However, alterations in potassium-triggered stimulated DA release were detected in nerve-injured  $\Delta$ ETorA rats within the contralateral striatum (time main effect:  $F_{21,373} = 113.4$ ,  $p < 0.0001$ ; time x groups interaction:  $F_{63,373} = 3.270$ ,  $p < 0.0001$ ; Figure 21 A) and the ipsilateral striatum (time main effect:  $F_{21,349} = 99.69$ ,  $p < 0.0001$ ; Figure 21 B). Striatal DA levels were significantly higher in  $\Delta$ ETorA crush rats compared to wt ctrl,  $\Delta$ ETorA ctrl and wt crush animals in the contralateral (Figure 21 A) as well as in the ipsilateral (Figure 21 B) brain hemisphere. A maximum DA level was observed in the samples collected 45 min after high potassium stimulation without showing a significant difference when comparing the contralateral striatum ( $16.23 \pm 2.25$  nM) to the ipsilateral striatum ( $14.27 \pm 2.02$  nM).

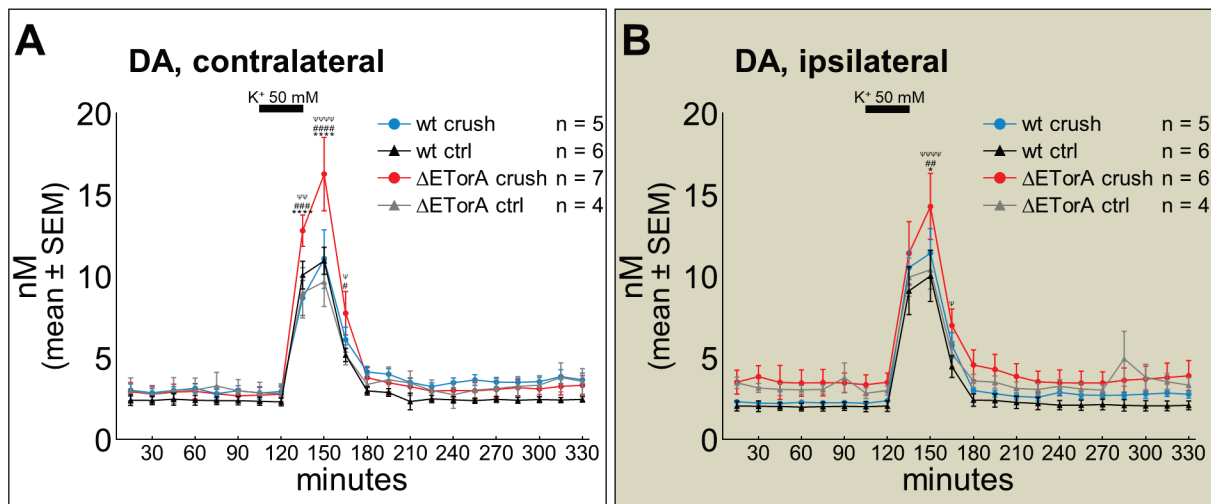


**Figure 21: High potassium is stimulating the striatal DA release**

Striatal DA levels of microdialysis samples of the contralateral side (A) and ipsilateral side (B) to nerve crush are analyzed from microdialysis samples twelve weeks after nerve crush injury by HPLC. Six baseline samples were collected before a high concentration of KCl (50 mM) was administered directly in the striatum through perfusion of the microdialysis probe for 30 min, starting 90 min (beginning of sample 7) after the stabilization period, after which further 14 samples were collected. Mixed-effects model with Dunn's multiple comparisons test;  $\Psi$   $p < 0.05$ ,  $\Psi\Psi$   $p < 0.01$ ,  $\Psi\Psi\Psi$   $p < 0.0001$  wt ctrl vs  $\Delta$ ETorA crush; #  $p < 0.05$ , ##  $p < 0.01$ , ###  $p < 0.001$ , ####  $p < 0.0001$   $\Delta$ ETorA ctrl vs  $\Delta$ ETorA crush; \*  $p < 0.05$ , \*\*\*\*  $p < 0.0001$  wt crush vs  $\Delta$ ETorA crush.

To investigate the DA metabolism, the DA metabolites DOPAC (Figure 22) and HVA (Figure 23) were analyzed. DOPAC from the striatum contralateral to the nerve crush showed the highest level in nerve-injured  $\Delta$ ETorA rats and an elevated level in wt crush rats (time main effect:  $F_{21,374} = 24.21$ ,  $p < 0.0001$ ; groups main effect:  $F_{3,18} = 9.749$ ,  $p < 0.0005$ ; time x groups interaction:  $F_{63,374} = 2.076$ ,  $p < 0.0001$ ; Figure 22 A). A comparably increased DOPAC level was observed in  $\Delta$ ETorA crush rats compared to wt crush rats of the striatum ipsilateral to the nerve crush during the whole microdialysis experiment (time main effect:  $F_{21,346} = 10.06$ ,  $p < 0.0001$ ; groups main effect:  $F_{3,17} = 3.785$ ,  $p < 0.05$ ; Figure 22 C). Striatal DOPAC concentrations of the contralateral side to nerve crush were significantly increased in  $\Delta$ ETorA crush rats compared to wt ctrl and  $\Delta$ ETorA ctrl rats as well as in samples perfused with aCSF when comparing wt ctrl and wt crush rats. There was also a tendency for higher baseline DOPAC levels in  $\Delta$ ETorA crush compared to wt crush animals in the striatum contralateral to nerve crush. In the striatum ipsilateral to nerve crush, DOPAC levels were significantly increased in baseline samples of  $\Delta$ ETorA crush rats compared to wt ctrl rats.

DOPAC/DA ratio is a metabolic index reflecting the DA turnover to the metabolite DOPAC. The striatal DOPAC/DA turnover of both hemispheres was increased in wt crush rats and slightly decreased in  $\Delta$ ETorA ctrl rats compared to wt ctrl rats (Figure 22 B, D). The highest level of DOPAC/DA ratio was observed in the contralateral striatum of  $\Delta$ ETorA crush rats, whereas the DOPAC/DA ratio in the ipsilateral striatum of  $\Delta$ ETorA crush rats was comparable to the level of wt ctrl rats. In the striatum contralateral to the nerve crush, a significant time main effect ( $F_{21,370} = 48.55$ ,  $p < 0.0001$ ) and significant time x groups interaction ( $F_{63,370} = 2.058$ ,  $p < 0.0001$ ) of the DOPAC/DA ratio was detected with a significant increase in baseline samples of  $\Delta$ ETorA crush rats compared to wt ctrl and  $\Delta$ ETorA ctrl rats. A significant time main effect ( $F_{21,344} = 54.11$ ,  $p < 0.0001$ ) and significant time x groups interaction ( $F_{63,344} = 1.675$ ,  $p < 0.01$ ) of the DOPAC/DA ratio was found in the striatum ipsilateral to nerve crush.

There was a tendency towards higher DOPAC levels and DOPAC/DA ratios in the contralateral striatum compared to the ipsilateral striatum to nerve crush in  $\Delta$ ETorA crush rats without statistical significance at any time point. Even if the high potassium stimulation led to increased DOPAC levels in all conditions, DOPAC showed higher levels in  $\Delta$ ETorA crush rats compared to control groups in the contralateral striatum to the nerve crush.

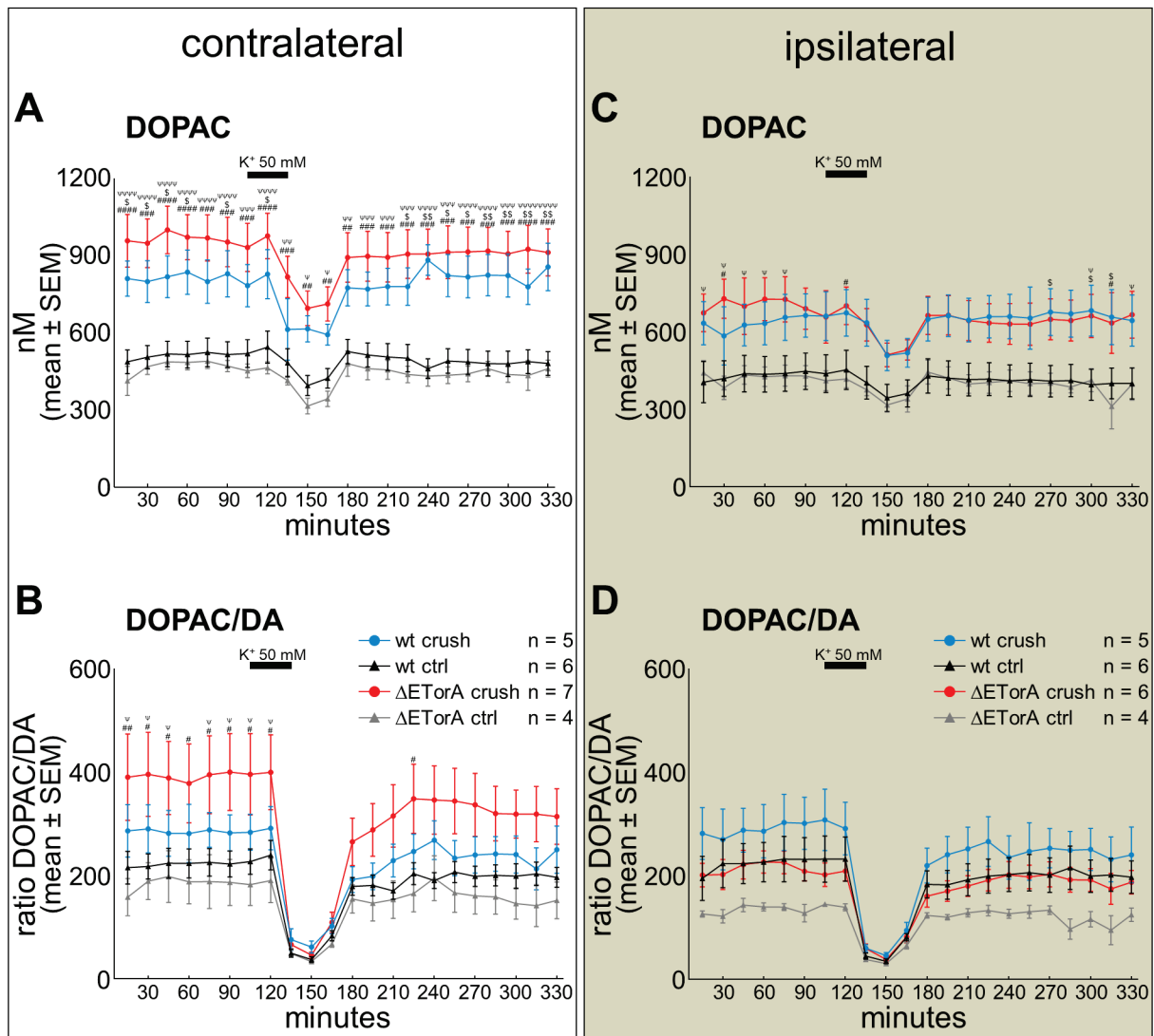


**Figure 22: Increased striatal DOPAC levels and striatal DOPAC/DA ratio in nerve-injured  $\Delta$ ETorA rats**

Striatal DOPAC levels of the contralateral side (A) and ipsilateral side (C) to nerve crush are analyzed from microdialysis samples twelve weeks after nerve crush injury by HPLC. The DOPAC/DA turnover rate was computed for the contralateral striatum (B) and ipsilateral striatum (D). Six baseline samples were collected before a high concentration of KCl (50 mM) was administered directly in the striatum through perfusion of the microdialysis probe for 30 min, starting 90 min (beginning of sample 7) after the stabilization period, after which further 14 samples were collected. Mixed-effects model with Dunn's multiple comparisons test;  $\Psi$   $p < 0.05$ ,  $\Psi\Psi$   $p < 0.01$ ,  $\Psi\Psi\Psi$   $p < 0.001$ ,  $\Psi\Psi\Psi\Psi$   $p < 0.0001$  wt ctrl vs  $\Delta$ ETorA crush; #  $p < 0.05$ , ##  $p < 0.01$ , ###  $p < 0.001$ , ####  $p < 0.0001$   $\Delta$ ETorA ctrl vs  $\Delta$ ETorA crush; \$  $p < 0.05$ , \$\$  $p < 0.01$  wt ctrl vs wt crush.

Elevated striatal HVA levels were found in nerve-injured wt rats and  $\Delta$ ETorA rats contralateral to the nerve crush with a time main effect ( $F_{21,374} = 61.89$ ,  $p < 0.0001$ ), a groups main effect ( $F_{3,18} = 7.849$ ,  $p < 0.01$ ), and a time x groups interaction ( $F_{63,374} = 2.629$ ,  $p < 0.0001$ ). HVA was significantly increased in  $\Delta$ ETorA crush rats compared to

wt ctrl and  $\Delta$ ETorA ctrl rats as well as in wt crush rats compared to wt ctrl rats, except in the perfusates in response to the high potassium concentration, where the HVA levels were decreasing (Figure 23 A). In the ipsilateral striatum, a time main effect ( $F_{21,347} = 19.37$ ,  $p < 0.0001$ ) could be observed. A tendency towards higher extracellular HVA concentrations was observed in the ipsilateral striatum in  $\Delta$ ETorA crush rats compared to wt crush, wt ctrl, and  $\Delta$ ETorA ctrl animals (Figure 23 C).

DA turnover to HVA in the contralateral striatum showed a time main effect ( $F_{21,370} = 55.54$ ,  $p < 0.0001$ ) and a time x groups interaction ( $F_{63,370} = 1.76$ ,  $p < 0.001$ ) as well as a time main effect in the ipsilateral striatum ( $F_{21,345} = 55.05$ ,  $p < 0.0001$ ) (Figure 23 B,D). HVA/DA ratios seem to be higher in nerve-injured rats compared to ctrl rats in the striatum contralateral to nerve crush.

$\Delta$ ETorA rats had similar striatal extracellular HVA levels in both hemispheres. However, a non-significant higher striatal HVA/DA ratio at the contralateral side compared to the ipsilateral side to the nerve crush was observed.

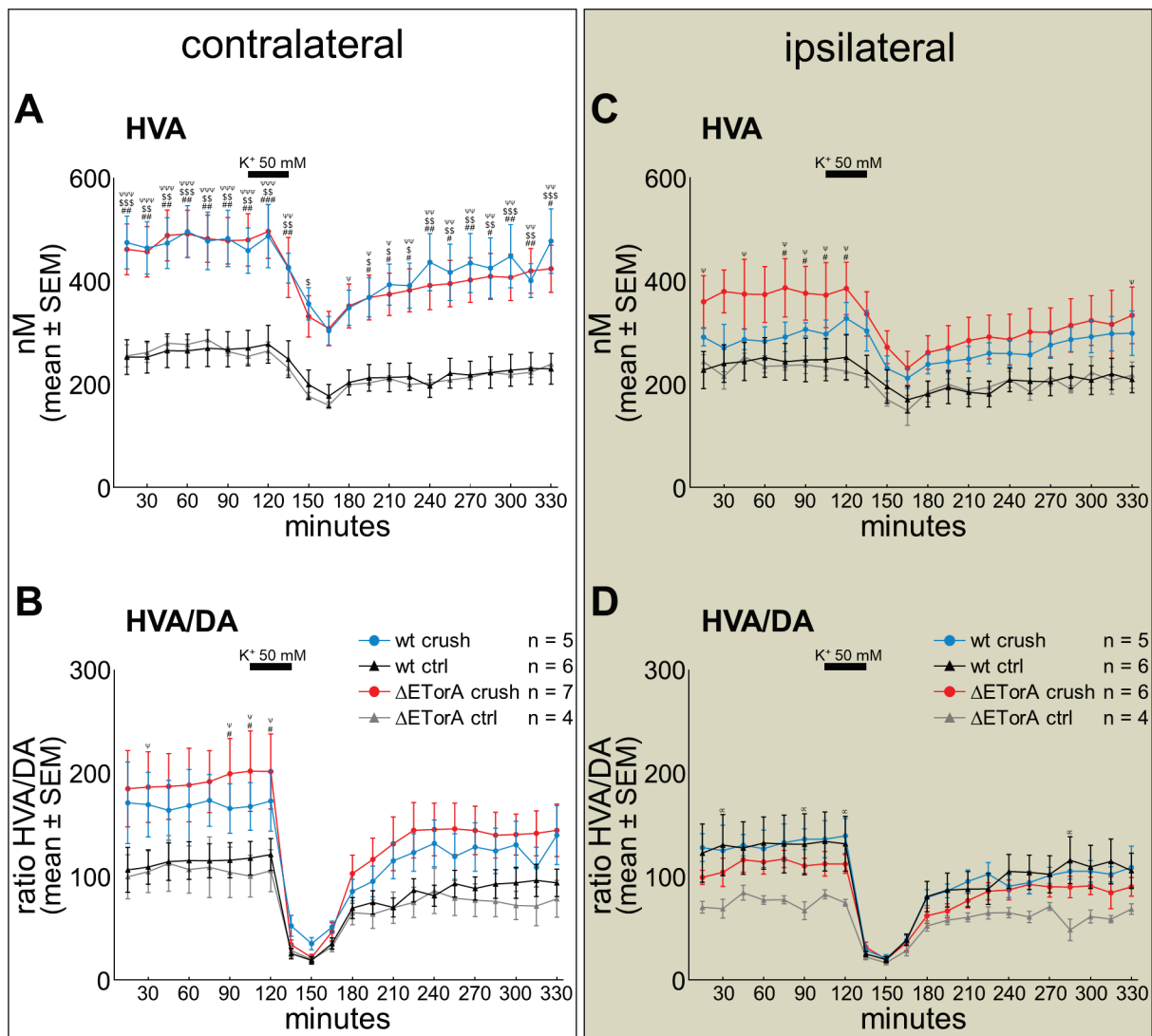


**Figure 23: Nerve crush injury affects the HVA levels in the striatum**

Striatal HVA levels of the contralateral side (A) and ipsilateral side (C) to nerve crush are analyzed from microdialysis samples twelve weeks after nerve crush injury by HPLC, and the turnover rate of HVA/DA was computed for the contralateral striatum (B) and ipsilateral striatum (D) to the nerve crush. Six baseline samples were collected before a high concentration of KCl (50 mM) was administered directly in the striatum through perfusion of the microdialysis probe for 30 min, starting 90 min (beginning of sample 7) after the stabilization period, after which further 14 samples were collected. Mixed-effects model with Dunn's multiple comparisons test;  $\Psi$   $p < 0.05$ ,  $\Psi\Psi$   $p < 0.01$ ,  $\Psi\Psi\Psi$   $p < 0.001$  wt ctrl vs  $\Delta$ ETorA crush; #  $p < 0.05$ , ##  $p < 0.01$ , ###  $p < 0.001$   $\Delta$ ETorA ctrl vs  $\Delta$ ETorA crush; \$  $p < 0.05$ , \$\$  $p < 0.01$ , \$\$\$  $p < 0.001$  wt ctrl vs wt crush;  $\infty$   $p < 0.05$  wt ctrl vs  $\Delta$ ETorA ctrl.

Overall, the baseline DA level did not differ between all groups. Only when the DA release was triggered by high potassium did DA levels increase significantly in nerve-injured  $\Delta$ ETorA rats. In nerve-injured  $\Delta$ ETorA rats, alterations in the DA metabolism were detected by showing significantly higher DOPAC levels in all conditions. The DOPAC/DA turnover was also significantly higher in baseline samples in the striatum

contralateral to the nerve crush. The DA metabolite HVA was significantly elevated to a comparable level of nerve-injured  $\Delta$ ETorA and wt rats in the striatum contralateral to the nerve crush. However, the high potassium stimulation did not significantly affect HVA levels in nerve-injured animals. Differences were detectable in levels for DA and DA metabolites when comparing the contralateral striatum to the ipsilateral striatum.

To explore the impact of DA targets in the DYT-TOR1A pathophysiology, DAT protein levels were examined by western blot (Figure 24 A) and mRNA expression levels of DA receptors ( $D_1$ R (*Drd1*) –  $D_5$ R (*Drd5*)) by qPCR in the striatum contralateral to the nerve crush. A reduction of DAT in  $\Delta$ ETorA after sciatic nerve crush injury was shown, yet without any statistical significance (Figure 24 B). In addition, the mRNA expression levels of striatal DA receptors were unaffected (Figure 24 C-G). Therefore, neither genetic background nor peripheral trauma influences the gene expression levels of striatal dopaminergic receptors.

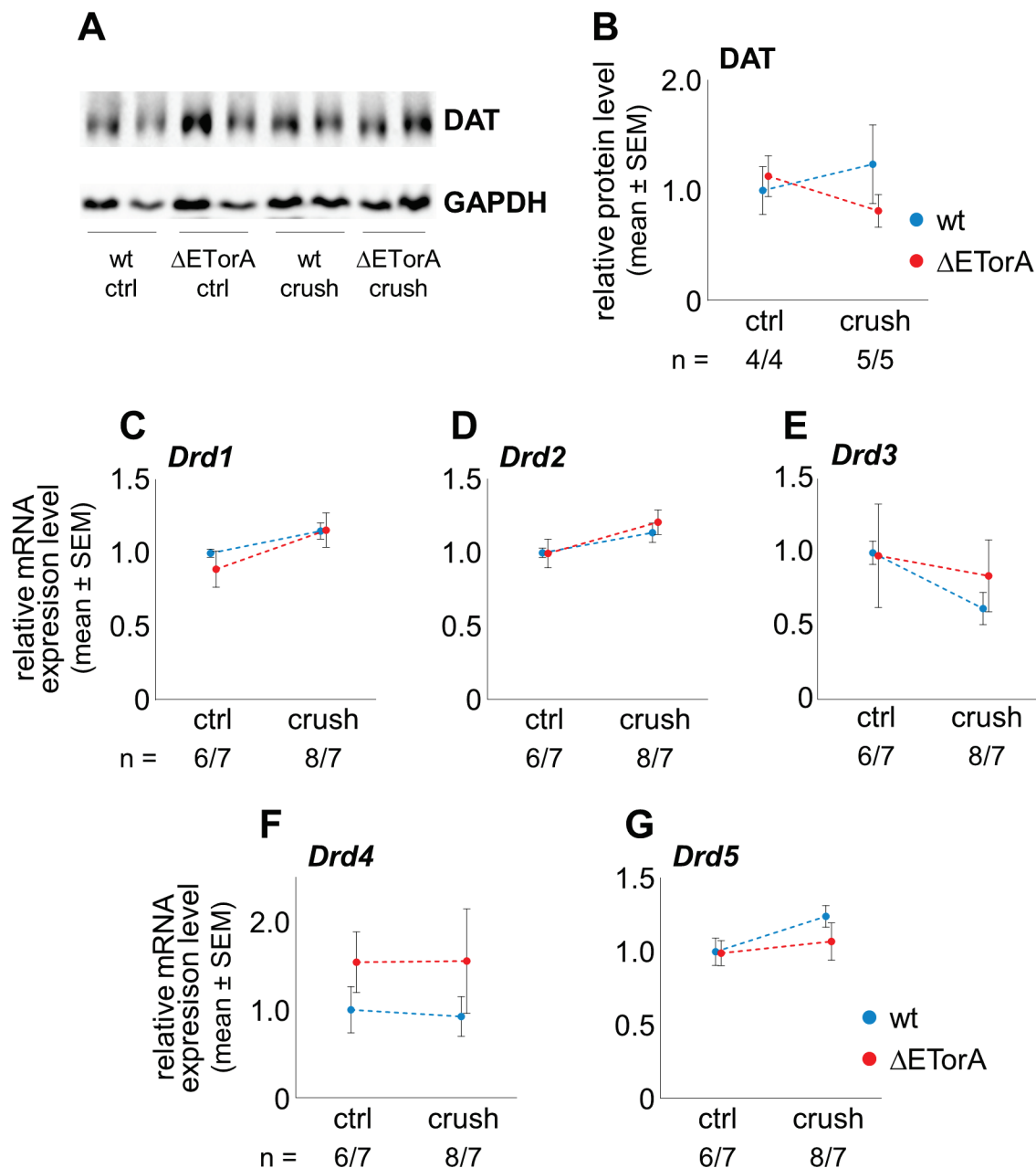


**Figure 24: Lack of evidence for dysregulation of DAT and dopaminergic receptors**

(A) Protein levels of DAT are detected at approximal 75 kDa and GAPDH at 36 kDa by western blot. (B) No significant dysregulation of striatal DAT was observed. DAT protein levels are normalized to GAPDH. Data are presented relative to wt ctrl rats. (C-G) DA receptors are not differently expressed on mRNA levels. qPCR data are normalized to *Gapdh* and to wt ctrl rats. Analysis of dopaminergic targets is performed from tissue of the contralateral striatum twelve weeks after sciatic nerve crush when comparing wt and  $\Delta$ ETorA rats in ctrl and crush state.

Alterations of 5-HT in dystonia has already been described.<sup>49,122,123</sup> Moreover, 5-HT can also influence the dopaminergic system.<sup>124</sup> Therefore, 5-HT and the metabolite 5-HIAA were analyzed on the protein level by HPLC and 5-HT receptors on mRNA

expression levels by qPCR in striatal tissue of wt and  $\Delta$ ETorA rats in control state and twelve weeks after sciatic nerve crush injury.

The analysis of 5-HT and the metabolite 5-HIAA in striatal tissue by HPLC showed increased 5-HT and 5-HIAA protein levels in nerve-injured  $\Delta$ ETorA rats compared to control  $\Delta$ ETorA rats in the striatum contralateral and ipsilateral to the nerve crush. Only 5-HIAA protein level was significantly higher in nerve-injured  $\Delta$ ETorA rats compared to  $\Delta$ ETorA rats in the striatum contralateral to the nerve crush ( $H$ : 8.370,  $p < 0.05$ ; Figure 25 B). The proteins level of 5-HT and 5-HIAA remained unchanged in wt rats after nerve crush injury compared to wt ctrl rats on both sides of the striatum. Moreover, the turnover of 5-HT and 5-HIAA was not altered after nerve crush injury in wt and  $\Delta$ ETorA rats compared to control animals in both sides of the striatum (Figure 25).

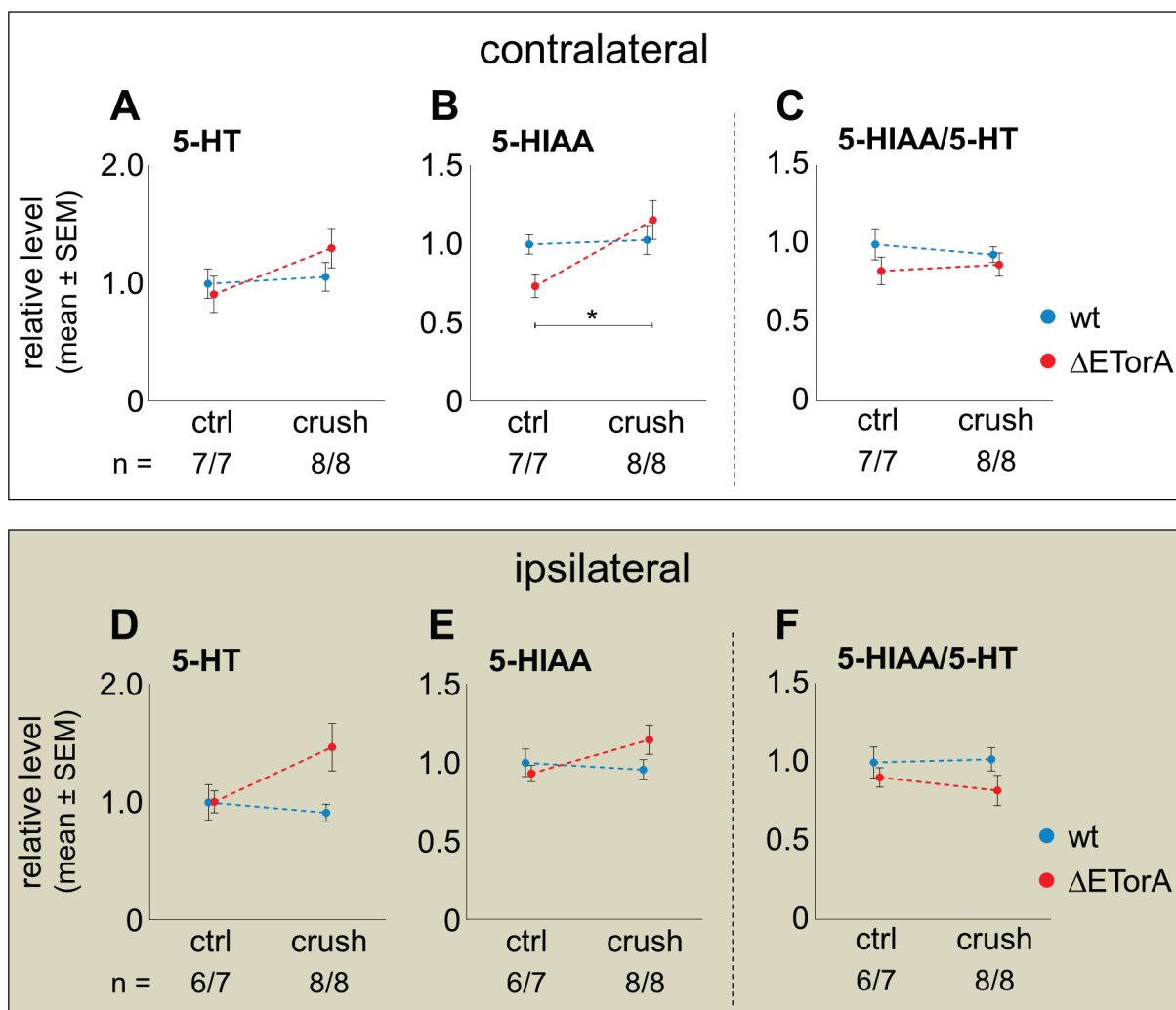


**Figure 25: Alterations in the striatal serotonergic metabolism in  $\Delta$ ETorA rats**

HPLC analysis of 5-HT and 5-HT metabolite from striatal tissue twelve weeks after nerve crush injury contralateral (A-C) and ipsilateral to the nerve crush (D-F). A significantly increased amount of 5-HIAA is detected in  $\Delta$ ETorA crush rats compared to  $\Delta$ ETorA ctrl rats ( $p < 0.05$ ). Data are normalized to wt ctrl rats. Kruskal-Wallis test with Dunn's multiple comparisons test; \*  $p < 0.05$ .

mRNA expression levels of 5-HT receptors were validated by qPCR. No differences could be detected in the expression levels of the transcripts for 5-HT receptor 1A (*Htr1a*) and 2A (*Htr2a*) in the striatum contralateral to the nerve crush when comparing wt and  $\Delta$ ETorA rats in control and nerve-injured state (Figure 26).

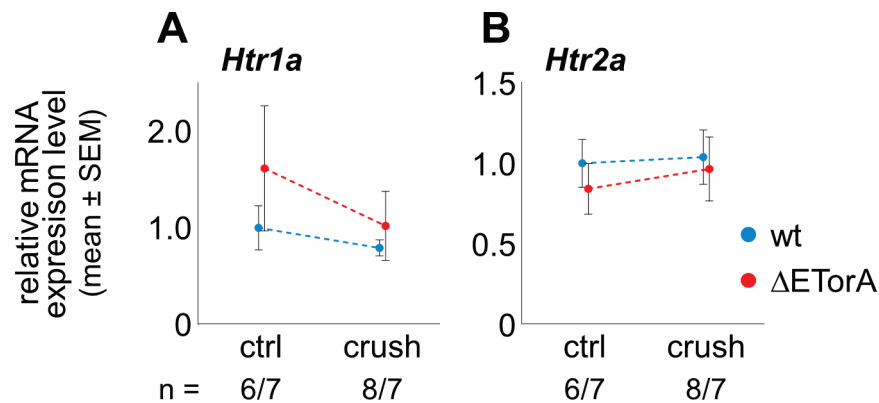


**Figure 26: Gene expression levels of 5-HT receptors remain unchanged**

(A-B) Relative mRNA gene expression levels of 5-HT receptors as revealed by qPCR do not show alterations in the contralateral striatum 12 weeks after sciatic nerve crush when comparing wt and  $\Delta$ ETorA rats in ctrl and crush state. Data are normalized to *Gapdh* and wt ctrl rats.

### 3.7 Transcriptome analysis by RNA-Seq of the striatum

The availability of an animal model with a dystonic phenotype on a DYT-TOR1A genetic background offers major experimental advantages, since a whole transcriptome analysis can be conducted, potentially generating new hypotheses in the pathophysiology of dystonia. RNA-Seq in striatal tissue of ctrl and nerve-injured wt and  $\Delta$ ETorA rats twelve weeks after nerve crush injury was performed. Only a small number of DEGs using the criteria of an adjusted p-value ( $p_{adj}$ ) of  $< 0.05$  and a  $\log_2$  fold change ( $\log_2FC$ ) of  $\geq 2$  were present in the analyzed samples; therefore, the cut-off criteria for calling the DEGs were set to  $p_{adj}$  of  $< 0.05$  without considering  $\log_2FC$  values.

The number of DEGs was determined by comparing all four analyzed groups in a pairwise manner, and the total up-regulated and down-regulated DEGs for each comparison are displayed in Figure 27. The highest number of DEGs could be detected when comparing wt crush with  $\Delta$ ETorA ctrl rats. The lowest number of DEGs was found when comparing wt ctrl with  $\Delta$ ETorA ctrl rats.

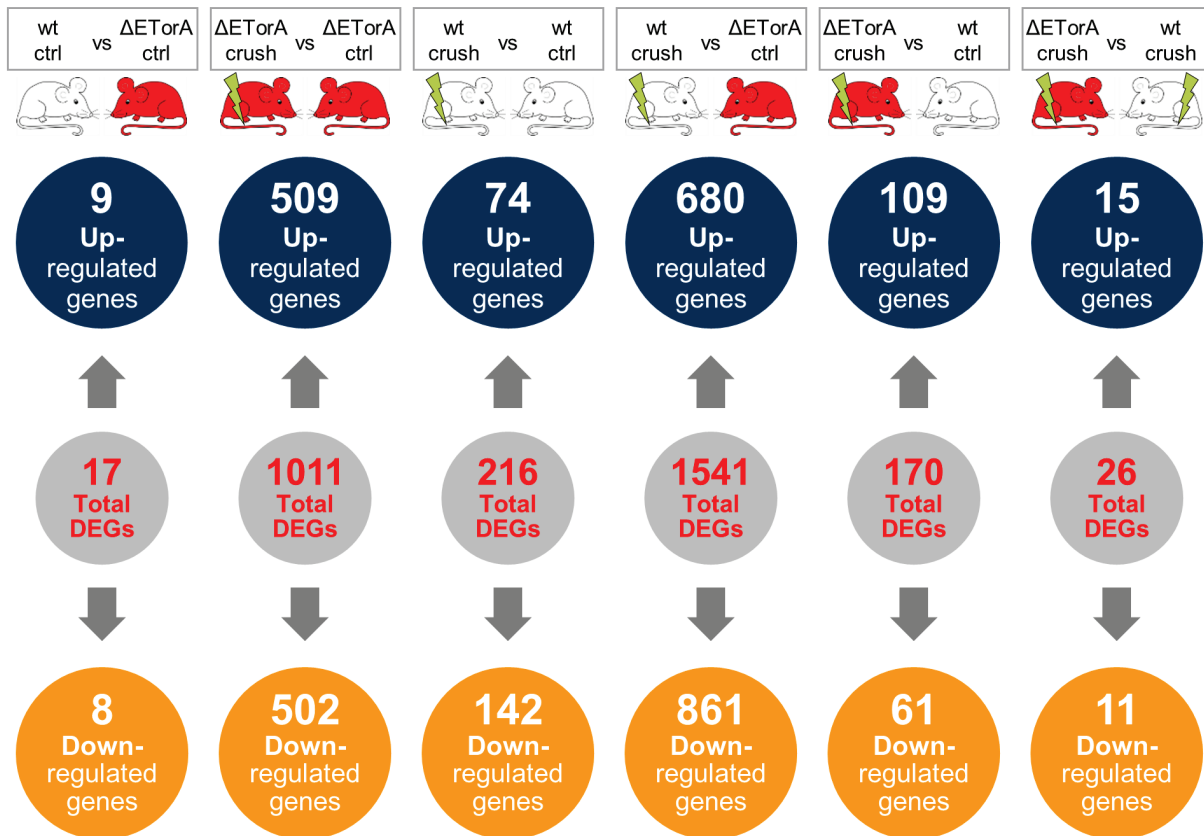


**Figure 27: Differentially expressed genes (DEGs) identified by RNA-Seq in the striatum**

RNA-Seq analysis of striatal tissue contralateral to the nerve crush twelve weeks after nerve crush injury and ctrl conditions in wt and  $\Delta$ ETorA rats. Diagram of DEGs showing the number of total, up-regulated or down-regulated genes by a two-group comparison between wt ctrl (n = 8), wt crush (n = 6),  $\Delta$ ETorA ctrl (n = 8),  $\Delta$ ETorA crush (n = 6). Used cutoff criteria: padj: 0.05; log<sub>2</sub>FC: 0.00.

For the investigation of regulated pathways, a gene set enrichment analysis of total DEGs was implemented by using the webserver Enrichr with the gene set library Wikipathways 2019 Human for each comparison group (Figure 28; Table S 1, Table S 2, Table S 3, Table S 4, Table S 5, Table S 6). The highest-ranked and most recurring pathways in almost all comparison groups were embedded globally in the pathway of the “circadian” rhythm and “energy metabolism”. Pathway terms included in circadian rhythm pathway were “Circadian rhythm related genes”, “Melatonin metabolism and effects”, “Exercise-induced Circadian Regulation”. “Fatty Acid Beta Oxidation”, “Synthesis and Degradation of Ketone Bodies”, “Metabolism of Sphingolipids in ER and Golgi apparatus”, “Sphingolipid pathway” and “Signal Transduction of S1P Receptor” pathway terms were combined into the energy metabolism pathway.

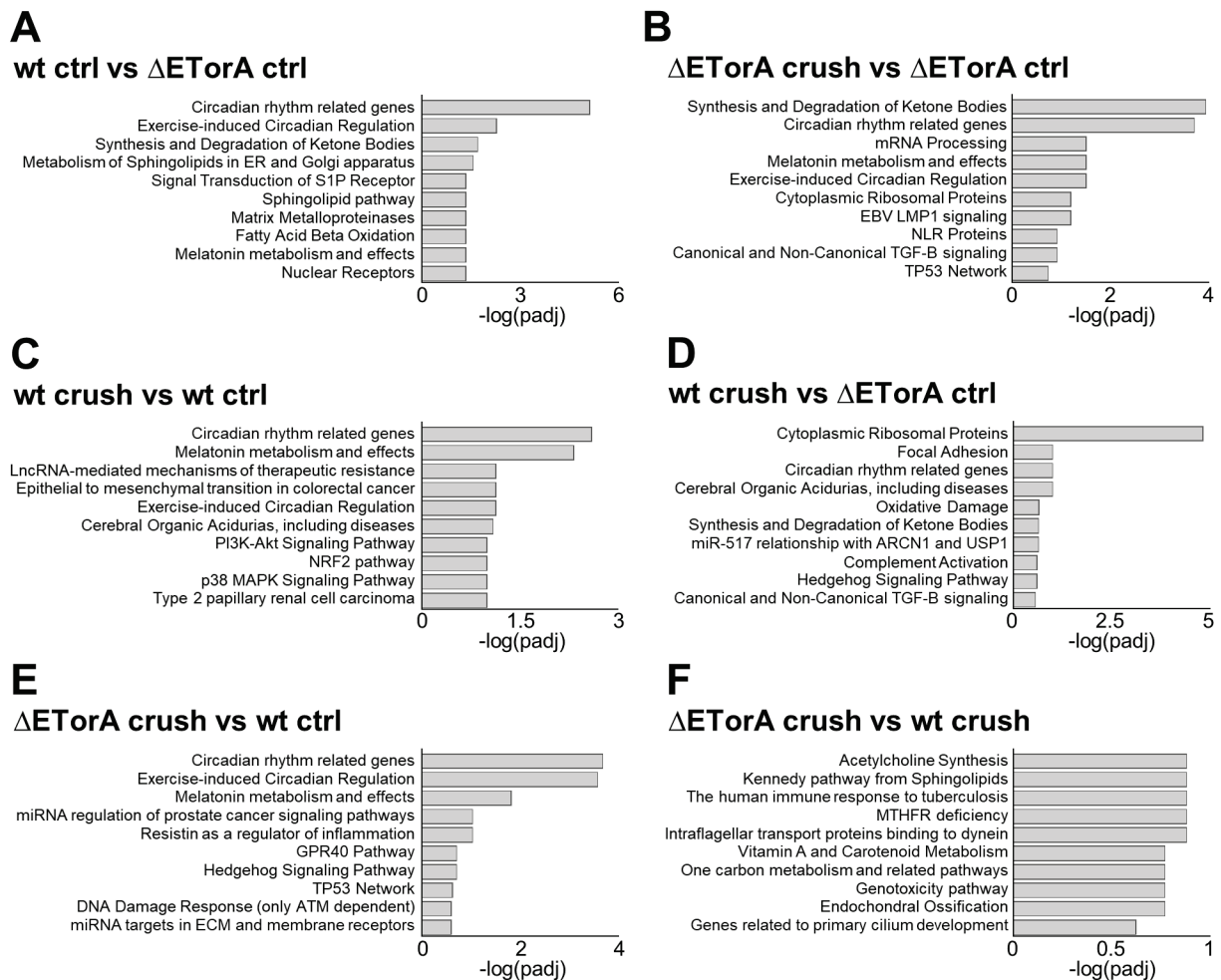


**Figure 28: Striatal top regulated pathways based on RNA-Seq data**

(A-F) Enrichment analysis of DEGs in the striatum reveals top regulated pathways by using the WikiPathways 2019 Human of the Enrichr database by a two-group comparison between wt ctrl (n = 8), wt crush (n = 6),  $\Delta$ ETorA ctrl (n = 8),  $\Delta$ ETorA crush (n = 6). Used cutoff criteria: padj: 0.05; log<sub>2</sub>FC: 0.00.

For the pathways of circadian rhythm (Figure 29 A) and the energy metabolism (Figure 29 B), heat maps were generated by using the log<sub>2</sub>FC values of DEGs which were included with the corresponding pathway terms.

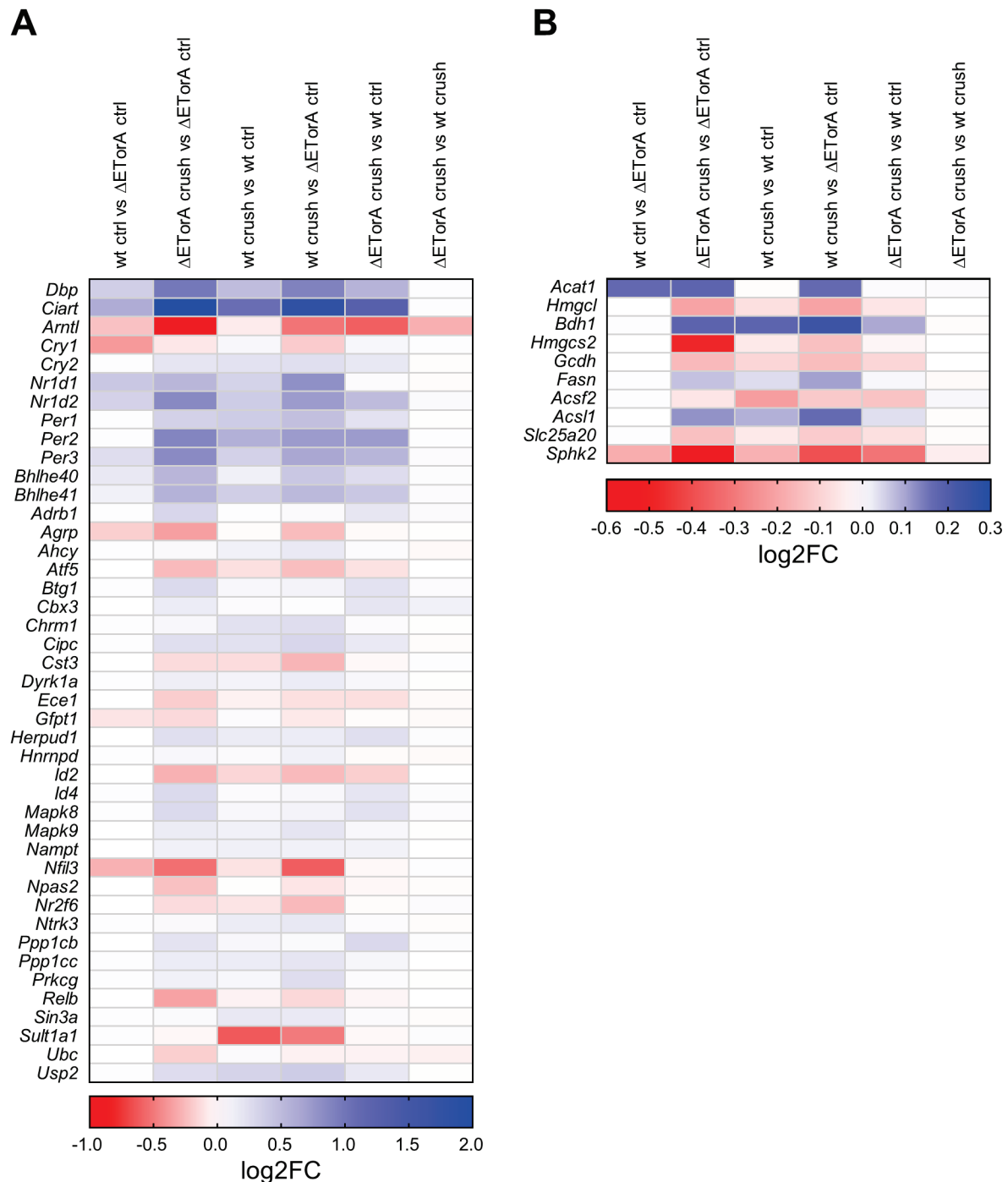


**Figure 29: Heat maps of two top regulated pathways representing color-coded expression levels of DEGs based on RNA-Seq data**

Heat maps of RNA-Seq expression data of the striatum using log<sub>2</sub>FC values. Two top regulated pathways circadian rhythm (A) and energy metabolism (B) are selected. Selected genes have to fulfill the cutoff criteria: padj: 0.05; log<sub>2</sub>FC: 0.00 in at least one comparison group between wt ctrl (n = 8), wt crush (n = 6),  $\Delta$ ETorA ctrl (n = 8),  $\Delta$ ETorA crush (n = 6). Negative values indicate a lower expression level of the comparison library (first listed group) compared to the reference library (second listed group). Positive values indicate a higher expression level of the comparison library (first listed group) compared to the reference library (second listed group).

RNA-Seq data were controlled by the reads of kilobase per million (RPKM) values (a normalized unit of transcript expression) of the human *TOR1A* and the rat *Tor1a* and *Tor1b*. Expression levels of human *TOR1A* were highly increased in all  $\Delta$ ETorA rats compared to wt rats (Figure 30 A). Comparable expression levels of rat *Tor1a* and *Tor1b* were detected in wt and  $\Delta$ ETorA naive rats in all conditions (Figure 30 B-C). As expected, rat *Tor1a* and *Tor1b* should not be differently expressed in  $\Delta$ ETorA rats, whereas the human *TOR1A* is overexpressed in  $\Delta$ ETorA rats compared to wt rats.

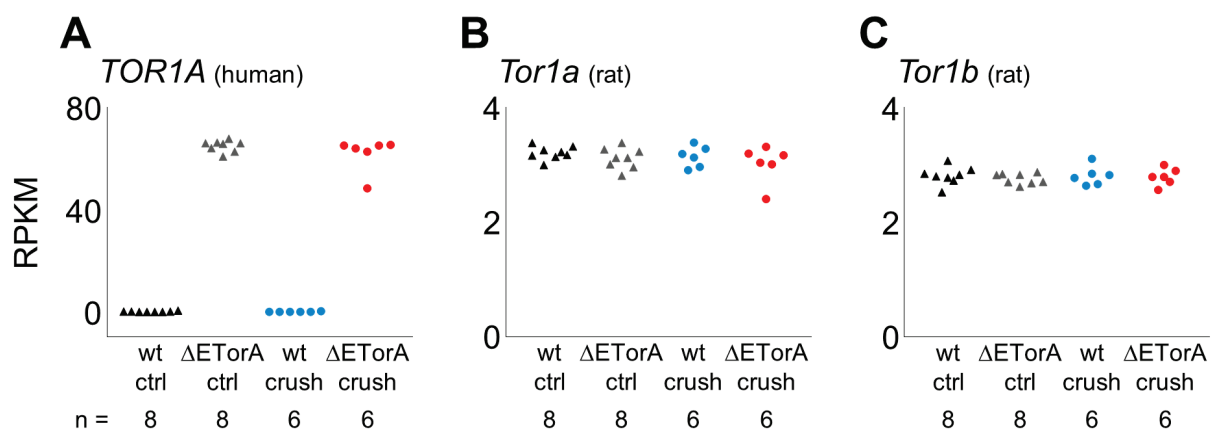


**Figure 30: Validation of RNA-Seq results by RPKM values**

Distribution of RPKM values *TOR1A* (A), *Tor1a* (B), and *Tor1b* (C) demonstrates the reliability of the RNA-Seq results.

Additional specifically selected genes of the energy metabolism were verified by comparing RPKM values of RNA-Seq analysis (Figure 31 A-J) with the relative mRNA expressions levels of qPCR analysis (Figure 31 A<sup>q</sup>-J<sup>q</sup>). All ten analyzed genes showed comparable patterns of expression levels from data generated by the different analysis techniques RNA-Seq and qPCR. Similar gene expression levels could be traced in qPCR data compared to gene expression levels of RNA-Seq data (*Pex11 $\alpha$*  = RNA-Seq *H*: 10.79,  $p < 0.05$ , (Figure 31 A); qPCR *H*: 9.396,  $p < 0.05$  (Figure 31 A<sup>q</sup>); *Acacb* = RNA-Seq *H*: 10.24,  $p < 0.05$ , (Figure 31 B); qPCR *H*: 5.709,  $p = 0.127$  (Figure 31 B<sup>q</sup>); *Hk2* = RNA-Seq *H*: 8.12,  $p < 0.05$ , (Figure 31 C); qPCR *H*: 4.964,  $p = 0.174$  (Figure 31 C<sup>q</sup>); *Cpt1a* = RNA-Seq *H*: 9.561,  $p < 0.05$ , (Figure 31 D); qPCR *H*: 2.825,  $p = 0.420$  (Figure 31 D<sup>q</sup>); *Acadm* = RNA-Seq *H*: 12.96,  $p < 0.01$ , (Figure 31 E); qPCR *H*: 7.216,  $p = 0.065$  (Figure 31 E<sup>q</sup>); *Bdh1* = RNA-Seq *H*: 11.44,  $p < 0.01$ , (Figure 31 F); qPCR *H*: 8.224,  $p < 0.05$  (Figure 31 F<sup>q</sup>); *Acat1* = RNA-Seq *H*: 14.36,  $p < 0.01$ , (Figure 31 G); qPCR *H*: 10.63,  $p < 0.05$  (Figure 31 G<sup>q</sup>); *Mct12* = RNA-Seq *H*: 14.76,  $p < 0.01$ , (Figure 31 H); qPCR *H*: 12.64,  $p < 0.01$  (Figure 31 H<sup>q</sup>); *Atf6* = RNA-Seq *H*: 11.62,  $p < 0.01$ ,

(Figure 31 I); qPCR  $H$ : 4.898,  $p = 0.1794$  (Figure 31 I<sup>q</sup>); *Kirrel3* = RNA-Seq  $H$ : 10.08,  $p < 0.01$ , (Figure 31 J); qPCR  $H$ : 4.47,  $p = 0.215$  (Figure 31 J<sup>q</sup>).

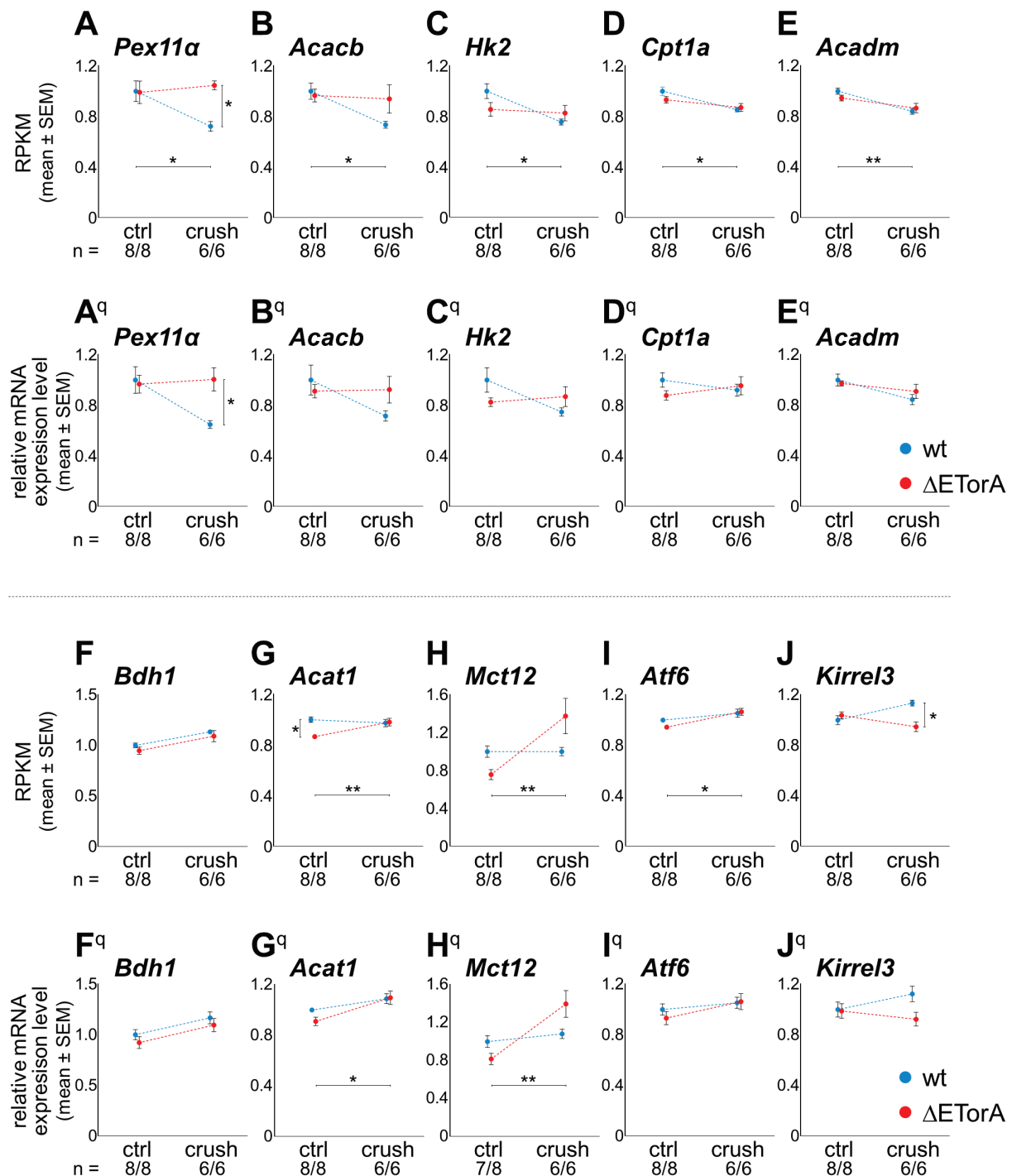


**Figure 31: Validation of RNA-Seq results by qPCR of selected DEGs from the energy metabolism**  
Validation of RNA-Seq data by comparing RPKM values of RNA-Seq analysis (A-J) with relative mRNA expression level of qPCR analysis (A<sup>q</sup>-J<sup>q</sup>) of striatal tissue contralateral to the nerve crush twelve weeks after nerve injury. Genes involved in the energy metabolism are selected for validation. Normalized to *Gapdh* (qPCR) and wt ctrl rats (RNA-Seq and qPCR). Kruskal-Wallis test with Dunn's multiple comparisons test; \*  $p < 0.05$ ; \*\*  $p < 0.01$ .

## 4 Discussion

Dystonia is a central network disorder still with an unclear pathophysiology. The essential clinical feature of reduced penetrance in DYT-TOR1A dystonia supports the assumption that additional disease modifiers such as environmental factors are needed to trigger dystonia in genetically predisposed subjects. Reflecting several studies about the development of dystonia, peripheral trauma was associated with dystonia and described as an environmental risk factor.<sup>130,133-135</sup> Because of ethical considerations, it is not feasible to analyze the pathophysiology of dystonia in humans on all biological levels. Model organisms are excellent alternatives for analyzing human diseases and performing multiscale analyses to deepen our understanding of the pathomechanism behind these. For DYT-TOR1A dystonia no model organism exists, which reflects the whole pathology of DYT-TOR1A dystonia. DYT-TOR1A rodent models either show a dystonic phenotype without a genetically DYT-TOR1A background, or the genetically modified animal models do not display a dystonic phenotype. Therefore, it is as yet not possible to mimic the complete human DYT-TOR1A dystonia pathology in an animal model and to correctly translate the findings to the human disease. With this work we aimed to generate a model organism for DYT-TOR1A dystonia which closely resembles the human pathological condition by combining genetical background with an environmental factor to elicit dystonia. In a rat model ( $\Delta$ ETorA), which expresses the human mutant TOR1A protein, a peripheral nerve trauma was implemented as an environmental factor. For this, the sciatic nerve, which provides motor and sensory innervation to and from the leg, was traumatized by a unilateral crush injury to disturb the sensorimotor integration. Behavioral analyses were then performed to assess if a sciatic nerve crush injury can trigger DLM in  $\Delta$ ETorA rats and a multiscale analysis was conducted to understand the pathophysiology behind DYT-TOR1A dystonia.

### 4.1 Nerve-injured $\Delta$ ETorA rats as a new DYT-TOR1A rodent model with DLM on a DYT-TOR1A genetic background

For the first time, a new symptomatic DYT-TOR1A rat model could be evolved by combining the DYT-TOR1A genetic background with an environmental factor. DLM could be triggered in  $\Delta$ ETorA rats through a unilateral sciatic nerve crush by showing abnormal, repetitive movements and contractions of the nerve-injured hind limb with a tendency towards spreading DLM to the contralateral side during TST. Additional

functional assessment was used to exclude impaired nerve regeneration and to show correlative theta oscillation abnormalities, as observed in human DYT-TOR1A patients.

To assess DLM severity, a novel DLM scoring system for the hindlimbs was developed. During the first weeks after sciatic nerve injury, both  $\Delta$ ETorA and wt rats developed a similarly high DLM severity score. We assume that in this early stage after nerve crush injury, DLM is caused by peripheral deafferentation of the injured nerve, a phenomenon called “pseudodystonia”.<sup>1</sup> Nine weeks after sciatic nerve crush, DLM in wt rats were decreasing to a level comparable to control groups. However, in  $\Delta$ ETorA rats the DLM always remained at a significantly higher DLM level from week nine until the end of the experiment (week twelve). Based on these results, we consider DLM within this time frame from week nine to week twelve after sciatic crush injury in  $\Delta$ ETorA rats to be “genuine” dystonia. Even if no generally accepted clinical criteria can clearly validate dystonic movements in humans as well as DLM in our  $\Delta$ ETorA rats, we found a similar phenotype in dystonia patients and in  $\Delta$ ETorA rats after a peripheral nerve trauma.

Dystonia is a disease of the CNS; consequently, it had to be excluded that DLM arose directly from the PNS due to the sciatic nerve crush. Eleven weeks after nerve injury, ENG recordings demonstrated in both genotypes slower NCVs and reduced CMAPs in the crushed sciatic nerves compared to control nerves. Thus, the genotype itself did not affect peripheral nerve conduction, and impaired nerve regeneration in  $\Delta$ ETorA rats after sciatic nerve injury could be excluded as the cause for an increase of DLM. This finding indicated that the peripheral trauma in  $\Delta$ ETorA rats is capable of inducing an alteration of the CNS, thereby triggering DLM.

Since neuronal activity in the primary motor cortex mainly contributes to the control of movement execution, we analyzed synchronized neuronal activity in the CNS of  $\Delta$ ETorA rats with DLM by LFP recordings. LFPs reflect the sum of extracellular neuronal postsynaptic potentials. The observed increased theta oscillations in hyperkinetic disorders like dystonia, tics or L-DOPA-induced dyskinesia is discussed controversially with respect of their impact in disease manifestation.<sup>32,216-218</sup> In previous studies, dystonia was associated with an increased oscillatory pallidal activity of the theta frequency band (4–12 Hz).<sup>31-33</sup> Higher oscillatory activity represents a higher

degree of synchronization between neurons, thereby assuming an alteration of information processing, which may then contribute to the dystonic phenotype. It was hypothesized that in dystonia, an increased pallidal low-frequency synchronization might lead to the loss of pallido-cerebellar coupling or disruption of cortico-pallidal coupling.<sup>36</sup> Even if the causal role of theta oscillation in the pathophysiology of dystonia is still unclear, it is already described as a pallidal physiomaer in cervical dystonia.<sup>35</sup> Moreover, a connectivity between the prokinetic pallidal theta power and the cortical motor areas as well as to dystonic symptom severity was described in human dystonia studies.<sup>34-36</sup> Indeed, for the first time we could demonstrate altered oscillatory activity in the EP and primary motor cortex in a dystonia rat model by confirming similar oscillatory patterns as in human dystonia patients, which strengthens the validity of our DYT-TOR1A rodent model. LFP recordings revealed a significant increase of the theta power (4 – 7 Hz) in EP and the motor cortex area MC1 in nerve-injured  $\Delta$ ETorA rats compared to wt rats. Simultaneously, the beta power (14 – 35 Hz) in the EP was significantly decreased in  $\Delta$ ETorA crush rats compared to wt rats. Similar observations have been described for dystonia patients compared to either treated or untreated PD, in which pallidal LFP recordings revealed a decreased beta power with a concurrent elevated theta power.<sup>33</sup> Additionally, the negative correlation between pallidal theta activity and physiological motor cortical beta oscillations revealed a cortico-pallidal coupling in dystonia patients. All these findings clarify the importance of the pallidum and cortical targets in the pathophysiology of dystonia.<sup>36,219</sup>

#### **4.2 DBS as a beneficial therapeutic approach in nerve-injured $\Delta$ ETorA rats**

For dystonia patients, DBS of the GPi is described as a safe and effective treatment.<sup>138,139</sup> Interestingly, it was shown that dystonic DYT-TOR1A patients responded better to pallidal DBS than other forms of dystonia. A reduction in disease burden between 50% to 94% was described (for review see Panov et al. 2013).<sup>142,148,220</sup> As a proof-of-principle experiment, we analyzed whether HFS of the EP that is recognized as the rodent GPi analog is effective in reducing DLM in DYT-TOR1A rats. Indeed, HFS of the EP in nerve-injured  $\Delta$ ETorA rats for three weeks led to a significant reduction of DLM, thereby demonstrating that modulation of the EP affects the behavioral outcome in these rats.

Several DBS studies of dystonia patients analyzed the effect of DBS on disease outcome or electrophysiological changes in the brain.<sup>34,149,221-223</sup> These studies should gain a better understanding of the mechanism of DBS in dystonia, which is not fully understood. It is assumed that the synchronization of neuronal activity in the theta band, which was already described for dystonia patients, can be disrupted through pallidal HFS by decreasing the theta oscillation. This desynchronization may modulate the synaptic plasticity back to a physiological level, which turns into an improvement of dystonic symptoms.<sup>34,51,149,152</sup> A reduced theta power in the GPi through DBS was verified. However, the suppression of GPi theta activity was only found in dystonia patients with a phasic phenotype, but not in dystonia patients with a tonic phenotype.<sup>34</sup> It must be mentioned that LFP recordings in human dystonia were performed one to seven days after DBS-electrode implantation.<sup>34-36</sup> The effect of pallidal DBS on oscillation patterns in the GPi of dystonia patients was analyzed by LFP recordings during a short test stimulation of 150 s.<sup>34</sup> However, the important long-term effect of HFS in the GPi could not be analyzed because usually DBS-mediated improvement of dystonic symptoms was obtained between minutes to month depending on the type of dystonia.<sup>81,143</sup> A study of patients with cervical dystonia reported a correlation between theta peak amplitudes with the clinical benefit after three months of GPi-HFS.<sup>35</sup> It is also interesting to note that it is not just the GPi, as the stimulated target, that seems to be modulated by DBS. DBS-induced changes in the cortex-basal ganglia network is assumed. This was clarified in a study of dystonia patients in which pallidal DBS led to alterations of EEG-GPi-LFP coherence.<sup>34</sup> Our evaluation of the theta power by LFP recordings revealed a significant reduction in MC2 and a non-significant reduction in MC1 and EP of nerve-injured  $\Delta$ ETorA rats within three weeks of EP-HFS. A significant higher coherence was found in EP-MC2 compared to EP-MC1 in the theta power of  $\Delta$ ETorA crush rats three weeks after EP-DBS, indicating that DBS is influencing the cortex–basal ganglia network through different level of connectivity between EP and the primary motor cortex areas. A disruptive technical aspect of our experiment could be that the EP-HFS had to be turned off for LFP recordings. Thus, approximately 10 min after switching off the HFS, LFP recordings were performed. This possibly led to a loss of temporary signals of oscillations patterns affected by HFS. Nevertheless, also under consideration of the time lag between EP-HFS and LFP recording in our study, a suppressed theta power in the EP of nerve-injured  $\Delta$ ETorA rats was observed after

EP-HFS which is comparable to the suppressed theta power in the GPi found in patients with phasic dystonic movements after pallidal-HFS.<sup>34</sup>

### **4.3 Peripheral trauma has an impact on brain glucose metabolism in the central motor network**

Brain neuronal activity demands high levels of energy that is provided by glucose as the primary source of energy. In adult humans, 20% of the total body glucose is consumed by the brain.<sup>215</sup> Functional brain imaging demonstrated a direct link between brain activity and neuronal glucose metabolism. Additionally, neurons were described as the principal locus of glucose uptake.<sup>224</sup>

Functional alterations of the central motor network in the CNS were observed in dystonia patients. FDG/positron emission tomography (PET) studies of human individuals reported altered glucose metabolism in non-manifesting as well as manifesting DYT-TOR1A mutation carriers. Increased glucose metabolism was detected in the putamen, GP, supplementary motor area, and the cerebellum. These FDG/PET studies were also performed under movement free conditions as well as in non-manifesting carriers. Consequently, dystonic contractions can be excluded as the cause of metabolic changes in these studies.<sup>28,225</sup>

To assess whether alteration of neuronal activity on a large-scale level could also be detected in  $\Delta$ ETorA rats with DLM, the CNS of  $\Delta$ ETorA and wt rats with and without nerve injury was analyzed by FDG autoradiography twelve weeks after nerve crush injury. In our study, alterations of the glucose uptake, and thereby alterations of neuronal activity, were observed bilaterally in the MC, the SC, and striatum in nerve-injured  $\Delta$ ETorA rats. However, the glucose metabolism was only significantly increased in the contralateral MC and SC of nerve-injured  $\Delta$ ETorA rats compared to wt control animals.  $\Delta$ ETorA ctrl rats revealed a tendency towards elevated glucose metabolism in the MC and SC of both hemispheres compared to wt control rats.  $\Delta$ ETorA ctrl rats reflected non-manifesting DYT-TOR1A gene carriers, and  $\Delta$ ETorA crush rats the manifesting DYT-TOR1A gene carriers, which showed comparable results in the areas of the striatum and cortices. Differences in glucose metabolism in the cerebellum could not be detected in  $\Delta$ ETorA rats. In human studies, FDG/PET scans were used for measuring the glucose uptake. In our study, we choose the FDG autoradiography because of higher sensitivity and better resolution. However, only 60  $\mu$ m of the whole rat cerebellum could be analyzed by autoradiography in our settings, whereas a PET

scan can capture the entire brain structure. Inconsistent data are most likely the result of the analysis of different cerebellar regions in human studies and our study. The cerebellar areas of the human studies were not defined more precisely. Only representative pictures of the FDG/PET scans were shown.<sup>28,225</sup> It was unfeasible to analyze the EP in our animal model because of the small size of this structure and the insufficient resolution of the FDG autoradiography for this size.

Already in a PD model, changes in the glucose metabolism were detected by using the functional neuroimaging FDG/PET. The 6-hydroxydopamine (6-OHDA) rat is an acute model of the hypokinetic disorder PD, induced by a unilateral neurotoxin lesion with 6-OHDA. FDG/PET data of 6-OHDA rats revealed glucose hypometabolism in the ipsilateral SN, primary motor cortex and pedunculo-pontine tegmental nucleus compared to baseline data. Additionally, a correlation between the degree of behavioral response and the change in metabolic activity in the ipsilateral SN, primary motor cortex and pedunculo-pontine tegmental nucleus was shown.<sup>226</sup> As assumed, this hypokinetic PD model showed decreased glucose metabolic changes, whereas our hyperkinetic  $\Delta$ ETorA rats demonstrated increased glucose metabolic changes in brain areas involved in movement generation.

A surprising result of our study was that nerve-injured wt rats revealed the highest glucose uptake. The glucose metabolism was significantly increased in MC, SC, and the striatum of both hemispheres. At present, we do not have an explanation for this. We can only suggest that compensatory mechanisms are involved, finally leading to a rat model without DLM after nerve crush injury.

Our study indicates that a peripheral trauma affects the neuronal activity by showing alterations of glucose metabolism in various regions of the central motor network.

#### **4.4 $\Delta$ ETorA rats display no alterations in striatal neuron cell number and striatal glutamatergic and cholinergic gene expression profiles**

Changes in cellular levels are described as a pathophysiological aspect in dystonia. Neurodegeneration was not observed in DYT-TOR1A patients and DYT-TOR1A rodent models, but structural abnormalities in the brain were identified (for review see Breakefield et al. 2008 and Dauer et al. 2014).<sup>4,193,227</sup> Enlarged dopaminergic cell bodies in the SN and perinuclear ubiquitin/torsinA-positive inclusion bodies in the brainstem and midbrain could be shown in DYT-TOR1A patients.<sup>109,191</sup> In naive  $\Delta$ ETorA rats, altered ultrastructures of the NE have been observed in the cortex,

striatum, and SN, amongst other CNS regions.<sup>188</sup> In addition, transgenic mice expressing human  $\Delta E$ -torsinA, revealed ubiquitin/torsinA-positive inclusion bodies in the brainstem.<sup>107</sup> Studies with various DYT-TOR1A mouse models focused on striatal interneurons. The impaired modulatory effect of striatal interneurons on MSNs could be a potential feature in the pathophysiology of dystonia.<sup>102</sup> Only one study showed a loss of CINs, which could not be confirmed in other mouse models. Except for enlarged cell bodies of striatal ACh- and PV-positive interneurons, no further alterations in GABAergic striatal neurons were described.<sup>101,102</sup> In our study, we analyzed the striatum as the primary input and output structure of the basal ganglia, where changes can affect the motor network, and finally in the pathophysiology of dystonia. Quantification of the absolute cell number of the whole striatum by unbiased stereology did not yield any differences in the number of CINs, PV<sup>+</sup>-, nNOS<sup>+</sup>- and CR<sup>+</sup>-GABAergic interneuron populations, and Nissl<sup>+</sup> cells comparing  $\Delta E$ TorA and wt rats with and without nerve crush injury. Additionally, gene expression levels of the striatal interneuron markers (encoded by *Pvalb*, *Nos1*, *Calb2*, *ChAT*) and the neuronal marker (*Darpp32*) revealed no differences between  $\Delta E$ TorA and wt rats with and without nerve crush injury. Our results confirm the assumption that DYT-TOR1A dystonia is not a neurodegenerative disease, as described by the majority of available literature (for review see Breakefield et al. 2008 and Dauer et al. 2014).<sup>4,227</sup> The morphology of striatal neurons was not further investigated, therefore no conclusion can be made about cell size, dendrite and spine density, length of dendrites and axons.

The gene expression levels of selected glutamatergic receptors and cholinergic receptors as well as the transcripts of *Ache* and *VACht*, were determined by qPCR. This experiment was performed to evaluate the availability of these targets in the striatum twelve weeks after nerve crush injury in wt and  $\Delta E$ TorA rats with and without nerve injury, which can influence processing of neurotransmission.

The neurotransmitter glutamate is involved in corticostriatal and intrastriatal signaling. These projections play a central role in movement control and could therefore also be valuable in the pathophysiology of dystonia. The three families of glutamate receptors (AMPA-receptors (GluR1-4), NMDA-receptors (GluN1, 2A-D, 3A, B), and kainate-receptors (GluK1-5)) modulate the striatal MSN activity in different ways.<sup>228</sup> Alterations of the glutamatergic transmission are associated with several movement disorders, such as PD and tardive dyskinesia.<sup>229,230</sup> Corticostriatal glutamatergic overactivity

resulted in dystonic symptoms in the paroxysmal dystonia *dt<sup>sz</sup>* hamster model.<sup>231</sup> Additionally, only juvenile (P26) knock-in *Tor1a<sup>+/ $\Delta$ gag</sup>* mice revealed a reduced NMDA-receptor/AMPA-receptor ratio at corticostriatal synapses compared to wt mice. Alterations of the NMDA-receptor/AMPA-receptor ratio was not observed in adult (P60) knock-in *Tor1a<sup>+/ $\Delta$ gag</sup>* mice. In the same study, a “premature” GluN2A/GluN2B switch was suggested, indicating molecular and morphological early maturation of the excitatory synapse in knock-in *Tor1a<sup>+/ $\Delta$ gag</sup>* mice.<sup>232</sup> Additionally, humans with *de novo* *GRIN2B* variants frequently revealed movement disorders.<sup>233</sup> GluR4 is a further glutamatergic receptor to mention. Some *de novo* heterozygous variants of glutamatergic receptor GluR4 resulted in gait abnormalities of human individuals.<sup>234</sup> Also, a loss-of-function mutation in a human AMPA receptor-associated protein, ferric chelate reductase 1-like (*FRRS1L*), led to hyperkinetic movement disorders.<sup>235</sup> *Frrs1<sup>-/-</sup>* mice showed significantly reduced levels of GluR1, GluR2 and GluR4 in the cerebellum and abnormalities in movement and muscle force compared to wt controls.<sup>236</sup> However, no differences were observed in the gene expression levels of the transcripts for the glutamatergic receptors GluR4 (*Gria4*) and GluN2B (*Grin2b*) in wt and  $\Delta$ ETorA rats with and without nerve injury.

The cholinergic system is described as a key player in synaptic plasticity, motor learning, and motor dysfunction in movement disorders, where an increased ACh release by interneurons is triggered through diminished striatal dopaminergic signaling.<sup>237</sup> In  $\Delta$ ETorA rats as well in hMT mice, DYT-TOR1A mouse models expressing the mutant human torsinA protein revealed impaired LTD and synaptic depotentiation in MSNs.<sup>71,188</sup> These effects could be restored by a mAChR M1 antagonist.<sup>71,188</sup> Additionally, it is assumed for dystonia that mAChRs M1 and M2/M4 as well as nAChRs are involved in cholinergic dysregulation by modulating MSNs activity via AChRs in the striatum.<sup>237-240</sup> In our study, the gene expression levels of striatal mAChRs (encoded by *Chrm1*, *Chrm2*, *Chrm4*), nAChR subunit *Chrn2b*, VACHT, and biosynthetic enzyme AChE appeared normal in control and nerve-injured  $\Delta$ ETorA rats compared to littermate controls. A study of DYT-TOR1A patients has already revealed no significant alterations in the striatal protein levels of AChE and VACHT.<sup>101</sup> It appears that gene expression levels of the analyzed cholinergic and glutamatergic markers do not influence DLM of the nerve-injured  $\Delta$ ETorA rats in our study. Further work is required to analyze functionality of the striatal cholinergic and

glutamatergic neurotransmission by electrophysiology or specific PET scans. Our methods could not evaluate this aspect.

#### **4.5 $\Delta$ ETorA rats exhibit abnormalities in catecholamine metabolism after peripheral trauma**

There is a clear link between monoamines and the pathophysiology of dystonia underscored by DRD, myoclonus-dystonia, and dystonia caused through mutations in genes encoding for TH or D<sub>5</sub>R.<sup>38,241-243</sup> Treatments with antipsychotic drugs, which block DA receptors, resulted in tardive dystonia.<sup>39,244,245</sup> It is assumed that monoamines have a modulatory effect on the DYT-TOR1A pathophysiology. However, monoamines do not appear as the unique factor in DYT-TOR1A dystonia.

Alteration of the dopaminergic system is described in several studies of DYT-TOR1A dystonia. Postmortem studies in a small cohort of three DYT-TOR1A patients revealed an elevated DOPAC/DA ratio in the striatum.<sup>44</sup> Additionally, enlarged dopaminergic cell bodies in the SN were described for DYT-TOR1A patients.<sup>109,246</sup> Some asymptomatic rodent models of DYT-TOR1A showed unaltered striatal levels of DA and its metabolites DOPAC and HVA.<sup>45,199,202</sup> However, increased striatal DOPAC levels were detected in h $\Delta$ GAG transgenic mice. Furthermore, hMT1 transgenic mice showed elevated DOPAC and HVA concentrations and DA turnover (DOPAC/DA and HVA/DA).<sup>49,247</sup> At baseline, no alterations in the extracellular striatal DA levels could be found in  $\Delta$ ETorA compared to wt rats. In addition, the nerve injury did not affect baseline DA release, analyzed by microdialysis. Potassium-evoked DA release was significantly elevated in nerve-injured  $\Delta$ ETorA rats, and even more pronounced in the contralateral striatum than the ipsilateral striatum. Significantly increased levels of the DA metabolites DOPAC and HVA were detected in nerve-injured  $\Delta$ ETorA rats compared to wt control animals. However, nerve-injured wt rats showed similar HVA levels compared to nerve-injured  $\Delta$ ETorA rats. In line with the microdialysis results, the analysis of contralateral striatal tissue revealed significantly elevated baseline levels of DOPAC and no difference in DA in nerve-injured  $\Delta$ ETorA rats compared to control  $\Delta$ ETorA rats. The difference between these two analysis methods is that tissue analysis discloses intracellular and extracellular contents whereas microdialysis displays only the extracellular levels. Stress-induced neurotransmitter release can only be simulated in microdialysis through potassium-evoked depolarization, and stress

trigger seems a critical feature in dystonia. These results correspond to findings of human and rodent DYT-TOR1A studies. Alterations in the dopaminergic system appears to be restricted to nerve injury with a more pronounced effect in the striatum contralateral to the nerve crush. It reflects that DLM are linked to the dopaminergic system, which emphasizes maladaptive changes in the basal ganglia loop and its involvement in the pathophysiology of dystonia.

Connections between the dopaminergic system and oscillation patterns of the basal ganglia reinforces the assumption of the involvement of the dopaminergic system in dystonia. Interestingly, PD studies found suppressed exaggerated basal ganglia beta activity by dopaminergic medication with L-DOPA, including improved motor symptoms.<sup>248-250</sup> Additionally, a study with dystonia patients treated with tetrabenazine, a monoamine-depleting agent by inhibiting VMAT2, showed an increased pallidal beta power in a hypodopamine state.<sup>251,252</sup> These results, as well as our finding of an altered dopaminergic system in  $\Delta$ ETorA rats, reflect the involvement of the dopaminergic system in the cortico-basal ganglia-thalamo-cortical circuit and finally in the pathophysiology of dystonia. However, concerning our data, no conclusion can be made about a correlation between DA and theta power.

For dopaminergic transmission, the mechanisms for DA release and reuptake are essential features. A great importance is attributed to DAT. In DYT-TOR1A dystonia, it is assumed that torsinA can influence protein processing because of the primary location of torsinA in the ER. It could be shown that overexpression of torsinA leads to a reduced cell-surface distribution of DAT.<sup>110</sup> In  $\Delta$ ETorA rats, the striatal DAT baseline levels tended to be decreased after nerve crush injury. A slight elevation of DAT levels was observed in nerve-injured wt rats. Nevertheless, these studies do not disclose information about DAT activity and functionality, yet reduced DAT activity and reduced DAT binding was observed in two different DYT-TOR1A mouse models.<sup>50,253</sup> There is evidence of altered DA dynamics due to a reduced DAT availability and functionality in DYT-TOR1A dystonia. While complete loss of DAT function resulted in five times higher basal DA levels, Hewett et al. suggested that a gradual loss of DAT function can lead to no detectable changes in DA levels, which match with our results of nerve-injured  $\Delta$ ETorA rats.<sup>50,254</sup>

Dopaminergic receptors are also essential targets in the dopaminergic transmission. Their specific activation defines the direction of voluntary movements through the direct or indirect pathway. Control and nerve-injured  $\Delta$ ETorA rats revealed no alterations in the striatal DA receptor mRNA expression levels. In a previous study of naive  $\Delta$ ETorA rats, altered D<sub>2</sub>R responsiveness could be observed in electrophysiological analysis.<sup>188</sup> However, changes for dopaminergic receptors, predominantly for D<sub>2</sub>, were found in different DYT-TOR1A human and animal studies. These studies showed a reduction in striatal D<sub>2</sub>R binding, partially also in striatal D<sub>1</sub>R, and striatal D<sub>2</sub>R protein levels even with normal mRNA levels of D<sub>2</sub>R.<sup>40,44,255-257</sup> This indicates a posttranslational defect through altered ER activity influenced by torsinA, as already mentioned for DAT.<sup>110</sup> Alterations in dopaminergic transmission through D<sub>2</sub>R leads to abnormal activation and inappropriate firing of cholinergic interneurons and GABAergic medium spiny neurons, which can finally result in an altered communication between CINs and MSNs.<sup>258-260</sup> Not only can DA influence CINs, but CINs can also trigger DA release through nicotinic receptors.<sup>90</sup> Therefore, it can be assumed that altered striatal synaptic plasticity in the aforementioned complex striatal neurotransmitter network results in irregular motor control. Functional assessment for the dopaminergic system as well as for other neurotransmitter systems was not performed in this study but could be applied in further studies by using techniques such as electrophysiological recordings, or specific PET and autoradiography setups.

For the monoamine 5-HT, a functional role can be attributed to the basal ganglia. Serotonergic axon terminals of neurons from dorsal and median raphe nucleus are innervated to all basal ganglia components, predominantly to the SN, striatum, and GPi, which emphasizes the importance of 5-HT/DA interaction.<sup>121</sup> In general, the serotonergic system is attributed to impulsivity and aggression behavior, and 5-HT deficiency leads to a hyperactivity phenotype and disrupted circadian behavior patterns.<sup>261,262</sup> The involvement of the serotonergic system in different types of dystonia was reviewed by Smit et al.<sup>122</sup> In post mortem tissue of two patients with early-onset primary dystonia, decreased levels of 5-HT in the dorsal raphe nuclei, increased levels of 5-HT in the GP, and increased levels of 5-HIAA in the raphe nuclei obscurus as well as in the GP were detected.<sup>123,263</sup> In a transgenic DYT-TOR1A mouse model (h $\Delta$ GAG) increased levels of 5-HT and 5-HIAA were observed in the brainstem, but not in the striatum.<sup>49</sup> *dt<sup>sz</sup>* hamsters, a phenotypic model of paroxysmal dystonia, revealed increased levels of 5-HT and/or 5-HIAA in the olfactory bulb, cortex, striatum,

hypothalamus, pons, and medulla oblongata. However, in most regions, the 5-HIAA/5-HT ratio was not significantly altered in *dt<sup>sz</sup>* hamsters.<sup>264</sup> A prominent clinical feature of the serotonergic system is the treatment by serotonergic drugs, which can elicit or improve dystonia depending on the specific serotonergic target and dystonia etiology.<sup>122</sup> Important serotonergic targets are 5-HT<sub>1A</sub> and 5-HT<sub>2A</sub> receptors. Inhibition of serotonergic neurons firing by the 5-HT<sub>1A</sub> agonist influences GABAergic, glutaminergic, cholinergic, and dopaminergic activity.<sup>265</sup> *dt* rats, a genetic animal model of dystonia musculorum deformans, showed a 6-fold higher sensitivity to the 5-HT<sub>1A</sub> agonist compared to wt rats, suggesting an integral role of the 5-HT system and 5-HT<sub>1A</sub> receptor in abnormal movements.<sup>266</sup> Importance should be given to the 5-HT<sub>1A</sub> receptor because of its high affinity for 5-HT.<sup>267</sup> 5-HT<sub>2A/2C</sub> is a further interesting serotonergic receptor. A blockage of 5-HT<sub>2A/2C</sub> led to 5-HT<sub>2A/2C</sub> receptor-mediated inhibition of DA release in the striatum, activation of cholinergic interneurons in the striatum, and inhibition of dopaminergic neurons in the SN.<sup>265</sup> Only a few studies about DYT-TOR1A dystonia and the serotonergic system are available. Indeed, we could show some similarities in nerve-injured  $\Delta$ ETorA rats to previous studies. Nerve-injured  $\Delta$ ETorA rats demonstrated a significant striatal increase of 5-HIAA. Alterations in protein levels of 5-HT levels, 5-HT/5-HIAA ratios, and mRNA expression levels of the 5-HT receptors *Htr1a* and *Htr2a* have not been found in nerve-injured  $\Delta$ ETorA rats. All this data postulate that the serotonergic system is a putative target in dystonia through potential changes in the synaptic transmission.

#### **4.6 Evidence of new potential pathways in DYT-TOR1A dystonia by whole-transcriptome analysis**

An unbiased RNA-Seq approach was implemented to identify dysregulated genes and pathways in nerve-injured  $\Delta$ ETorA rats in comparison to untreated  $\Delta$ ETorA and wt rats as well as nerve-injured wt rats. RNA-Seq was performed in the striatum contralateral to the nerve crush twelve weeks after nerve injury, where apparent differences of DLM were observed in nerve-injured  $\Delta$ ETorA rats compared to all indicated control groups.

Our data demonstrate genotype-dependent transcriptomics changes of the CNS after peripheral nerve crush injury. Genes from  $\Delta$ ETorA rats were most affected by the central mechanisms induced by nerve crush injury with 1011 DEGs. Nerve crush injury had a smaller impact on modulating gene expression of animals with wt background.

Only 216 DEGs were observed in rats with wt background compared to animals with a transgenic background. A low number of DEGs were found when comparing wt ctrl and transgenic ctrl animals, as well as wt crush and transgenic crush animals. Based on the small number of DEGs, the cut-off criteria were set to  $p_{adj} < 0.05$  due to low levels of  $\log_2FC$ . The low levels of  $\log_2FC$  point to a multifactorial disease, which suggests an involvement of different pathways in the pathophysiology of dystonia. It must be taken into consideration that the analysis was performed from whole striatal tissue lysate, which includes different cell types as well as extracellular and intracellular components. A more precise analysis could be achieved by using a single-cell approach. Nevertheless, to give credence to the data, a minimum of six replicates (each replicate is an individual animal) were used per group. Additionally, the RNA-Seq data were verified and confirmed by qPCR.

Multiple dysregulated pathways were highlighted in the enrichment analysis of DEGs in the striatum by using the WikiPathways 2019 human database. A specific pathway database for rats was not available in Enrichr. Therefore, the human database was selected. The expression of the human torsinA in  $\Delta ETorA$  rats and the aim of comparing the results of this animal study to the human DYT-TOR1A pathophysiology justified this selection. The pathway analysis of our transcriptome data revealed the circadian rhythm and energy metabolism as new potential mechanisms in the pathophysiology of dystonia of our DYT-TOR1A rat model.

There is little information regarding the involvement of the circadian rhythm in dystonia. For DYT-TOR1A dystonia, nothing has yet been described. Our data showed differentially regulated pathways of the circadian clock. Many core clock genes were significantly altered with highly regulated gene-levels. Additionally, in almost every two-group comparison, striatal differentially regulated pathways related to the circadian rhythm were detected. The circadian clock is a genetically encoded endogenous timekeeper, located in nearly all cells and tissues.<sup>268,269</sup> The principal circadian clock resides in the suprachiasmatic nucleus (SCN) of the hypothalamus, directing molecular rhythm of approximately 24 h intervals and synchronizing independent circadian clocks throughout the body.<sup>270-272</sup> The mechanisms of circadian rhythm is based on intrinsic transcriptional–translational feedback loops and depends fundamentally on the two master genes *CLOCK* and *BMAL1* (*ARNTL*) of the core clock.<sup>269,273</sup> These two transcription factors drive rhythmic gene expression and regulate biological functions

under circadian control by interacting with their targets Period (PER1, PER2, PER3), Cryptochrome (CRY1, CRY2), REV-ERB $\alpha$  (NR1D1), and REV-ERB $\beta$  (NR1D2) of the core clock.<sup>272,274,275</sup> Core clock targets are responsible for timekeeping and generating circadian oscillations next to hundreds to thousands of other targets expressed with a circadian rhythm.<sup>270,276</sup> A disrupted circadian rhythm has an effect on different pathologies, such as obesity, metabolic syndrome, diabetes, cardiovascular diseases, inflammation, sleep disorders, and tumorigenic processes based on circadian oscillatory output in metabolism, energy levels, hormone secretion, neurotransmitter secretion, cellular homeostasis, and further biological pathways.<sup>269,272,277</sup> DYT-TOR1A rodent models as well as our  $\Delta$ ETorA rats showed alterations in the above-mentioned targets, which can be disrupted by the circadian rhythm. Obesity, metabolic syndrome, and diabetes are correlated with glucose metabolism. In the  $\Delta$ ETorA rat model, glucose metabolism seems to be affected. Grundmann et al. have already described late-onset diabetes mellitus in  $\Delta$ ETorA rats of line 4.<sup>188</sup> Additionally, our study revealed glucose metabolic changes in nerve-injured  $\Delta$ ETorA rats by autoradiography and dysregulations of the energy metabolism by transcriptome analysis. Furthermore, it appears that the serotonergic system is also a component of the circadian clock. The SCN receives serotonergic input from the dorsal and median raphe nucleus.<sup>278</sup> Alteration of the serotonergic system was already described for different DYT-TOR1A rodent models.<sup>49,264</sup> We could also show that the serotonergic system is altered in nerve-injured  $\Delta$ ETorA rats. DA is another relevant target referring to the circadian clock. It is suggested that the circadian clock can change the dopaminergic system at different levels.<sup>278</sup> In 1986, Kafka et al. described a circadian rhythm in levels of DA and its related metabolites and receptors in different brain areas.<sup>279</sup> Furthermore, circadian clock genes affect the dopaminergic system by influencing the expression patterns of DA, DA metabolites, DAT, TH, MAO, D<sub>1</sub>R and D<sub>2</sub>R.<sup>278,280-282</sup> Conversely, the circadian expression of clock genes can be regulated by DA in the dorsal striatum through D1 and D2 receptor binding.<sup>283-285</sup> The circadian clock regulates biological timing of time-related processes. It includes time-related processes of various temporal domains like microsecond and seconds-to-minutes rhythms.<sup>278</sup> The millisecond range seems to be important for motor control, depending on sensory-motor circuits.<sup>286,287</sup> Some fundamental behaviors, such as learning, memory, and decision-making were assigned to the seconds-to-minutes range by the involvement of cortico-striatal circuits.<sup>288-290</sup> An impaired seconds-to-minutes range was already described for

movement disorders with alterations in the dopaminergic system like PD and HD.<sup>288,291</sup> A correlation between circadian rhythm and dystonia has so far been described for dopa-responsive dystonia DYT-GCH1 (DYT5a) and DYT2-like dystonia. These types of dystonia are associated with dysfunctions in the dopaminergic system.<sup>292,293</sup> This cross-link between dystonia and different targets as well as to different brain regions suggests a potential involvement of the circadian clock in the pathophysiology of dystonia. The circadian clock is very delicate concerning tissue preparation and timing. To exclude false positive results, the tissue preparation was performed in a randomized order according to the different animal groups.

Pathways of energy metabolism were further main topics, found in the whole transcriptome analysis. The energy demand of the brain is very high. The brain consumes 20% of the total body glucose, even though the brain accounts for only 2% of the whole body mass.<sup>215,294</sup> ATP is a high potential molecule providing energy for cellular processes. There are different substrate sources for energy metabolism in the brain. Through various mechanisms, all substrates are converted to acetyl-CoA, which finally enters the common pathway of the tricarboxylic acid (TCA) cycle in the mitochondria for ATP synthesizing through oxidative phosphorylation. Glucose is the primary energy source in the brain for both neurons and glial cells, however with different metabolic profiles.<sup>215</sup> Glucose enters the CNS from the blood through the blood-brain-barrier (BBB) primarily by glucose transporter 1 (GLUT1).<sup>295</sup> GLUT3 is next to GLUT1, a further primary glucose transporter in the CNS which delivers glucose into neurons and glial cells.<sup>296</sup> Besides glucose, lactate, ketone bodies, and fatty acids are additional substrates for energy metabolism. Lactate is used as an energy substrate, especially during periods of intense physical activity.<sup>297</sup> Neurons and astrocytes can fully oxidize lactate in their mitochondria.<sup>298</sup> Lactate is oxidized to pyruvate, pyruvate is further converted to acetyl-CoA and finally enters the TCA cycle. Fatty acids are energy substrates that belong to the class of lipids, such as triacylglycerols, phospholipids, sterol lipids, and sphingolipids.<sup>299</sup> Fatty acids are mainly produced in the liver and adipose tissue. They enter the CNS through the BBB by fatty acid transport protein-1 and -4 (FATP-1 and FATP-4). Fatty acids are taken up mainly by glia cells and oxidized to acetyl-CoA.<sup>300,301</sup> Long-chain fatty acids are converted to acetyl-CoA by  $\beta$ -oxidation in mitochondria. A further important cell organelle for fatty acids is the peroxisome. Branched and very long chain fatty acids were only shortened, but not fully converted to acetyl-CoA by  $\alpha$ - and  $\beta$ -oxidation in peroxisomes.<sup>302,303</sup> An

essential role in neurodevelopment, neurotransmission and repair processes is attributed to energy metabolism of fatty acids.<sup>304,305</sup> Ketone bodies (acetoacetate, 3-hydroxybutyrate, and acetone) are derived from the liver and are formed predominantly from fatty acids through the metabolic pathway ketogenesis, infiltrating the brain through BBB by monocarboxylate transporter 1 and 2 (MCT1 and MCT2).<sup>306,307</sup> During maturation at a young age as well as prolonged fasting, ketone bodies are essential energy substrates of the brain by neurons and glial cells when glucose is less available.<sup>306</sup> Ketone bodies can supply up to 60% of the brain energy during prolonged fasting.<sup>308</sup> Furthermore, neuroprotection and synthesis of lipids are attributed functions of ketone bodies.<sup>306,309</sup> A balanced energy metabolism provided from different substrates is necessary for physiological processes in the brain. An energy shift can have an impact on alterations of various cellular processes through an insufficient supply of ATP. For example, presynaptic and postsynaptic signaling are fast processes which consume approximately 80% of the ATP. Additionally, ATP is required quickly for these processes. These requirements cannot be fulfilled by all energy substrates.<sup>215,301</sup> An energy shift to fatty acids, where a rapid ATP supply is not guaranteed regarding the slow  $\beta$ -oxidation, can also lead to disadvantages like hypoxia and oxidative stress in neurons as well as to a disturbed neuronal signaling.<sup>305</sup>

Our study provided alterations in different pathways of energy metabolism by RNA-Seq. Our FDG autoradiography data showed differences in the glucose metabolism in  $\Delta$ ETorA rats. Combining all these data of our DYT-TOR1A rat model, an energy shift can be suggested. Different studies have already revealed alterations in the lipid metabolism for DYT-TOR1A. In a drosophila model of DYT-TOR1A, it could be shown that torsinA regulated lipid metabolism, resulting in membrane proliferation and increased cellular lipid content. Additionally, in DYT-TOR1A mouse models and DYT-TOR1A patient-derived cells, alterations in the key lipid metabolizing enzyme lipin were described.<sup>310</sup> Also, a mutation of the *MECR* gene, encoding the mitochondrial trans-2-enoyl-coenzyme A-reductase involved in human mitochondrial fatty acid synthesis, caused childhood-onset dystonia.<sup>311</sup> Alterations in pathways of sphingolipids appeared during whole transcriptome analysis. Sphingolipids are a subgroup of lipids involved in cellular membrane structure, the regulation of cell growth, differentiation, senescence, and apoptosis.<sup>312</sup> In  $\Delta$ ETorA rats, differential expression of sphingosine kinase-2 (SPHK2) was detected, which was already observed for the movement disorders PD

and HD. Several observations of the  $\Delta$ ETorA animals indicated alterations in energy metabolism, concerning mainly the lipid metabolism.

New potential pathways emerged out of the whole genome analysis. However, these pathways require detailed analysis in order to provide unambiguous information. Analysis of cell specificity, protein expression, target interaction and functionality are necessary to examine. Analysis can range from cell sorting to the use of specific knock out models.

#### **4.7 Synopsis**

In conclusion, a novel DYT-TOR1A rodent model with a dystonia-like phenotype on a genetic background and pathophysiological features, which were already described for human dystonia, was generated. It could be confirmed that peripheral nerve injury triggers DLM in an asymptomatic transgenic DYT-TOR1A rat model, supporting our “second hit” hypothesis. Furthermore, peripheral nerve injury induced pathophysiological alterations in the CNS of  $\Delta$ ETorA animals in different levels of the nervous system. The pathophysiology of DYT-TOR1A dystonia can be considered to arise from the interactions between genetics and environmental triggers, which influences molecular and cellular mechanisms, followed by microcircuitry changes right up to large-scale network alterations, finally resulting in dystonia. This novel  $\Delta$ ETorA rat model is one of the rare available DYT-TOR1A animal models combining genetics and phenotype by translating a similar human dystonia endophenotype into a DYT-TOR1A rodent model. It provides many opportunities to investigate mechanisms and pathways in the pathophysiology of dystonia in close conformity to human DYT-TOR1A dystonia. The beneficial effect of EP-DBS treatment in nerve-injured  $\Delta$ ETorA rats provides entirely new possibilities for verifying novel DBS approaches by different stimulation parameters and different stimulation targets. The opportunity to combine DBS with a broad diversity of analytical methods in the  $\Delta$ ETorA rat model gives excellent leverage to understand the mechanisms behind the HFS and to translate observations from the laboratory to the clinic.

However, there are some limitations to this study. Several confounding factors and technical limitations are associated with LFP recordings. One confounding factor could be anesthesia during recordings, even if the anesthesia was set to comparable levels

in all animals, with a minimized isoflurane level. A better approach would be recordings in free-moving animals, which was not feasible with our current electrophysiological setup. Additionally, it must be noted that brain edema due to surgical intervention could have an impact on the data. This not only concerns our animal study, but human studies are also affected. A further disadvantage was the delay of LFP recordings in EP-DBS conditions. However, there was no other possibility to implement these recordings with our current setup. The use of comparative groups should compensate for these confounding factors in LFP recordings, which is a big advantage for animal studies, whereas human studies have weak controls or lack controls. Additionally, animal studies benefit from comparable external factors such as housing, noise, food and specialized tissue preparation which is not given in human studies. Particularly for targets, like monoamines or circadian clock, the environment as well as tissue preparation influences results. This study mainly concentrated on the analysis of the striatum. Further studies are necessary to investigate the cortex, thalamus, and cerebellum, which also seems to be relevant in the pathophysiology of DYT-TOR1A. Moreover, the used techniques are not sufficient to explain the mechanisms behind dysregulations on protein and mRNA levels. Further studies are required to address functionality and mechanism.

## 5 References

- 1 Albanese, A. *et al.* Phenomenology and classification of dystonia: a consensus update. *Mov Disord* 28, 863-873, doi:10.1002/mds.25475 (2013).
- 2 Oppenheim, H. Über eine eigenartige Krampfkrankheit des kindlichen und jugendlichen Alters (Dysbasia lordotica progressiva, Dystonia musculorum deformans). *Neurologisches Centralblatt* 30, 1090-1107 (1911).
- 3 Fahn, S. Concept and classification of dystonia. *Adv Neurol* 50, 1-8 (1988).
- 4 Breakefield, X. O. *et al.* The pathophysiological basis of dystonias. *Nat Rev Neurosci* 9, 222-234, doi:10.1038/nrn2337 (2008).
- 5 Nadaf, S. N., Chakor, R. T., Kothari, K. V. & Bharote, H. Progressive delayed hemidystonia following clinically mild traumatic brain injury. *BMJ Case Rep* 2017, doi:10.1136/bcr-2017-220334 (2017).
- 6 Albanese, A. *et al.* "Complex" dystonia is not a category in the new 2013 consensus classification. *Mov Disord* 31, 1758-1759, doi:10.1002/mds.26764 (2016).
- 7 Klein, C. *et al.* Reply letter to Jinnah "Locus pocus" and Albanese "Complex dystonia is not a category in the new 2013 consensus classification": Necessary evolution, no magic! *Mov Disord* 31, 1760-1762, doi:10.1002/mds.26763 (2016).
- 8 Klein, C., Lohmann, K., Marras, C. & Münchau, A. in *Hereditary Dystonia Overview; GeneReviews® [Internet]* Vol. 1993-2019 (eds Adam MP, Ardinger HH, & Pagon RA) (University of Washington, Seattle, 2003 Oct 28 [Updated 2017 Jun 22]).
- 9 Marras, C. *et al.* Nomenclature of genetic movement disorders: Recommendations of the international Parkinson and movement disorder society task force. *Mov Disord* 31, 436-457, doi:10.1002/mds.26527 (2016).
- 10 Marras, C., Lohmann, K., Lang, A. & Klein, C. Fixing the broken system of genetic locus symbols: Parkinson disease and dystonia as examples. *Neurology* 78, 1016-1024, doi:10.1212/WNL.0b013e31824d58ab (2012).
- 11 Jinnah, H. A. Locus Pocus. *Mov Disord* 31, 1759-1760, doi:10.1002/mds.26765 (2016).
- 12 Neychev, V. K., Gross, R. E., Lehericy, S., Hess, E. J. & Jinnah, H. A. The functional neuroanatomy of dystonia. *Neurobiol Dis* 42, 185-201, doi:10.1016/j.nbd.2011.01.026 (2011).
- 13 Geyer, H. L. & Bressman, S. B. The diagnosis of dystonia. *Lancet Neurol* 5, 780-790, doi:10.1016/S1474-4422(06)70547-6 (2006).
- 14 Marsden, C. D., Obeso, J. A., Zarranz, J. J. & Lang, A. E. The anatomical basis of symptomatic hemidystonia. *Brain* 108 ( Pt 2), 463-483, doi:10.1093/brain/108.2.463 (1985).
- 15 Obeso, J. A. & Gimenez-Roldan, S. Clinicopathological correlation in symptomatic dystonia. *Adv Neurol* 50, 113-122 (1988).
- 16 Pettigrew, L. C. & Jankovic, J. Hemidystonia: a report of 22 patients and a review of the literature. *J Neurol Neurosurg Psychiatry* 48, 650-657, doi:10.1136/jnnp.48.7.650 (1985).
- 17 Bhatia, K. P. & Marsden, C. D. The behavioural and motor consequences of focal lesions of the basal ganglia in man. *Brain* 117 ( Pt 4), 859-876, doi:10.1093/brain/117.4.859 (1994).
- 18 LeDoux, M. S. & Brady, K. A. Secondary cervical dystonia associated with structural lesions of the central nervous system. *Mov Disord* 18, 60-69, doi:10.1002/mds.10301 (2003).
- 19 Burguera, J. A., Bataller, L. & Valero, C. Action hand dystonia after cortical parietal infarction. *Mov Disord* 16, 1183-1185 (2001).
- 20 Cho, C. & Samkoff, L. M. A lesion of the anterior thalamus producing dystonic tremor of the hand. *Arch Neurol* 57, 1353-1355 (2000).
- 21 Kim, J. W. & Lee, P. H. Dystonic head tremor associated with a parietal lesion. *Eur J Neurol* 14, e32-33, doi:10.1111/j.1468-1331.2006.01495.x (2007).
- 22 Scott, B. L. & Jankovic, J. Delayed-onset progressive movement disorders after static brain lesions. *Neurology* 46, 68-74, doi:10.1212/wnl.46.1.68 (1996).

- 23 Tanabe, L. M., Kim, C. E., Alagem, N. & Dauer, W. T. Primary dystonia: molecules and mechanisms. *Nat Rev Neurol* 5, 598-609, doi:10.1038/nrneuro.2009.160 (2009).
- 24 Delmaire, C. *et al.* Structural abnormalities in the cerebellum and sensorimotor circuit in writer's cramp. *Neurology* 69, 376-380, doi:10.1212/01.wnl.0000266591.49624.1a (2007).
- 25 Draganski, B., Thun-Hohenstein, C., Bogdahn, U., Winkler, J. & May, A. "Motor circuit" gray matter changes in idiopathic cervical dystonia. *Neurology* 61, 1228-1231, doi:10.1212/01.wnl.0000094240.93745.83 (2003).
- 26 Etgen, T., Muhlau, M., Gaser, C. & Sander, D. Bilateral grey-matter increase in the putamen in primary blepharospasm. *J Neurol Neurosurg Psychiatry* 77, 1017-1020, doi:10.1136/jnnp.2005.087148 (2006).
- 27 Garraux, G. *et al.* Changes in brain anatomy in focal hand dystonia. *Ann Neurol* 55, 736-739, doi:10.1002/ana.20113 (2004).
- 28 Eidelberg, D. *et al.* Functional brain networks in DYT1 dystonia. *Ann Neurol* 44, 303-312, doi:10.1002/ana.410440304 (1998).
- 29 Starr, P. A. *et al.* Spontaneous pallidal neuronal activity in human dystonia: comparison with Parkinson's disease and normal macaque. *J Neurophysiol* 93, 3165-3176, doi:10.1152/jn.00971.2004 (2005).
- 30 Gernert, M., Bennay, M., Fedrowitz, M., Rehders, J. H. & Richter, A. Altered discharge pattern of basal ganglia output neurons in an animal model of idiopathic dystonia. *J Neurosci* 22, 7244-7253, doi:20026724 (2002).
- 31 Liu, X. *et al.* Involvement of the medial pallidum in focal myoclonic dystonia: A clinical and neurophysiological case study. *Mov Disord* 17, 346-353 (2002).
- 32 Liu, X. *et al.* The sensory and motor representation of synchronized oscillations in the globus pallidus in patients with primary dystonia. *Brain* 131, 1562-1573, doi:10.1093/brain/awn083 (2008).
- 33 Silberstein, P. *et al.* Patterning of globus pallidus local field potentials differs between Parkinson's disease and dystonia. *Brain* 126, 2597-2608, doi:10.1093/brain/awg267 (2003).
- 34 Barow, E. *et al.* Deep brain stimulation suppresses pallidal low frequency activity in patients with phasic dystonic movements. *Brain* 137, 3012-3024, doi:10.1093/brain/awu258 (2014).
- 35 Neumann, W. J. *et al.* A localized pallidal physiomarker in cervical dystonia. *Ann Neurol* 82, 912-924, doi:10.1002/ana.25095 (2017).
- 36 Neumann, W. J. *et al.* Cortico-pallidal oscillatory connectivity in patients with dystonia. *Brain* 138, 1894-1906, doi:10.1093/brain/awv109 (2015).
- 37 Coubes, P., Roubertie, A., Vayssiere, N., Hemm, S. & Echenne, B. Treatment of DYT1-generalised dystonia by stimulation of the internal globus pallidus. *Lancet* 355, 2220-2221, doi:10.1016/S0140-6736(00)02410-7 (2000).
- 38 Nygaard, T. G., Marsden, C. D. & Duvoisin, R. C. Dopa-responsive dystonia. *Adv Neurol* 50, 377-384 (1988).
- 39 Pinninti, N. R., Mago, R. & Adityanjee. Tardive dystonia-associated prescription of aripiprazole. *J Neuropsychiatry Clin Neurosci* 18, 426-427, doi:10.1176/jnp.2006.18.3.426a (2006).
- 40 Asanuma, K. *et al.* Decreased striatal D2 receptor binding in non-manifesting carriers of the DYT1 dystonia mutation. *Neurology* 64, 347-349, doi:10.1212/01.WNL.0000149764.34953.BF (2005).
- 41 Black, K. J. *et al.* Spatial reorganization of putaminal dopamine D2-like receptors in cranial and hand dystonia. *PLoS One* 9, e88121, doi:10.1371/journal.pone.0088121 (2014).
- 42 Carbon, M. *et al.* Abnormal striatal and thalamic dopamine neurotransmission: Genotype-related features of dystonia. *Neurology* 72, 2097-2103, doi:10.1212/WNL.0b013e3181aa538f (2009).
- 43 Karimi, M. *et al.* Striatal dopamine D1-like receptor binding is unchanged in primary focal dystonia. *Mov Disord* 28, 2002-2006, doi:10.1002/mds.25720 (2013).

- 44 Augood, S. J. *et al.* Dopamine transmission in DYT1 dystonia: a biochemical and autoradiographical study. *Neurology* 59, 445-448, doi:10.1212/wnl.59.3.445 (2002).
- 45 Balcioglu, A. *et al.* Dopamine release is impaired in a mouse model of DYT1 dystonia. *J Neurochem* 102, 783-788, doi:10.1111/j.1471-4159.2007.04590.x (2007).
- 46 Dang, M. T. *et al.* Generation and characterization of Dyt1 DeltaGAG knock-in mouse as a model for early-onset dystonia. *Exp Neurol* 196, 452-463, doi:10.1016/j.expneurol.2005.08.025 (2005).
- 47 Dang, M. T., Yokoi, F., Pence, M. A. & Li, Y. Motor deficits and hyperactivity in Dyt1 knockdown mice. *Neurosci Res* 56, 470-474, doi:10.1016/j.neures.2006.09.005 (2006).
- 48 Furukawa, Y., Hornykiewicz, O., Fahn, S. & Kish, S. J. Striatal dopamine in early-onset primary torsion dystonia with the DYT1 mutation. *Neurology* 54, 1193-1195, doi:10.1212/wnl.54.5.1193 (2000).
- 49 Grundmann, K. *et al.* Overexpression of human wildtype torsinA and human DeltaGAG torsinA in a transgenic mouse model causes phenotypic abnormalities. *Neurobiol Dis* 27, 190-206, doi:10.1016/j.nbd.2007.04.015 (2007).
- 50 Hewett, J., Johanson, P., Sharma, N., Standaert, D. & Balcioglu, A. Function of dopamine transporter is compromised in DYT1 transgenic animal model in vivo. *J Neurochem* 113, 228-235, doi:10.1111/j.1471-4159.2010.06590.x (2010).
- 51 Quartarone, A. & Hallett, M. Emerging concepts in the physiological basis of dystonia. *Mov Disord* 28, 958-967, doi:10.1002/mds.25532 (2013).
- 52 Hallett, M. Pathophysiology of dystonia. *J Neural Transm Suppl*, 485-488 (2006).
- 53 Berardelli, A. *et al.* The pathophysiology of primary dystonia. *Brain* 121 ( Pt 7), 1195-1212, doi:10.1093/brain/121.7.1195 (1998).
- 54 Cohen, L. G. & Hallett, M. Hand cramps: clinical features and electromyographic patterns in a focal dystonia. *Neurology* 38, 1005-1012, doi:10.1212/wnl.38.7.1005 (1988).
- 55 Hallett, M. Neurophysiology of dystonia: The role of inhibition. *Neurobiol Dis* 42, 177-184, doi:10.1016/j.nbd.2010.08.025 (2011).
- 56 Berardelli, A., Rothwell, J. C., Day, B. L. & Marsden, C. D. Pathophysiology of blepharospasm and oromandibular dystonia. *Brain* 108 ( Pt 3), 593-608, doi:10.1093/brain/108.3.593 (1985).
- 57 Bara-Jimenez, W., Shelton, P. & Hallett, M. Spatial discrimination is abnormal in focal hand dystonia. *Neurology* 55, 1869-1873, doi:10.1212/wnl.55.12.1869 (2000).
- 58 Scontrini, A. *et al.* Somatosensory temporal discrimination in patients with primary focal dystonia. *J Neurol Neurosurg Psychiatry* 80, 1315-1319, doi:10.1136/jnnp.2009.178236 (2009).
- 59 Flanders, M. What is the biological basis of sensorimotor integration? *Biol Cybern* 104, 1-8, doi:10.1007/s00422-011-0419-9 (2011).
- 60 Pastor, M. A., Day, B. L., Macaluso, E., Friston, K. J. & Frackowiak, R. S. The functional neuroanatomy of temporal discrimination. *J Neurosci* 24, 2585-2591, doi:10.1523/JNEUROSCI.4210-03.2004 (2004).
- 61 Restuccia, D. *et al.* Functional changes of the primary somatosensory cortex in patients with unilateral cerebellar lesions. *Brain* 124, 757-768, doi:10.1093/brain/124.4.757 (2001).
- 62 Manto, M. *et al.* Consensus paper: roles of the cerebellum in motor control--the diversity of ideas on cerebellar involvement in movement. *Cerebellum* 11, 457-487, doi:10.1007/s12311-011-0331-9 (2012).
- 63 Ghilardi, M. F. *et al.* Impaired sequence learning in carriers of the DYT1 dystonia mutation. *Ann Neurol* 54, 102-109, doi:10.1002/ana.10610 (2003).
- 64 Bliss, T. V. & Lomo, T. Long-lasting potentiation of synaptic transmission in the dentate area of the anaesthetized rabbit following stimulation of the perforant path. *J Physiol* 232, 331-356, doi:10.1113/jphysiol.1973.sp010273 (1973).
- 65 Quartarone, A. & Pisani, A. Abnormal plasticity in dystonia: Disruption of synaptic homeostasis. *Neurobiol Dis* 42, 162-170, doi:10.1016/j.nbd.2010.12.011 (2011).

- 66 Quartarone, A. *et al.* Abnormal associative plasticity of the human motor cortex in writer's cramp. *Brain* 126, 2586-2596, doi:10.1093/brain/awg273 (2003).
- 67 Quartarone, A. *et al.* Enhanced long-term potentiation-like plasticity of the trigeminal blink reflex circuit in blepharospasm. *J Neurosci* 26, 716-721, doi:10.1523/JNEUROSCI.3948-05.2006 (2006).
- 68 Edwards, M. J., Huang, Y. Z., Mir, P., Rothwell, J. C. & Bhatia, K. P. Abnormalities in motor cortical plasticity differentiate manifesting and nonmanifesting DYT1 carriers. *Mov Disord* 21, 2181-2186, doi:10.1002/mds.21160 (2006).
- 69 Quartarone, A. *et al.* Abnormal plasticity of sensorimotor circuits extends beyond the affected body part in focal dystonia. *J Neurol Neurosurg Psychiatry* 79, 985-990, doi:10.1136/jnnp.2007.121632 (2008).
- 70 Byl, N. N., Merzenich, M. M. & Jenkins, W. M. A primate genesis model of focal dystonia and repetitive strain injury: I. Learning-induced dedifferentiation of the representation of the hand in the primary somatosensory cortex in adult monkeys. *Neurology* 47, 508-520, doi:10.1212/wnl.47.2.508 (1996).
- 71 Martella, G. *et al.* Impairment of bidirectional synaptic plasticity in the striatum of a mouse model of DYT1 dystonia: role of endogenous acetylcholine. *Brain* 132, 2336-2349, doi:10.1093/brain/awp194 (2009).
- 72 Quartarone, A., Rizzo, V. & Morgante, F. Clinical features of dystonia: a pathophysiological revisit. *Curr Opin Neurol* 21, 484-490, doi:10.1097/WCO.0b013e328307bf07 (2008).
- 73 Lanciego, J. L., Luquin, N. & Obeso, J. A. Functional neuroanatomy of the basal ganglia. *Cold Spring Harb Perspect Med* 2, a009621, doi:10.1101/cshperspect.a009621 (2012).
- 74 Bolam, J. P., Hanley, J. J., Booth, P. A. & Bevan, M. D. Synaptic organisation of the basal ganglia. *J Anat* 196 ( Pt 4), 527-542, doi:10.1046/j.1469-7580.2000.19640527.x (2000).
- 75 Calabresi, P., Picconi, B., Tozzi, A., Ghiglieri, V. & Di Filippo, M. Direct and indirect pathways of basal ganglia: a critical reappraisal. *Nat Neurosci* 17, 1022-1030, doi:10.1038/nn.3743 (2014).
- 76 Do, J., Kim, J. I., Bakes, J., Lee, K. & Kaang, B. K. Functional roles of neurotransmitters and neuromodulators in the dorsal striatum. *Learn Mem* 20, 21-28, doi:10.1101/lm.025015.111 (2012).
- 77 Ding, J. B., Guzman, J. N., Peterson, J. D., Goldberg, J. A. & Surmeier, D. J. Thalamic gating of corticostriatal signaling by cholinergic interneurons. *Neuron* 67, 294-307, doi:10.1016/j.neuron.2010.06.017 (2010).
- 78 Gerfen, C. R. *et al.* D1 and D2 dopamine receptor-regulated gene expression of striatonigral and striatopallidal neurons. *Science* 250, 1429-1432 (1990).
- 79 Groenewegen, H. J. The basal ganglia and motor control. *Neural Plast* 10, 107-120, doi:10.1155/NP.2003.107 (2003).
- 80 Nobrega, J. N., Richter, A., Jiwa, D., Raymond, R. & Loscher, W. Regional alterations in neuronal activity in dystonic hamster brain determined by quantitative cytochrome oxidase histochemistry. *Neuroscience* 83, 1215-1223 (1998).
- 81 Reese, R. & Volkmann, J. Deep Brain Stimulation for the Dystonias: Evidence, Knowledge Gaps, and Practical Considerations. *Mov Disord Clin Pract* 4, 486-494, doi:10.1002/mdc3.12519 (2017).
- 82 Simonyan, K., Cho, H., Hamzehei Sichani, A., Rubien-Thomas, E. & Hallett, M. The direct basal ganglia pathway is hyperfunctional in focal dystonia. *Brain* 140, 3179-3190, doi:10.1093/brain/awx263 (2017).
- 83 Kawaguchi, Y., Wilson, C. J., Augood, S. J. & Emson, P. C. Striatal interneurons: chemical, physiological and morphological characterization. *Trends Neurosci* 18, 527-535 (1995).
- 84 Tepper, J. M. & Bolam, J. P. Functional diversity and specificity of neostriatal interneurons. *Curr Opin Neurobiol* 14, 685-692, doi:10.1016/j.conb.2004.10.003 (2004).

- 85 Tepper, J. M., Tecuapetla, F., Koos, T. & Ibanez-Sandoval, O. Heterogeneity and diversity of striatal GABAergic interneurons. *Front Neuroanat* 4, 150, doi:10.3389/fnana.2010.00150 (2010).
- 86 Doig, N. M., Magill, P. J., Apicella, P., Bolam, J. P. & Sharott, A. Cortical and thalamic excitation mediate the multiphasic responses of striatal cholinergic interneurons to motivationally salient stimuli. *J Neurosci* 34, 3101-3117, doi:10.1523/JNEUROSCI.4627-13.2014 (2014).
- 87 English, D. F. *et al.* GABAergic circuits mediate the reinforcement-related signals of striatal cholinergic interneurons. *Nat Neurosci* 15, 123-130, doi:10.1038/nn.2984 (2011).
- 88 Maurice, N. *et al.* D2 dopamine receptor-mediated modulation of voltage-dependent Na<sup>+</sup> channels reduces autonomous activity in striatal cholinergic interneurons. *J Neurosci* 24, 10289-10301, doi:10.1523/JNEUROSCI.2155-04.2004 (2004).
- 89 Koos, T. & Tepper, J. M. Dual cholinergic control of fast-spiking interneurons in the neostriatum. *J Neurosci* 22, 529-535 (2002).
- 90 Threlfell, S. *et al.* Striatal dopamine release is triggered by synchronized activity in cholinergic interneurons. *Neuron* 75, 58-64, doi:10.1016/j.neuron.2012.04.038 (2012).
- 91 Bernard, V., Normand, E. & Bloch, B. Phenotypical characterization of the rat striatal neurons expressing muscarinic receptor genes. *J Neurosci* 12, 3591-3600 (1992).
- 92 Kreitzer, A. C. Physiology and pharmacology of striatal neurons. *Annu Rev Neurosci* 32, 127-147, doi:10.1146/annurev.neuro.051508.135422 (2009).
- 93 Higley, M. J. *et al.* Cholinergic interneurons mediate fast VGLUT3-dependent glutamatergic transmission in the striatum. *PLoS One* 6, e19155, doi:10.1371/journal.pone.0019155 (2011).
- 94 Tepper, J. M. *et al.* Heterogeneity and Diversity of Striatal GABAergic Interneurons: Update 2018. *Front Neuroanat* 12, 91, doi:10.3389/fnana.2018.00091 (2018).
- 95 Centonze, D., Gubellini, P., Pisani, A., Bernardi, G. & Calabresi, P. Dopamine, acetylcholine and nitric oxide systems interact to induce corticostriatal synaptic plasticity. *Rev Neurosci* 14, 207-216 (2003).
- 96 Calabresi, P. *et al.* A critical role of the nitric oxide/cGMP pathway in corticostriatal long-term depression. *J Neurosci* 19, 2489-2499 (1999).
- 97 Assous, M. & Tepper, J. M. Excitatory extrinsic afferents to striatal interneurons and interactions with striatal microcircuitry. *Eur J Neurosci* 49, 593-603, doi:10.1111/ejn.13881 (2019).
- 98 Levy, L. M. & Hallett, M. Impaired brain GABA in focal dystonia. *Ann Neurol* 51, 93-101 (2002).
- 99 Gittis, A. H. *et al.* Selective inhibition of striatal fast-spiking interneurons causes dyskinesias. *J Neurosci* 31, 15727-15731, doi:10.1523/JNEUROSCI.3875-11.2011 (2011).
- 100 Gernert, M., Hamann, M., Bennay, M., Loscher, W. & Richter, A. Deficit of striatal parvalbumin-reactive GABAergic interneurons and decreased basal ganglia output in a genetic rodent model of idiopathic paroxysmal dystonia. *J Neurosci* 20, 7052-7058 (2000).
- 101 Pappas, S. S. *et al.* Forebrain deletion of the dystonia protein torsinA causes dystonic-like movements and loss of striatal cholinergic neurons. *Elife* 4, e08352, doi:10.7554/eLife.08352 (2015).
- 102 Song, C. H. *et al.* Subtle microstructural changes of the striatum in a DYT1 knock-in mouse model of dystonia. *Neurobiol Dis* 54, 362-371, doi:10.1016/j.nbd.2013.01.008 (2013).
- 103 Ayano, G. Dopamine: Receptors, Functions, Synthesis, Pathways, Locations and Mental Disorders: Review of Literatures. *J Ment Disord Treat* 2, doi:10.4172/2471-271X.1000120 (2016).
- 104 Meiser, J., Weindl, D. & Hiller, K. Complexity of dopamine metabolism. *Cell Commun Signal* 11, 34, doi:10.1186/1478-811X-11-34 (2013).

- 105 Bracci, E., Centonze, D., Bernardi, G. & Calabresi, P. Dopamine excites fast-spiking interneurons in the striatum. *J Neurophysiol* 87, 2190-2194, doi:10.1152/jn.00754.2001 (2002).
- 106 Centonze, D. *et al.* Activation of dopamine D1-like receptors excites LTS interneurons of the striatum. *Eur J Neurosci* 15, 2049-2052 (2002).
- 107 Shashidharan, P. *et al.* Transgenic mouse model of early-onset DYT1 dystonia. *Hum Mol Genet* 14, 125-133, doi:10.1093/hmg/ddi012 (2005).
- 108 Song, C. H., Fan, X., Exeter, C. J., Hess, E. J. & Jinnah, H. A. Functional analysis of dopaminergic systems in a DYT1 knock-in mouse model of dystonia. *Neurobiol Dis* 48, 66-78, doi:10.1016/j.nbd.2012.05.009 (2012).
- 109 Rostasy, K. *et al.* TorsinA protein and neuropathology in early onset generalized dystonia with GAG deletion. *Neurobiol Dis* 12, 11-24 (2003).
- 110 Torres, G. E., Sweeney, A. L., Beaulieu, J. M., Shashidharan, P. & Caron, M. G. Effect of torsinA on membrane proteins reveals a loss of function and a dominant-negative phenotype of the dystonia-associated DeltaE-torsinA mutant. *Proc Natl Acad Sci U S A* 101, 15650-15655, doi:10.1073/pnas.0308088101 (2004).
- 111 Augood, S. J. *et al.* Distribution and ultrastructural localization of torsinA immunoreactivity in the human brain. *Brain Res* 986, 12-21 (2003).
- 112 Augood, S. J. *et al.* Distribution of the mRNAs encoding torsinA and torsinB in the normal adult human brain. *Ann Neurol* 46, 761-769 (1999).
- 113 Lv, J. & Liu, F. The Role of Serotonin beyond the Central Nervous System during Embryogenesis. *Front Cell Neurosci* 11, 74, doi:10.3389/fncel.2017.00074 (2017).
- 114 Fidalgo, S., Ivanov, D. K. & Wood, S. H. Serotonin: from top to bottom. *Biogerontology* 14, 21-45, doi:10.1007/s10522-012-9406-3 (2013).
- 115 Di Matteo, V. *et al.* Serotonin modulation of the basal ganglia circuitry: therapeutic implication for Parkinson's disease and other motor disorders. *Prog Brain Res* 172, 423-463, doi:10.1016/S0079-6123(08)00921-7 (2008).
- 116 Erickson, J. D., Schafer, M. K., Bonner, T. I., Eiden, L. E. & Weihe, E. Distinct pharmacological properties and distribution in neurons and endocrine cells of two isoforms of the human vesicular monoamine transporter. *Proc Natl Acad Sci U S A* 93, 5166-5171, doi:10.1073/pnas.93.10.5166 (1996).
- 117 Filip, M. & Bader, M. Overview on 5-HT receptors and their role in physiology and pathology of the central nervous system. *Pharmacol Rep* 61, 761-777 (2009).
- 118 Marston, O. J., Garfield, A. S. & Heisler, L. K. Role of central serotonin and melanocortin systems in the control of energy balance. *Eur J Pharmacol* 660, 70-79, doi:10.1016/j.ejphar.2010.12.024 (2011).
- 119 Best, J., Nijhout, H. F. & Reed, M. Serotonin synthesis, release and reuptake in terminals: a mathematical model. *Theor Biol Med Model* 7, 34, doi:10.1186/1742-4682-7-34 (2010).
- 120 Sandyk, R. & Fisher, H. Serotonin in involuntary movement disorders. *Int J Neurosci* 42, 185-208 (1988).
- 121 Wallman, M. J., Gagnon, D. & Parent, M. Serotonin innervation of human basal ganglia. *Eur J Neurosci* 33, 1519-1532, doi:10.1111/j.1460-9568.2011.07621.x (2011).
- 122 Smit, M. *et al.* Serotonergic perturbations in dystonia disorders-a systematic review. *Neurosci Biobehav Rev* 65, 264-275, doi:10.1016/j.neubiorev.2016.03.015 (2016).
- 123 Hornykiewicz, O., Kish, S. J., Becker, L. E., Farley, I. & Shannak, K. Brain neurotransmitters in dystonia musculorum deformans. *N Engl J Med* 315, 347-353, doi:10.1056/NEJM198608073150602 (1986).
- 124 Di Giovanni, G., Esposito, E. & Di Matteo, V. Role of serotonin in central dopamine dysfunction. *CNS Neurosci Ther* 16, 179-194, doi:10.1111/j.1755-5949.2010.00135.x (2010).
- 125 Kramer, P. L. *et al.* The DYT1 gene on 9q34 is responsible for most cases of early limb-onset idiopathic torsion dystonia in non-Jews. *Am J Hum Genet* 55, 468-475 (1994).
- 126 Saunders-Pullman, R. *et al.* Narrowing the DYT6 dystonia region and evidence for locus heterogeneity in the Amish-Mennonites. *Am J Med Genet A* 143A, 2098-2105, doi:10.1002/ajmg.a.31887 (2007).

- 127 Ichinose, H. *et al.* Hereditary progressive dystonia with marked diurnal fluctuation caused by mutations in the GTP cyclohydrolase I gene. *Nat Genet* 8, 236-242, doi:10.1038/ng1194-236 (1994).
- 128 Edwards, M., Wood, N. & Bhatia, K. Unusual phenotypes in DYT1 dystonia: a report of five cases and a review of the literature. *Mov Disord* 18, 706-711, doi:10.1002/mds.10411 (2003).
- 129 Saint Hilaire, M. H., Burke, R. E., Bressman, S. B., Brin, M. F. & Fahn, S. Delayed-onset dystonia due to perinatal or early childhood asphyxia. *Neurology* 41, 216-222, doi:10.1212/wnl.41.2\_part\_1.216 (1991).
- 130 Jankovic, J. Peripherally induced movement disorders. *Neurol Clin* 27, 821-832, vii, doi:10.1016/j.ncl.2009.04.005 (2009).
- 131 Risch, N. J., Bressman, S. B., Senthil, G. & Ozelius, L. J. Intragenic Cis and Trans modification of genetic susceptibility in DYT1 torsion dystonia. *Am J Hum Genet* 80, 1188-1193, doi:10.1086/518427 (2007).
- 132 Martino, D. *et al.* Extragenetic factors and clinical penetrance of DYT1 dystonia: an exploratory study. *J Neurol* 260, 1081-1086, doi:10.1007/s00415-012-6765-2 (2013).
- 133 Jankovic, J. & Van der Linden, C. Dystonia and tremor induced by peripheral trauma: predisposing factors. *J Neurol Neurosurg Psychiatry* 51, 1512-1519, doi:10.1136/jnnp.51.12.1512 (1988).
- 134 Macerollo, A. *et al.* Peripheral trauma and risk of dystonia: What are the evidences and potential co-risk factors from a population insurance database? *PLoS One* 14, e0216772, doi:10.1371/journal.pone.0216772 (2019).
- 135 Kumar, H. & Jog, M. Peripheral trauma induced dystonia or post-traumatic syndrome? *Can J Neurol Sci* 38, 22-29, doi:10.1017/s0317167100011057 (2011).
- 136 Cloud, L. J. & Jinnah, H. A. Treatment strategies for dystonia. *Expert Opin Pharmacother* 11, 5-15, doi:10.1517/14656560903426171 (2010).
- 137 Jinnah, H. A. & Factor, S. A. Diagnosis and treatment of dystonia. *Neurol Clin* 33, 77-100, doi:10.1016/j.ncl.2014.09.002 (2015).
- 138 Kupsch, A. *et al.* Pallidal deep-brain stimulation in primary generalized or segmental dystonia. *N Engl J Med* 355, 1978-1990, doi:10.1056/NEJMoa063618 (2006).
- 139 Vidailhet, M. *et al.* Bilateral deep-brain stimulation of the globus pallidus in primary generalized dystonia. *N Engl J Med* 352, 459-467, doi:10.1056/NEJMoa042187 (2005).
- 140 Tagliati, M., Shils, J., Sun, C. & Alterman, R. Deep brain stimulation for dystonia. *Expert Rev Med Devices* 1, 33-41, doi:10.1586/17434440.1.1.33 (2004).
- 141 Krauss, J. K., Yianni, J., Loher, T. J. & Aziz, T. Z. Deep brain stimulation for dystonia. *J Clin Neurophysiol* 21, 18-30 (2004).
- 142 Isaias, I. U., Alterman, R. L. & Tagliati, M. Outcome predictors of pallidal stimulation in patients with primary dystonia: the role of disease duration. *Brain* 131, 1895-1902, doi:10.1093/brain/awn120 (2008).
- 143 Yianni, J. *et al.* Post-operative progress of dystonia patients following globus pallidus internus deep brain stimulation. *Eur J Neurol* 10, 239-247 (2003).
- 144 Cif, L. *et al.* Long-term follow-up of DYT1 dystonia patients treated by deep brain stimulation: an open-label study. *Mov Disord* 25, 289-299, doi:10.1002/mds.22802 (2010).
- 145 Vidailhet, M. *et al.* Bilateral, pallidal, deep-brain stimulation in primary generalised dystonia: a prospective 3 year follow-up study. *Lancet Neurol* 6, 223-229, doi:10.1016/S1474-4422(07)70035-2 (2007).
- 146 Cif, L. *et al.* Treatment of dystonic syndromes by chronic electrical stimulation of the internal globus pallidus. *J Neurosurg Sci* 47, 52-55 (2003).
- 147 Coubes, P. *et al.* Electrical stimulation of the globus pallidus internus in patients with primary generalized dystonia: long-term results. *J Neurosurg* 101, 189-194, doi:10.3171/jns.2004.101.2.0189 (2004).
- 148 Panov, F. *et al.* Deep brain stimulation in DYT1 dystonia: a 10-year experience. *Neurosurgery* 73, 86-93; discussion 93, doi:10.1227/01.neu.0000429841.84083.c8 (2013).

- 149 Ruge, D. *et al.* Shaping reversibility? Long-term deep brain stimulation in dystonia: the relationship between effects on electrophysiology and clinical symptoms. *Brain* 134, 2106-2115, doi:10.1093/brain/awr122 (2011).
- 150 Grabli, D. *et al.* Interruption of deep brain stimulation of the globus pallidus in primary generalized dystonia. *Mov Disord* 24, 2363-2369, doi:10.1002/mds.22827 (2009).
- 151 DeLong, M. R. & Wichmann, T. Circuits and circuit disorders of the basal ganglia. *Arch Neurol* 64, 20-24, doi:10.1001/archneur.64.1.20 (2007).
- 152 Albanese, A. Deep brain stimulation for cervical dystonia. *Lancet Neurol* 13, 856-857, doi:10.1016/S1474-4422(14)70178-4 (2014).
- 153 Ozelius, L. J. *et al.* The early-onset torsion dystonia gene (DYT1) encodes an ATP-binding protein. *Nat Genet* 17, 40-48, doi:10.1038/ng0997-40 (1997).
- 154 Granata, A. & Warner, T. T. The role of torsinA in dystonia. *Eur J Neurol* 17 Suppl 1, 81-87, doi:10.1111/j.1468-1331.2010.03057.x (2010).
- 155 Ozelius, L. & Lubarr, N. in *GeneReviews((R))* (eds M. P. Adam *et al.*) (1993).
- 156 Klein, C., Lohmann, K., Marras, C. & Munchau, A. in *GeneReviews((R))* (eds M. P. Adam *et al.*) (1993).
- 157 Muller, U. The monogenic primary dystonias. *Brain* 132, 2005-2025, doi:10.1093/brain/awp172 (2009).
- 158 Kamm, C. Early onset torsion dystonia (Oppenheim's dystonia). *Orphanet J Rare Dis* 1, 48, doi:10.1186/1750-1172-1-48 (2006).
- 159 Krauss, J. K. Deep brain stimulation for dystonia in adults. Overview and developments. *Stereotact Funct Neurosurg* 78, 168-182, doi:10.1159/000068963 (2002).
- 160 Kustedjo, K., Bracey, M. H. & Cravatt, B. F. Torsin A and its torsion dystonia-associated mutant forms are luminal glycoproteins that exhibit distinct subcellular localizations. *J Biol Chem* 275, 27933-27939, doi:10.1074/jbc.M910025199 (2000).
- 161 Hanson, P. I. & Whiteheart, S. W. AAA+ proteins: have engine, will work. *Nat Rev Mol Cell Biol* 6, 519-529, doi:10.1038/nrm1684 (2005).
- 162 Maurizi, M. R. & Li, C. C. AAA proteins: in search of a common molecular basis. International Meeting on Cellular Functions of AAA Proteins. *EMBO Rep* 2, 980-985, doi:10.1093/embo-reports/kve229 (2001).
- 163 Shashidharan, P., Kramer, B. C., Walker, R. H., Olanow, C. W. & Brin, M. F. Immunohistochemical localization and distribution of torsinA in normal human and rat brain. *Brain Res* 853, 197-206 (2000).
- 164 Xiao, J., Gong, S., Zhao, Y. & LeDoux, M. S. Developmental expression of rat torsinA transcript and protein. *Brain Res Dev Brain Res* 152, 47-60, doi:10.1016/j.devbrainres.2004.05.012 (2004).
- 165 Augood, S. J. *et al.* Expression of the early-onset torsion dystonia gene (DYT1) in human brain. *Ann Neurol* 43, 669-673, doi:10.1002/ana.410430518 (1998).
- 166 Goodchild, R. E. & Dauer, W. T. The AAA+ protein torsinA interacts with a conserved domain present in LAP1 and a novel ER protein. *J Cell Biol* 168, 855-862, doi:10.1083/jcb.200411026 (2005).
- 167 Brown, R. S., Zhao, C., Chase, A. R., Wang, J. & Schlieker, C. The mechanism of Torsin ATPase activation. *Proc Natl Acad Sci U S A* 111, E4822-4831, doi:10.1073/pnas.1415271111 (2014).
- 168 Kamm, C. *et al.* The early onset dystonia protein torsinA interacts with kinesin light chain 1. *J Biol Chem* 279, 19882-19892, doi:10.1074/jbc.M401332200 (2004).
- 169 Goodchild, R. E. & Dauer, W. T. Mislocalization to the nuclear envelope: an effect of the dystonia-causing torsinA mutation. *Proc Natl Acad Sci U S A* 101, 847-852, doi:10.1073/pnas.0304375101 (2004).
- 170 Naismith, T. V., Heuser, J. E., Breakefield, X. O. & Hanson, P. I. TorsinA in the nuclear envelope. *Proc Natl Acad Sci U S A* 101, 7612-7617, doi:10.1073/pnas.0308760101 (2004).
- 171 Granata, A., Watson, R., Collinson, L. M., Schiavo, G. & Warner, T. T. The dystonia-associated protein torsinA modulates synaptic vesicle recycling. *J Biol Chem* 283, 7568-7579, doi:10.1074/jbc.M704097200 (2008).

- 172 Ferrari-Toninelli, G., Paccioretti, S., Francisconi, S., Uberti, D. & Memo, M. TorsinA negatively controls neurite outgrowth of SH-SY5Y human neuronal cell line. *Brain Res* 1012, 75-81, doi:10.1016/j.brainres.2004.02.080 (2004).
- 173 Helfand, B. T., Chang, L. & Goldman, R. D. The dynamic and motile properties of intermediate filaments. *Annu Rev Cell Dev Biol* 19, 445-467, doi:10.1146/annurev.cellbio.19.111401.092306 (2003).
- 174 Hewett, J. W., Zeng, J., Niland, B. P., Bragg, D. C. & Breakefield, X. O. Dystonia-causing mutant torsinA inhibits cell adhesion and neurite extension through interference with cytoskeletal dynamics. *Neurobiol Dis* 22, 98-111, doi:10.1016/j.nbd.2005.10.012 (2006).
- 175 Hewett, J. W. *et al.* Mutant torsinA interferes with protein processing through the secretory pathway in DYT1 dystonia cells. *Proc Natl Acad Sci U S A* 104, 7271-7276, doi:10.1073/pnas.0701185104 (2007).
- 176 Nery, F. C. *et al.* TorsinA participates in endoplasmic reticulum-associated degradation. *Nat Commun* 2, 393, doi:10.1038/ncomms1383 (2011).
- 177 Cao, S., Gelwix, C. C., Caldwell, K. A. & Caldwell, G. A. Torsin-mediated protection from cellular stress in the dopaminergic neurons of *Caenorhabditis elegans*. *J Neurosci* 25, 3801-3812, doi:10.1523/JNEUROSCI.5157-04.2005 (2005).
- 178 Chen, P. *et al.* The early-onset torsion dystonia-associated protein, torsinA, is a homeostatic regulator of endoplasmic reticulum stress response. *Hum Mol Genet* 19, 3502-3515, doi:10.1093/hmg/ddq266 (2010).
- 179 Hewett, J. *et al.* TorsinA in PC12 cells: localization in the endoplasmic reticulum and response to stress. *J Neurosci Res* 72, 158-168, doi:10.1002/jnr.10567 (2003).
- 180 Kuner, R. *et al.* TorsinA protects against oxidative stress in COS-1 and PC12 cells. *Neurosci Lett* 350, 153-156 (2003).
- 181 Goodchild, R. E., Kim, C. E. & Dauer, W. T. Loss of the dystonia-associated protein torsinA selectively disrupts the neuronal nuclear envelope. *Neuron* 48, 923-932, doi:10.1016/j.neuron.2005.11.010 (2005).
- 182 Naismith, T. V., Dalal, S. & Hanson, P. I. Interaction of torsinA with its major binding partners is impaired by the dystonia-associated DeltaGAG deletion. *J Biol Chem* 284, 27866-27874, doi:10.1074/jbc.M109.020164 (2009).
- 183 Demircioglu, F. E., Sosa, B. A., Ingram, J., Ploegh, H. L. & Schwartz, T. U. Structures of TorsinA and its disease-mutant complexed with an activator reveal the molecular basis for primary dystonia. *Elife* 5, doi:10.7554/eLife.17983 (2016).
- 184 Kustedjo, K., Deechongkit, S., Kelly, J. W. & Cravatt, B. F. Recombinant expression, purification, and comparative characterization of torsinA and its torsion dystonia-associated variant Delta E-torsinA. *Biochemistry* 42, 15333-15341, doi:10.1021/bi0349569 (2003).
- 185 Giles, L. M., Chen, J., Li, L. & Chin, L. S. Dystonia-associated mutations cause premature degradation of torsinA protein and cell-type-specific mislocalization to the nuclear envelope. *Hum Mol Genet* 17, 2712-2722, doi:10.1093/hmg/ddn173 (2008).
- 186 Gordon, K. L. & Gonzalez-Alegre, P. Consequences of the DYT1 mutation on torsinA oligomerization and degradation. *Neuroscience* 157, 588-595, doi:10.1016/j.neuroscience.2008.09.028 (2008).
- 187 Granata, A., Schiavo, G. & Warner, T. T. TorsinA and dystonia: from nuclear envelope to synapse. *J Neurochem* 109, 1596-1609, doi:10.1111/j.1471-4159.2009.06095.x (2009).
- 188 Grundmann, K. *et al.* Generation of a novel rodent model for DYT1 dystonia. *Neurobiol Dis* 47, 61-74, doi:10.1016/j.nbd.2012.03.024 (2012).
- 189 Gonzalez-Alegre, P. & Paulson, H. L. Aberrant cellular behavior of mutant torsinA implicates nuclear envelope dysfunction in DYT1 dystonia. *J Neurosci* 24, 2593-2601, doi:10.1523/JNEUROSCI.4461-03.2004 (2004).
- 190 Sharma, N. *et al.* Impaired motor learning in mice expressing torsinA with the DYT1 dystonia mutation. *J Neurosci* 25, 5351-5355, doi:10.1523/JNEUROSCI.0855-05.2005 (2005).

- 191 McNaught, K. S. *et al.* Brainstem pathology in DYT1 primary torsion dystonia. *Ann Neurol* 56, 540-547, doi:10.1002/ana.20225 (2004).
- 192 Walker, R. H., Brin, M. F., Sandu, D., Good, P. F. & Shashidharan, P. TorsinA immunoreactivity in brains of patients with DYT1 and non-DYT1 dystonia. *Neurology* 58, 120-124, doi:10.1212/wnl.58.1.120 (2002).
- 193 Pratt, D. *et al.* Diminishing evidence for torsinA-positive neuronal inclusions in DYT1 dystonia. *Acta Neuropathol Commun* 4, 85, doi:10.1186/s40478-016-0362-z (2016).
- 194 Wilson, B. K. & Hess, E. J. Animal models for dystonia. *Mov Disord* 28, 982-989, doi:10.1002/mds.25526 (2013).
- 195 Fredow, G. & Loscher, W. Effects of pharmacological manipulation of GABAergic neurotransmission in a new mutant hamster model of paroxysmal dystonia. *Eur J Pharmacol* 192, 207-219, doi:10.1016/0014-2999(91)90045-r (1991).
- 196 Loscher, W. *et al.* The sz mutant hamster: a genetic model of epilepsy or of paroxysmal dystonia? *Mov Disord* 4, 219-232, doi:10.1002/mds.870040304 (1989).
- 197 Pizoli, C. E., Jinnah, H. A., Billingsley, M. L. & Hess, E. J. Abnormal cerebellar signaling induces dystonia in mice. *J Neurosci* 22, 7825-7833 (2002).
- 198 Oleas, J., Yokoi, F., DeAndrade, M. P., Pisani, A. & Li, Y. Engineering animal models of dystonia. *Mov Disord* 28, 990-1000, doi:10.1002/mds.25583 (2013).
- 199 Yokoi, F., Dang, M. T., Mitsui, S., Li, J. & Li, Y. Motor deficits and hyperactivity in cerebral cortex-specific Dyt1 conditional knockout mice. *J Biochem* 143, 39-47, doi:10.1093/jb/mvm191 (2008).
- 200 Dang, M. T. *et al.* Disrupted motor learning and long-term synaptic plasticity in mice lacking NMDAR1 in the striatum. *Proc Natl Acad Sci U S A* 103, 15254-15259, doi:10.1073/pnas.0601758103 (2006).
- 201 Rossi, J. *et al.* Melanocortin-4 receptors expressed by cholinergic neurons regulate energy balance and glucose homeostasis. *Cell Metab* 13, 195-204, doi:10.1016/j.cmet.2011.01.010 (2011).
- 202 Page, M. E. *et al.* Cell-autonomous alteration of dopaminergic transmission by wild type and mutant (DeltaE) TorsinA in transgenic mice. *Neurobiol Dis* 39, 318-326, doi:10.1016/j.nbd.2010.04.016 (2010).
- 203 Oostenveld, R., Fries, P., Maris, E. & Schoffelen, J. M. FieldTrip: Open source software for advanced analysis of MEG, EEG, and invasive electrophysiological data. *Comput Intell Neurosci* 2011, 156869, doi:10.1155/2011/156869 (2011).
- 204 Nolte, G. *et al.* Identifying true brain interaction from EEG data using the imaginary part of coherency. *Clin Neurophysiol* 115, 2292-2307, doi:10.1016/j.clinph.2004.04.029 (2004).
- 205 Paxinos, G. & Watson, C. *The Rat Brain in Stereotaxic Coordinates*. 6th edn, (Academic Press, 2007).
- 206 Wang, Z., Gerstein, M. & Snyder, M. RNA-Seq: a revolutionary tool for transcriptomics. *Nat Rev Genet* 10, 57-63, doi:10.1038/nrg2484 (2009).
- 207 Dobin, A. *et al.* STAR: ultrafast universal RNA-seq aligner. *Bioinformatics* 29, 15-21, doi:10.1093/bioinformatics/bts635 (2013).
- 208 Liao, Y., Smyth, G. K. & Shi, W. featureCounts: an efficient general purpose program for assigning sequence reads to genomic features. *Bioinformatics* 30, 923-930, doi:10.1093/bioinformatics/btt656 (2014).
- 209 Love, M. I., Huber, W. & Anders, S. Moderated estimation of fold change and dispersion for RNA-seq data with DESeq2. *Genome Biol* 15, 550, doi:10.1186/s13059-014-0550-8 (2014).
- 210 Wagner, G. P., Kin, K. & Lynch, V. J. Measurement of mRNA abundance using RNA-seq data: RPKM measure is inconsistent among samples. *Theory Biosci* 131, 281-285, doi:10.1007/s12064-012-0162-3 (2012).
- 211 Chen, E. Y. *et al.* Enrichr: interactive and collaborative HTML5 gene list enrichment analysis tool. *BMC Bioinformatics* 14, 128, doi:10.1186/1471-2105-14-128 (2013).
- 212 Kuleshov, M. V. *et al.* Enrichr: a comprehensive gene set enrichment analysis web server 2016 update. *Nucleic Acids Res* 44, W90-97, doi:10.1093/nar/gkw377 (2016).

- 213 Lowry, O. H., Rosebrough, N. J., Farr, A. L. & Randall, R. J. Protein measurement with the Folin phenol reagent. *J Biol Chem* 193, 265-275 (1951).
- 214 Gioltzoglou, T., Milonas, I. & Lees, A. J. Case of DYT1 dystonia triggered by bite from a moray. *Mov Disord* 21, 1536-1537, doi:10.1002/mds.20994 (2006).
- 215 Attwell, D. & Laughlin, S. B. An energy budget for signaling in the grey matter of the brain. *J Cereb Blood Flow Metab* 21, 1133-1145, doi:10.1097/00004647-200110000-00001 (2001).
- 216 Sharott, A. *et al.* Is the synchronization between pallidal and muscle activity in primary dystonia due to peripheral afference or a motor drive? *Brain* 131, 473-484, doi:10.1093/brain/awm324 (2008).
- 217 Neumann, W. J. *et al.* Pallidal and thalamic neural oscillatory patterns in tourette's syndrome. *Ann Neurol* 84, 505-514, doi:10.1002/ana.25311 (2018).
- 218 Alegre, M. *et al.* Subthalamic activity during diphasic dyskinesias in Parkinson's disease. *Mov Disord* 27, 1178-1181, doi:10.1002/mds.25090 (2012).
- 219 Neumann, W. J. & Kuhn, A. A. Reply: Role of cortico-pallidal connectivity in the pathophysiology of dystonia. *Brain* 139, e49, doi:10.1093/brain/aww105 (2016).
- 220 Andrews, C., Aviles-Olmos, I., Hariz, M. & Foltynie, T. Which patients with dystonia benefit from deep brain stimulation? A metaregression of individual patient outcomes. *J Neurol Neurosurg Psychiatry* 81, 1383-1389, doi:10.1136/jnnp.2010.207993 (2010).
- 221 Isaias, I. U., Alterman, R. L. & Tagliati, M. Deep brain stimulation for primary generalized dystonia: long-term outcomes. *Arch Neurol* 66, 465-470, doi:10.1001/archneurol.2009.20 (2009).
- 222 Jinnah, H. A. *et al.* Deep brain stimulation for dystonia: a novel perspective on the value of genetic testing. *J Neural Transm (Vienna)* 124, 417-430, doi:10.1007/s00702-016-1656-9 (2017).
- 223 Ruge, D. *et al.* Deep brain stimulation effects in dystonia: time course of electrophysiological changes in early treatment. *Mov Disord* 26, 1913-1921, doi:10.1002/mds.23731 (2011).
- 224 Lundgaard, I. *et al.* Direct neuronal glucose uptake heralds activity-dependent increases in cerebral metabolism. *Nat Commun* 6, 6807, doi:10.1038/ncomms7807 (2015).
- 225 Trost, M. *et al.* Primary dystonia: is abnormal functional brain architecture linked to genotype? *Ann Neurol* 52, 853-856, doi:10.1002/ana.10418 (2002).
- 226 Jang, D. P. *et al.* Functional neuroimaging of the 6-OHDA lesion rat model of Parkinson's disease. *Neurosci Lett* 513, 187-192, doi:10.1016/j.neulet.2012.02.034 (2012).
- 227 Dauer, W. Inherited isolated dystonia: clinical genetics and gene function. *Neurotherapeutics* 11, 807-816, doi:10.1007/s13311-014-0297-7 (2014).
- 228 Vizcarra-Chacon, B. J. *et al.* Contribution of different classes of glutamate receptors in the corticostriatal polysynaptic responses from striatal direct and indirect projection neurons. *BMC Neurosci* 14, 60, doi:10.1186/1471-2202-14-60 (2013).
- 229 Klockgether, T. & Turski, L. Toward an understanding of the role of glutamate in experimental parkinsonism: agonist-sensitive sites in the basal ganglia. *Ann Neurol* 34, 585-593, doi:10.1002/ana.410340413 (1993).
- 230 Tsai, G. *et al.* Markers of glutamatergic neurotransmission and oxidative stress associated with tardive dyskinesia. *Am J Psychiatry* 155, 1207-1213, doi:10.1176/ajp.155.9.1207 (1998).
- 231 Nobrega, J. N., Raymond, R., Barlow, K., Hamann, M. & Richter, A. Changes in AMPA receptor binding in an animal model of inborn paroxysmal dystonia. *Exp Neurol* 176, 371-376, doi:10.1006/exnr.2002.7932 (2002).
- 232 Maltese, M. *et al.* Early structural and functional plasticity alterations in a susceptibility period of DYT1 dystonia mouse striatum. *Elife* 7, doi:10.7554/eLife.33331 (2018).
- 233 Platzer, K. *et al.* GRIN2B encephalopathy: novel findings on phenotype, variant clustering, functional consequences and treatment aspects. *J Med Genet* 54, 460-470, doi:10.1136/jmedgenet-2016-104509 (2017).

- 234 Martin, S. *et al.* De Novo Variants in GRIA4 Lead to Intellectual Disability with or without Seizures and Gait Abnormalities. *Am J Hum Genet* 101, 1013-1020, doi:10.1016/j.ajhg.2017.11.004 (2017).
- 235 Madeo, M. *et al.* Loss-of-Function Mutations in FRRS1L Lead to an Epileptic-Dyskinetic Encephalopathy. *Am J Hum Genet* 98, 1249-1255, doi:10.1016/j.ajhg.2016.04.008 (2016).
- 236 Stewart, M. *et al.* Loss of Frrs1l disrupts synaptic AMPA receptor function, and results in neurodevelopmental, motor, cognitive and electrographical abnormalities. *Dis Model Mech* 12, doi:10.1242/dmm.036806 (2019).
- 237 Pisani, A., Bernardi, G., Ding, J. & Surmeier, D. J. Re-emergence of striatal cholinergic interneurons in movement disorders. *Trends Neurosci* 30, 545-553, doi:10.1016/j.tins.2007.07.008 (2007).
- 238 Eskow Jaunarajs, K. L., Bonsi, P., Chesselet, M. F., Standaert, D. G. & Pisani, A. Striatal cholinergic dysfunction as a unifying theme in the pathophysiology of dystonia. *Prog Neurobiol* 127-128, 91-107, doi:10.1016/j.pneurobio.2015.02.002 (2015).
- 239 Hamann, M. *et al.* Alterations of M1 and M4 acetylcholine receptors in the genetically dystonic (dt(sz)) hamster and moderate antidystonic efficacy of M1 and M4 anticholinergics. *Neuroscience* 357, 84-98, doi:10.1016/j.neuroscience.2017.05.051 (2017).
- 240 Sciamanna, G. *et al.* Cholinergic dysregulation produced by selective inactivation of the dystonia-associated protein torsinA. *Neurobiol Dis* 47, 416-427, doi:10.1016/j.nbd.2012.04.015 (2012).
- 241 Placzek, M. R. *et al.* Cervical dystonia is associated with a polymorphism in the dopamine (D5) receptor gene. *J Neurol Neurosurg Psychiatry* 71, 262-264, doi:10.1136/jnnp.71.2.262 (2001).
- 242 Knappskog, P. M., Flatmark, T., Mallet, J., Ludecke, B. & Bartholome, K. Recessively inherited L-DOPA-responsive dystonia caused by a point mutation (Q381K) in the tyrosine hydroxylase gene. *Hum Mol Genet* 4, 1209-1212, doi:10.1093/hmg/4.7.1209 (1995).
- 243 Klein, C. *et al.* Association of a missense change in the D2 dopamine receptor with myoclonus dystonia. *Proc Natl Acad Sci U S A* 96, 5173-5176, doi:10.1073/pnas.96.9.5173 (1999).
- 244 Vercueil, L. & Foucher, J. Risperidone-induced tardive dystonia and psychosis. *Lancet* 353, 981, doi:10.1016/S0140-6736(99)00193-2 (1999).
- 245 Dunayevich, E. & Strakowski, S. M. Olanzapine-induced tardive dystonia. *Am J Psychiatry* 156, 1662, doi:10.1176/ajp.156.10.1662 (1999).
- 246 Iacono, D., Geraci-Erck, M., Peng, H., Rabin, M. L. & Kurlan, R. Hypertrophy of nigral neurons in Torsin1A deletion (DYT1) carriers manifesting dystonia. *Parkinsonism Relat Disord* 58, 63-69, doi:10.1016/j.parkreldis.2018.08.020 (2019).
- 247 Zhao, Y., DeCuypere, M. & LeDoux, M. S. Abnormal motor function and dopamine neurotransmission in DYT1 DeltaGAG transgenic mice. *Exp Neurol* 210, 719-730, doi:10.1016/j.expneurol.2007.12.027 (2008).
- 248 Kuhn, A. A., Kupsch, A., Schneider, G. H. & Brown, P. Reduction in subthalamic 8-35 Hz oscillatory activity correlates with clinical improvement in Parkinson's disease. *Eur J Neurosci* 23, 1956-1960, doi:10.1111/j.1460-9568.2006.04717.x (2006).
- 249 Tinkhauser, G. *et al.* Beta burst dynamics in Parkinson's disease OFF and ON dopaminergic medication. *Brain* 140, 2968-2981, doi:10.1093/brain/awx252 (2017).
- 250 Weinberger, M. *et al.* Beta oscillatory activity in the subthalamic nucleus and its relation to dopaminergic response in Parkinson's disease. *J Neurophysiol* 96, 3248-3256, doi:10.1152/jn.00697.2006 (2006).
- 251 Pettibone, D. J., Totaro, J. A. & Pflueger, A. B. Tetrabenazine-induced depletion of brain monoamines: characterization and interaction with selected antidepressants. *Eur J Pharmacol* 102, 425-430, doi:10.1016/0014-2999(84)90562-4 (1984).
- 252 Kuhn, A. A. *et al.* Increased beta activity in dystonia patients after drug-induced dopamine deficiency. *Exp Neurol* 214, 140-143, doi:10.1016/j.expneurol.2008.07.023 (2008).

- 253 Ip, C. W. *et al.* Tor1a<sup>+/-</sup> mice develop dystonia-like movements via a striatal dopaminergic dysregulation triggered by peripheral nerve injury. *Acta Neuropathol Commun* 4, 108, doi:10.1186/s40478-016-0375-7 (2016).
- 254 Giros, B., Jaber, M., Jones, S. R., Wightman, R. M. & Caron, M. G. Hyperlocomotion and indifference to cocaine and amphetamine in mice lacking the dopamine transporter. *Nature* 379, 606-612, doi:10.1038/379606a0 (1996).
- 255 Carbon, M. & Eidelberg, D. Abnormal structure-function relationships in hereditary dystonia. *Neuroscience* 164, 220-229, doi:10.1016/j.neuroscience.2008.12.041 (2009).
- 256 Bonsi, P. *et al.* RGS9-2 rescues dopamine D2 receptor levels and signaling in DYT1 dystonia mouse models. *EMBO Mol Med* 11, doi:10.15252/emmm.201809283 (2019).
- 257 Napolitano, F. *et al.* Dopamine D2 receptor dysfunction is rescued by adenosine A2A receptor antagonism in a model of DYT1 dystonia. *Neurobiol Dis* 38, 434-445, doi:10.1016/j.nbd.2010.03.003 (2010).
- 258 Pisani, A. *et al.* Altered responses to dopaminergic D2 receptor activation and N-type calcium currents in striatal cholinergic interneurons in a mouse model of DYT1 dystonia. *Neurobiol Dis* 24, 318-325, doi:10.1016/j.nbd.2006.07.006 (2006).
- 259 Sciamanna, G. *et al.* Impaired striatal D2 receptor function leads to enhanced GABA transmission in a mouse model of DYT1 dystonia. *Neurobiol Dis* 34, 133-145, doi:10.1016/j.nbd.2009.01.001 (2009).
- 260 Dang, M. T. *et al.* An anticholinergic reverses motor control and corticostriatal LTD deficits in Dyt1 DeltaGAG knock-in mice. *Behav Brain Res* 226, 465-472, doi:10.1016/j.bbr.2011.10.002 (2012).
- 261 Nautiyal, K. M. *et al.* Distinct Circuits Underlie the Effects of 5-HT1B Receptors on Aggression and Impulsivity. *Neuron* 86, 813-826, doi:10.1016/j.neuron.2015.03.041 (2015).
- 262 Whitney, M. S. *et al.* Adult Brain Serotonin Deficiency Causes Hyperactivity, Circadian Disruption, and Elimination of Siestas. *J Neurosci* 36, 9828-9842, doi:10.1523/JNEUROSCI.1469-16.2016 (2016).
- 263 Hornykiewicz, O., Kish, S. J., Becker, L. E., Farley, I. & Shannak, K. Biochemical evidence for brain neurotransmitter changes in idiopathic torsion dystonia (dystonia musculorum deformans). *Adv Neurol* 50, 157-165 (1988).
- 264 Loscher, W., Annies, R. & Richter, A. Marked regional disturbances in brain metabolism of monoaminergic neurotransmitters in the genetically dystonic hamster. *Brain Res* 658, 199-208, doi:10.1016/s0006-8993(09)90027-0 (1994).
- 265 Ohno, Y., Shimizu, S. & Tokudome, K. Pathophysiological roles of serotonergic system in regulating extrapyramidal motor functions. *Biol Pharm Bull* 36, 1396-1400, doi:10.1248/bpb.b13-00310 (2013).
- 266 Wieland, S. & Lucki, I. Altered behavioral responses mediated by serotonin receptors in the genetically dystonic (dt) rat. *Brain Res Bull* 26, 11-16, doi:10.1016/0361-9230(91)90185-m (1991).
- 267 Peroutka, S. J. 5-Hydroxytryptamine receptor subtypes. *Annu Rev Neurosci* 11, 45-60, doi:10.1146/annurev.ne.11.030188.000401 (1988).
- 268 Konopka, R. J. & Benzer, S. Clock mutants of *Drosophila melanogaster*. *Proc Natl Acad Sci U S A* 68, 2112-2116, doi:10.1073/pnas.68.9.2112 (1971).
- 269 Paganelli, R., Petrarca, C. & Di Gioacchino, M. Biological clocks: their relevance to immune-allergic diseases. *Clin Mol Allergy* 16, 1, doi:10.1186/s12948-018-0080-0 (2018).
- 270 Buhr, E. D. & Takahashi, J. S. Molecular components of the Mammalian circadian clock. *Handb Exp Pharmacol*, 3-27, doi:10.1007/978-3-642-25950-0\_1 (2013).
- 271 Partch, C. L., Green, C. B. & Takahashi, J. S. Molecular architecture of the mammalian circadian clock. *Trends Cell Biol* 24, 90-99, doi:10.1016/j.tcb.2013.07.002 (2014).
- 272 Aguilar-Arnal, L. & Sassone-Corsi, P. Chromatin landscape and circadian dynamics: Spatial and temporal organization of clock transcription. *Proc Natl Acad Sci U S A* 112, 6863-6870, doi:10.1073/pnas.1411264111 (2015).

- 273 Zhang, E. E. & Kay, S. A. Clocks not winding down: unravelling circadian networks. *Nat Rev Mol Cell Biol* 11, 764-776, doi:10.1038/nrm2995 (2010).
- 274 Puram, R. V. *et al.* Core Circadian Clock Genes Regulate Leukemia Stem Cells in AML. *Cell* 165, 303-316, doi:10.1016/j.cell.2016.03.015 (2016).
- 275 Menet, J. S., Pescatore, S. & Rosbash, M. CLOCK:BMAL1 is a pioneer-like transcription factor. *Genes Dev* 28, 8-13, doi:10.1101/gad.228536.113 (2014).
- 276 Silva, C. M., Sato, S. & Margolis, R. N. No time to lose: workshop on circadian rhythms and metabolic disease. *Genes Dev* 24, 1456-1464, doi:10.1101/gad.1948310 (2010).
- 277 Eckel-Mahan, K. & Sassone-Corsi, P. Metabolism and the circadian clock converge. *Physiol Rev* 93, 107-135, doi:10.1152/physrev.00016.2012 (2013).
- 278 Golombek, D. A., Bussi, I. L. & Agostino, P. V. Minutes, days and years: molecular interactions among different scales of biological timing. *Philos Trans R Soc Lond B Biol Sci* 369, 20120465, doi:10.1098/rstb.2012.0465 (2014).
- 279 Kafka, M. S. *et al.* Circadian rhythms in catecholamine metabolites and cyclic nucleotide production. *Chronobiol Int* 3, 101-115 (1986).
- 280 Hampp, G. & Albrecht, U. The circadian clock and mood-related behavior. *Commun Integr Biol* 1, 1-3, doi:10.4161/cib.1.1.6286 (2008).
- 281 Roybal, K. *et al.* Mania-like behavior induced by disruption of CLOCK. *Proc Natl Acad Sci U S A* 104, 6406-6411, doi:10.1073/pnas.0609625104 (2007).
- 282 Yoon, S. O. & Chikaraishi, D. M. Tissue-specific transcription of the rat tyrosine hydroxylase gene requires synergy between an AP-1 motif and an overlapping E box-containing dyad. *Neuron* 9, 55-67, doi:10.1016/0896-6273(92)90220-8 (1992).
- 283 Hood, S. *et al.* Endogenous dopamine regulates the rhythm of expression of the clock protein PER2 in the rat dorsal striatum via daily activation of D2 dopamine receptors. *J Neurosci* 30, 14046-14058, doi:10.1523/JNEUROSCI.2128-10.2010 (2010).
- 284 Yujnovsky, I., Hirayama, J., Doi, M., Borrelli, E. & Sassone-Corsi, P. Signaling mediated by the dopamine D2 receptor potentiates circadian regulation by CLOCK:BMAL1. *Proc Natl Acad Sci U S A* 103, 6386-6391, doi:10.1073/pnas.0510691103 (2006).
- 285 Imbesi, M. *et al.* Dopamine receptor-mediated regulation of neuronal "clock" gene expression. *Neuroscience* 158, 537-544, doi:10.1016/j.neuroscience.2008.10.044 (2009).
- 286 Mauk, M. D. & Buonomano, D. V. The neural basis of temporal processing. *Annu Rev Neurosci* 27, 307-340, doi:10.1146/annurev.neuro.27.070203.144247 (2004).
- 287 Bueti, D., Lasaponara, S., Cercignani, M. & Macaluso, E. Learning about time: plastic changes and interindividual brain differences. *Neuron* 75, 725-737, doi:10.1016/j.neuron.2012.07.019 (2012).
- 288 Buhusi, C. V. & Meck, W. H. What makes us tick? Functional and neural mechanisms of interval timing. *Nat Rev Neurosci* 6, 755-765, doi:10.1038/nrn1764 (2005).
- 289 Matell, M. S. & Meck, W. H. Cortico-striatal circuits and interval timing: coincidence detection of oscillatory processes. *Brain Res Cogn Brain Res* 21, 139-170, doi:10.1016/j.cogbrainres.2004.06.012 (2004).
- 290 Meck, W. H. Neuroanatomical localization of an internal clock: a functional link between mesolimbic, nigrostriatal, and mesocortical dopaminergic systems. *Brain Res* 1109, 93-107, doi:10.1016/j.brainres.2006.06.031 (2006).
- 291 Turek, F. W., Dugovic, C. & Zee, P. C. Current understanding of the circadian clock and the clinical implications for neurological disorders. *Arch Neurol* 58, 1781-1787, doi:10.1001/archneur.58.11.1781 (2001).
- 292 Segawa, M. Hereditary progressive dystonia with marked diurnal fluctuation. *Brain Dev* 33, 195-201, doi:10.1016/j.braindev.2010.10.015 (2011).
- 293 Chen, K. F., Lowe, S., Lamaze, A., Kratschmer, P. & Jepson, J. Neurocalcin regulates nighttime sleep and arousal in *Drosophila*. *Elife* 8, doi:10.7554/eLife.38114 (2019).
- 294 Belanger, M., Allaman, I. & Magistretti, P. J. Brain energy metabolism: focus on astrocyte-neuron metabolic cooperation. *Cell Metab* 14, 724-738, doi:10.1016/j.cmet.2011.08.016 (2011).

- 295 Farrell, C. L. & Pardridge, W. M. Blood-brain barrier glucose transporter is asymmetrically distributed on brain capillary endothelial luminal and abluminal membranes: an electron microscopic immunogold study. *Proc Natl Acad Sci U S A* 88, 5779-5783, doi:10.1073/pnas.88.13.5779 (1991).
- 296 Simpson, I. A. *et al.* The facilitative glucose transporter GLUT3: 20 years of distinction. *Am J Physiol Endocrinol Metab* 295, E242-253, doi:10.1152/ajpendo.90388.2008 (2008).
- 297 van Hall, G. *et al.* Blood lactate is an important energy source for the human brain. *J Cereb Blood Flow Metab* 29, 1121-1129, doi:10.1038/jcbfm.2009.35 (2009).
- 298 Zielke, H. R., Zielke, C. L. & Baab, P. J. Direct measurement of oxidative metabolism in the living brain by microdialysis: a review. *J Neurochem* 109 Suppl 1, 24-29, doi:10.1111/j.1471-4159.2009.05941.x (2009).
- 299 Tracey, T. J., Steyn, F. J., Wolvetang, E. J. & Ngo, S. T. Neuronal Lipid Metabolism: Multiple Pathways Driving Functional Outcomes in Health and Disease. *Front Mol Neurosci* 11, 10, doi:10.3389/fnmol.2018.00010 (2018).
- 300 Mitchell, R. W., On, N. H., Del Bigio, M. R., Miller, D. W. & Hatch, G. M. Fatty acid transport protein expression in human brain and potential role in fatty acid transport across human brain microvessel endothelial cells. *J Neurochem* 117, 735-746, doi:10.1111/j.1471-4159.2011.07245.x (2011).
- 301 Panov, A., Orynbayeva, Z., Vavilin, V. & Lyakhovich, V. Fatty acids in energy metabolism of the central nervous system. *Biomed Res Int* 2014, 472459, doi:10.1155/2014/472459 (2014).
- 302 Romano, A. *et al.* Fats for thoughts: An update on brain fatty acid metabolism. *Int J Biochem Cell Biol* 84, 40-45, doi:10.1016/j.biocel.2016.12.015 (2017).
- 303 Wanders, R. J. *et al.* Peroxisomal fatty acid alpha- and beta-oxidation in health and disease: new insights. *Adv Exp Med Biol* 544, 293-302, doi:10.1007/978-1-4419-9072-3\_37 (2003).
- 304 Davletov, B. & Montecucco, C. Lipid function at synapses. *Curr Opin Neurobiol* 20, 543-549, doi:10.1016/j.conb.2010.06.008 (2010).
- 305 Schonfeld, P. & Reiser, G. Why does brain metabolism not favor burning of fatty acids to provide energy? Reflections on disadvantages of the use of free fatty acids as fuel for brain. *J Cereb Blood Flow Metab* 33, 1493-1499, doi:10.1038/jcbfm.2013.128 (2013).
- 306 Morris, A. A. Cerebral ketone body metabolism. *J Inherit Metab Dis* 28, 109-121, doi:10.1007/s10545-005-5518-0 (2005).
- 307 Halestrap, A. P. & Price, N. T. The proton-linked monocarboxylate transporter (MCT) family: structure, function and regulation. *Biochem J* 343 Pt 2, 281-299 (1999).
- 308 Cahill, G. F., Jr. Fuel metabolism in starvation. *Annu Rev Nutr* 26, 1-22, doi:10.1146/annurev.nutr.26.061505.111258 (2006).
- 309 Wood, T. R., Stubbs, B. J. & Juul, S. E. Exogenous Ketone Bodies as Promising Neuroprotective Agents for Developmental Brain Injury. *Dev Neurosci* 40, 451-462, doi:10.1159/000499563 (2018).
- 310 Cascalho, A. *et al.* Inhibition of Lipin lipid phosphatase hyperactivity rescues TorsinA neurological disease. *BioRxiv*, doi:10.1101/606947 (2019).
- 311 Heimer, G. *et al.* MECR Mutations Cause Childhood-Onset Dystonia and Optic Atrophy, a Mitochondrial Fatty Acid Synthesis Disorder. *Am J Hum Genet* 99, 1229-1244, doi:10.1016/j.ajhg.2016.09.021 (2016).
- 312 Bartke, N. & Hannun, Y. A. Bioactive sphingolipids: metabolism and function. *J Lipid Res* 50 Suppl, S91-96, doi:10.1194/jlr.R800080-JLR200 (2009).

## 6 Appendix

### 6.1 Supplementary data

**Table S 1: Top ten regulated pathways through WikiPathways 2019 human in total regulated genes in the striatum of wt naive vs  $\Delta$ ETorA ctrl rats**

Term	padj	Overlap	Genes
Circadian rhythm related genes	0.000008	5/201	DBP;CRY1;NR1D2;NR1D1;CIART
Exercise-induced Circadian Regulation	0.005247	2/48	CRY1;NR1D2
Synthesis and Degradation of Ketone Bodies	0.019802	1/5	ACAT1
Metabolism of Spingolipids in ER and Golgi apparatus	0.026689	1/9	SPHK2
Signal Transduction of S1P Receptor	0.044557	1/25	SPHK2
Sphingolipid pathway	0.044557	1/27	SPHK2
Matrix Metalloproteinases	0.044557	1/30	MMP14
Fatty Acid Beta Oxidation	0.044557	1/34	ACAT1
Melatonin metabolism and effects	0.044557	1/37	CRY1
Nuclear Receptors	0.044557	1/38	NR1D2

**Table S 2: Top ten regulated pathways through WikiPathways 2019 human in total regulated genes in the striatum of  $\Delta$ ETorA crush vs  $\Delta$ ETorA ctrl rats**

Term	padj	Overlap	Genes
Synthesis and Degradation of Ketone Bodies	0.010665	4/5	HMGCL;BDH1;HMGCS2;ACAT1
Circadian rhythm related genes	0.013965	24/201	CIPC;GFPT1;USP2;BHLHE41;NR1D2;NR1D1;NPAS2;ARNTL;RELB;CIART;PER2;PER1;MAPK8;PER3;DBP;NFIL3;ID2;CRY2;UBC;BHLHE40;NAMPT;ID4;AGRP;ATF5
mRNA Processing	0.176014	15/126	RBM39;NCBP1;PRMT2;FUS;SUPT5H;CLK4;PTBP2;HNRNPM;LSM7;TRA2B;SRSF2;SRSF3;HNRNPC;RBMX;RBM5
Melatonin metabolism and effects	0.176014	7/37	PER2;PER1;PER3;CRY2;ECE1;ADRB1;ARNTL
Exercise-induced Circadian Regulation	0.176014	8/48	PER2;PER1;BTG1;CBX3;CRY2;NR1D2;ARNTL;HERPUD1
Cytoplasmic Ribosomal Proteins	0.250860	11/89	RPS15;RPS26;RPS14;RPS17;RPS28;RPS27;RPS16;RPS8;RPL14;RPL35;RPLP2
EBV LMP1 signaling	0.250860	5/23	MAPK8;TRAF1;IKBKG;MAP3K7;MAP3K14
NLR Proteins	0.346694	3/9	MAPK8;IKBKG;MAP3K7
Canonical and Non-Canonical TGF-B signaling	0.346694	4/17	MAPK8;SMAD3;LOX;LOXL1
TP53 Network	0.424226	4/19	CDKN1A;TNFSF10;ATM;BOK

**Table S 3: Top ten regulated pathways through WikiPathways 2019 human in total regulated genes in the striatum of wt crush vs wt ctrl rats**

Term	padj	Overlap	Genes
Circadian rhythm related genes	0.002546	11/201	PER2;PER1;PER3;DBP;CIPC;CRY2; USP;BHLHE41;NR1D2;NR1D1; CIART
Melatonin metabolism and effects	0.004753	5/37	PER2;SULT1A1;PER1;PER3;CRY2
LncRNA-mediated mechanisms of therapeutic resistance	0.073125	2/6	CDKN1A;HIF1A
Epithelial to mesenchymal transition in colorectal cancer	0.073125	7/159	TGFB2;SHC1;COL4A1;CLDN12; PIK3R3;HIF1A;MAP2K6
Exercise-induced Circadian Regulation	0.073125	4/48	PER2;PER1;CRY2;NR1D2
Cerebral Organic Acidurias, including diseases	0.080774	2/7	ADHFE1;IDH2
PI3K-Akt Signaling Pathway	0.100143	10/340	GH1;CDKN1A;IL4R;ANGPT2;LAMC3; COL4A1;CREB3L1;PIK3R3;ITGA7; PRL
NRF2 pathway	0.100143	6/146	NQO1;TGFB2;SLC6A15;SLC6A13; SLC6A20;EPHA3
p38 MAPK Signaling Pathway	0.100143	3/34	TGFB2;SHC1;MAP2K6
Type 2 papillary renal cell carcinoma	0.100143	3/34	CDKN1A;TGFB2;HIF1A

**Table S 4: Top ten regulated pathways through WikiPathways 2019 human in total regulated genes in the striatum of wt crush vs  $\Delta$ ETorA ctrl rats**

Term	padj	Overlap	Genes
Cytoplasmic Ribosomal Proteins	0.000015	24/89	RPL30;RPL21;RPL10;RPL31;RPS8; RPLP0;RPL35A;RPL8;RPS15; RPS26;RPS14;RPS17;RPS28; RPS27;RPS16;RPL18A;RPL14; RPL35;RPLP2;RPL38;RPS2;RPS11; RPS21;RPS23
Focal Adhesion	0.098618	29/198	SHC2;ITGB5;SRC;LAMC3;SHC1; ITGA2B;PIK3R3;PDGFA;THBS2; ACTG1;MYL12B;PPP1CC;MAPK9; CCND3;PDGFC;CAPN2;PAK4;VASP; PRKCG;SRMS;TNK2;VEGFB; PARVB;FGR;COL4A2;COL4A1; RAPGEF1;ITGA7;ITGA6
Circadian rhythm related genes	0.098618	29/201	AHCY;CHRM1;CIPC;BHLHE41; ARNTL;CIART;CST3;PPP1CC; MAPK9;DBP;NFIL3;SIN3A;NAMPT; PRKCG;NTRK3;USP2;DYRK1A; NR1D2;NR1D1;NR2F6;PER2;PER1; PER3;ID2;CRY2;BHLHE40;HNRNPD; AGRP;ATF5
Cerebral Organic Acidurias, including diseases	0.098618	4/7	GCDH;MDH2;ADHFE1;IDH2
Oxidative Damage	0.222427	9/40	C1QB;C1QA;CDKN1A;CDKN1B;C1S; TRAF3;C1R;TNK2;C1QC
Synthesis and Degradation of Ketone Bodies	0.222427	3/5	HMGCL;BDH1;ACAT1
miR-517 relationship with ARCN1 and USP1	0.222427	3/5	CDKN1A;ID2;ID1
Complement Activation	0.247317	6/22	C1QB;C3;C1QA;C1S;C1R;C1QC
Hedgehog Signaling Pathway	0.247317	5/16	GRK2;SMO;SIN3A;KIF7;ARNTL
Canonical and Non-Canonical TGF-B signaling	0.268737	5/17	MAPK9;TGFB1;SMAD3;LOX;LOXL1

**Table S 5: Top ten regulated pathways through WikiPathways 2019 human in total regulated genes in the striatum of  $\Delta$ ETorA crush vs wt ctrl rats**

Term	padj	Overlap	Genes
Circadian rhythm related genes	0.000211	11/201	PER2;PPP1CB;PER3;DBP;CIPC;CRY2;BHLHE40;BHLHE41;NR1D2;ARNTL;CIART
Exercise-induced Circadian Regulation	0.000269	6/48	PER2;CBX3;CRY2;NR1D2;ARNTL;HERPUD1
Melatonin metabolism and effects	0.015239	4/37	PER2;PER3;CRY2;ARNTL
miRNA regulation of prostate cancer signaling pathways	0.093351	3/33	CDKN1A;CREB3L1;KRAS
Resistin as a regulator of inflammation	0.093351	3/33	PLCB3;PLCD4;PLCD1
GPR40 Pathway	0.194705	2/15	PLCB3;PLCD1
Hedgehog Signaling Pathway	0.194705	2/16	GLI2;ARNTL
TP53 Network	0.238758	2/19	CDKN1A;BOK
DNA Damage Response (only ATM dependent)	0.253767	4/110	CDKN1A;KRAS;HMGB1;MAP3K7
miRNA targets in ECM and membrane receptors	0.253767	2/22	COL4A2;COL4A1

**Table S 6: Top ten regulated pathways through WikiPathways 2019 human in total regulated genes in the striatum of  $\Delta$ ETorA crush vs wt crush rats**

Term	padj	Overlap	Genes
Acetylcholine Synthesis	0.131234	1/7	CHKA
Kennedy pathway from Sphingolipids	0.131234	1/13	CHKA
The human immune response to tuberculosis	0.131234	1/23	IFIT1
MTHFR deficiency	0.131234	1/25	CHKA
Intraflagellar transport proteins binding to dynein	0.131234	1/27	IFT140
Vitamin A and Carotenoid Metabolism	0.168897	1/43	RETSAT
One carbon metabolism and related pathways	0.168897	1/52	CHKA
Genotoxicity pathway	0.168897	1/63	GXYLT1
Endochondral Ossification	0.168897	1/64	FGF18
Genes related to primary cilium development (based on CRISPR)	0.237517	1/103	IFT140

## 6.2 List of Figures

Figure 1: Potential concept of the pathophysiology of dystonia.....	14
Figure 2: Basal ganglia network .....	16
Figure 3: Biosynthesis and metabolism of DA in the brain .....	19
Figure 4: Biosynthesis and metabolism of 5-HT .....	20
Figure 5: Schematic illustration of the multiscale characterization in a DYT-TOR1A rat model ( $\Delta$ ETorA).....	29
Figure 6: Schematic illustration of the setup for DBS and LFP recordings in rats.....	46
Figure 7: Self-assembled microdialysis probe for rats .....	52
Figure 8: Schematic illustration of <i>in vivo</i> microdialysis perfusion coupled to HPLC	55
Figure 9: DLM and non-dystonic postures during TST .....	58
Figure 10: Sciatic nerve crush triggers DLM in $\Delta$ ETorA rats.....	60
Figure 11: Locomotor activity level is unaffected in $\Delta$ ETorA rats .....	61
Figure 12: Genetic background has no influence on peripheral nerve regeneration.	62
Figure 13: Alterations in theta and beta oscillations in $\Delta$ ETorA rats .....	63
Figure 14: DBS improves DLM in $\Delta$ ETorA rats.....	64
Figure 15: Modulating effect of DBS on theta and beta oscillations.....	66
Figure 16: Genetic and environmental factors have an impact on glucose metabolism .....	68
Figure 17: Neuronal cell numbers and gene expression of neuronal marker in the striatum.....	70
Figure 18: Gene expression levels of cholinergic targets are unaffected .....	71
Figure 19: Glutamate receptors are not differently expressed on mRNA levels .....	72
Figure 20: Alterations in the striatal dopaminergic metabolism in $\Delta$ ETorA rats .....	74
Figure 21: High potassium is stimulating the striatal DA release .....	76
Figure 22: Increased striatal DOPAC levels and striatal DOPAC/DA ratio in nerve-injured $\Delta$ ETorA rats .....	78
Figure 23: Nerve crush injury affects the HVA levels in the striatum .....	80
Figure 24: Lack of evidence for dysregulation of DAT and dopaminergic receptors.	82
Figure 25: Alterations in the striatal serotonergic metabolism in $\Delta$ ETorA rats .....	83
Figure 26: Gene expression levels of 5-HT receptors remain unchanged.....	84
Figure 27: Differentially expressed genes (DEGs) identified by RNA-Seq in the striatum.....	85
Figure 28: Striatal top regulated pathways based on RNA-Seq data.....	86

Figure 29: Heat maps of two top regulated pathways representing color-coded expression levels of DEGs based on RNA-Seq data.....	87
Figure 30: Validation of RNA-Seq results by RKPM values.....	88
Figure 31: Validation of RNA-Seq results by qPCR of selected DEGs from the energy metabolism .....	89

### 6.3 List of Tables

Table 1: Classification of dystonia by Albanese et al. 2013 <sup>1</sup> .....	9
Table 2: Primary antibodies used in immunohistochemistry .....	38
Table 3: Primary antibodies used for western blot.....	39
Table 4: Secondary antibodies used in immunohistochemistry .....	39
Table 5: Secondary antibodies used for western blot .....	39
Table 6: Newly developed DLM scoring system .....	59
Table S 1: Top ten regulated pathways through WikiPathways 2019 human in total regulated genes in the striatum of wt naive vs $\Delta$ ETorA ctrl rats.....	123
Table S 2: Top ten regulated pathways through WikiPathways 2019 human in total regulated genes in the striatum of $\Delta$ ETorA crush vs $\Delta$ ETorA ctrl rats.....	124
Table S 3: Top ten regulated pathways through WikiPathways 2019 human in total regulated genes in the striatum of wt crush vs wt ctrl rats .....	125
Table S 4: Top ten regulated pathways through WikiPathways 2019 human in total regulated genes in the striatum of wt crush vs $\Delta$ ETorA ctrl rats.....	126
Table S 5: Top ten regulated pathways through WikiPathways 2019 human in total regulated genes in the striatum of $\Delta$ ETorA crush vs wt ctrl rats.....	127
Table S 6: Top ten regulated pathways through WikiPathways 2019 human in total regulated genes in the striatum of $\Delta$ ETorA crush vs wt crush rats.....	128

## 6.4 Abbreviations

°C	Degree Celsius
<sup>18</sup> F	Fluorine-18
θ	Theta
β	Beta
3-MT	3-Methoxytyramine
5-HIAA	5-Hydroxyindole-3-acetic acid
5-HT	Serotonin, 5-hydroxytryptamine
5-HTP	5-hydroxytryptophan
6-OHDA	6-hydroxydopamine
ΔE	Trinucleotide GAG in-frame deletion of the <i>TOR1A</i> gene
A	Ampere
AAA+	ATPases associated with various cellular activities
AADC	Aromatic amino acid decarboxylase
ACh	Acetylcholine
AChE	Acetylcholinesterase
AChR	Acetylcholine receptor
ALDH	Aldehyde dehydrogenase
AP	Anterior – posterior
APS	Ammonium peroxodisulfate
ATP	Adenosine triphosphate
AUX	Auxiliary electrode
BBB	Blood–brain-barrier
bp	Base pair
BSA	Bovine serum albumin
CaCl <sub>2</sub>	Calcium chloride dihydrate
CC	Corpus callosum
cDNA	Complementary DNA
ChAT	Choline acetyltransferase
CIN	Cholinergic interneurons
CMAP	Compound muscle action potentials
CNS	Central nervous system
COMT	Catechol-O-methyl transferase
CR	Calretinin

D <sub>x</sub> R	Dopamine receptor D <sub>x</sub>
DA	Dopamine
DAB	Diaminobenzidine
DAT	Dopamine transporter
DBS	Deep brain stimulation
DC	Dorsal - ventral
DEG	Differentially expressed gene
DLM	Dystonia-like movements, Dystonie-ähnliche Bewegungen
DNA	Deoxyribonucleic acid
DYT1	Dystonia 1
DYT-TOR1A	Dystonia 1
dNTP	Deoxynucleosidtriphosphate
DOPAC	3,4-Dihydroxyphenylacetic acid
DRD	Dopa-responsive dystonia
DTPA	Diethylene triamine pentaacetic acid
DTT	DL-Dithiothreitol
DV	Dorsal-ventral
EDTA	Ethylenediamine tetraacetic acid
EEG	Electroencephalography
EMG	Electromyography
ENG	Electroneurography
EP	Entopeduncular nucleus, Nucleus entopeduncularis
ER	Endoplasmic reticulum
FAM	6-carboxyfluorescein
FATP	Fatty acid transport protein
FDG	Fluorodeoxyglucose
FSI	Fast-spiking interneuron
GABA	Gamma-aminobutyric acid
GAPDH	Glyceraldehyde 3-phosphate dehydrogenase
GSEA	Gene set enrichment analysis
GLUT	Glucose transporter
GP	Globus pallidus
GPe	Globus pallidus externus
GPi	Globus pallidus internus

h	Hour
H <sub>2</sub> O	Water
H <sub>3</sub> PO <sub>4</sub>	ortho-Phosphoric acid
HD	Huntington's disease
HFS	High-frequency stimulation, Hochfrequenz-Simulation
HPLC	High performance liquid chromatography
HRP	Horseradish peroxidase
HVA	Homovanillic acid
Hz	Hertz
IgG	Immunoglobulin G
ISAAC	In situ Ag/AgCl reference electrode
KCl	Potassium chloride
kDa	Kilodalton
KH <sub>2</sub> PO <sub>4</sub>	Potassium dihydrogen phosphate
KLC1	Kinesin light chain 1
LAP1	Lamina-associated protein1 (TOR1AIP1)
L-DOPA	L-3,4-dihydroxyphenylalanine, levodopa
LFP	Local field potential
log <sub>2</sub> FC	Log <sub>2</sub> fold change
LTD	Long-term depression
LTP	Long-term potentiation
LTS	Low-threshold spiking interneuron
LULL1	Luminal domain like LAP1 (TOR1AIP2)
mAChR	Muscarinic acetylcholine receptor
MAO	Monoamine oxidase
MBq	Megabecquerel
MC	Motor cortex
MCT	Monocarboxylate transporters
MECR	Mitochondrial trans-2-enoyl-coenzyme A-reductase
MgCl <sub>2</sub>	Magnesium chloride
min	Minute
ML	Medial – Lateral
mRNA	Messenger ribonucleic acid
MSN	Medium-sized densely spiny neuron

NA	L-Norepinephrine
Na <sub>2</sub> HPO <sub>4</sub>	di-Sodium hydrogen phosphate
nAChR	Nicotinic achetylcholine receptor
NaCl	Sodium chloride
NADPH-d	Nicotinamide adenine dinucleotide phosphate-diaphorase
NaH <sub>2</sub> PO <sub>4</sub>	Sodium dihydrogen phosphate
NCV	Nerve conduction velocity
NE	Nuclear envelope
NGS	Normal goat serum
nNOS	Neuronal nitric oxide synthase
NOS	Nitric oxide synthase
NRS	Normal rabbit serum
NPY	Neuropeptide Y
OF	Open field
OSA	Octane-1-sulphonic acid
padj	Adjusted p-value
PBS	Phosphate buffered saline
PCR	Polymerase chain reaction
PD	Parkinson's disease
PE	Polyethylene
PET	Positron emission tomography
PFA	Paraformaldehyde
PNS	Peripheral nervous system
PV	Parvalbumin
qPCR	Real-time PCR
RNA	Ribonucleic acid
RNA-Seq	RNA sequencing
ROI	Region of interest
RPC	Reversed-phase chromatography
RPKM	Reads per kilobase per million reads
rpm	Rounds per minute
RT	Room temperature
RT-PCR	Reverse transcriptase polymerase chain reaction
SC	Somatosensory cortex

SD	Standard deviation
SDS-PAGE	Sodium dodecyl sulfate polyacrylamide gel electrophoresis
sec	Second
SEM	Standard error of the mean
SERT	Serotonin reuptake transporter
SN	Substantia nigra
SNAP25	Synaptosomal associated protein of 25 kDa
SNc	Substantia nigra pars compacta
SNr	Substantia nigra pars reticulata
SOM	Somatostatin
SPHK2	Sphingosine kinase-2
stim	Stimulation
STN	Subthalamic nucleus
SV	Synaptic vesicle
TBE	Tris-borate-EDTA
TCA	Tricarboxylic acid
TEA	Triethylamine
TH	Tyrosine hydroxylase
THS	Tiefe Hirnstimulation
TPH	Tryptophan hydroxylase
TRIS	Tris(hydroxymethyl)aminomethane
TST	Tail suspension test
UV	Ultraviolet
V	Volt
VAChT	Vesicular acetylcholine transporter
VMAT2	Vesicular monoamine transporter 2
WE	Working electrode
wt	Wildtype

## 7 Curriculum vitae



## 8 Publications

Original articles in peer-reviewed international journals

**Knorr, S.**, L. Rauschenberger, U. Ramirez Pasos, K. Grundmann-Hauser, T. Ott, A. O'Leary, A. Reif, A. A. Kühn, P. Tovote, J. Volkmann, C. W. Ip. 'Trauma triggers striatal dopaminergic network dysfunction and dystonia-like movements in DYT1 rats', *submitted*.

Karikari A. A., R. Ribechini, R. Blum, V. Bruttel, **S. Knorr**, U. Keber, M. Gehmeyr, J. Volkmann, J. M. Brotchie, F. Ahsan, CM. Monoranu, A. Pagenstecher, J. Wischhusen, J. B. Koprach, M. B. Lutz, C. W. Ip. 'Neurodegeneration by  $\alpha$ -synuclein-specific T cells in A53T- $\alpha$ -synuclein Parkinson's disease mice', *in preparation*.

Rauschenberger, L., **S. Knorr**, Y. Al-Zuraiqi, P. Tovote, J. Volkmann, and C. W. Ip. 2019. 'Striatal dopaminergic dysregulation and dystonia-like movements induced by sensorimotor stress in a pharmacological mouse model of rapid-onset dystonia-parkinsonism', *Exp Neurol*, 323: 113109.

Ip, C. W., I. U. Isaias, B. B. Kusche-Tekin, D. Klein, J. Groh, A. O'Leary, **S. Knorr**, T. Higuchi, J. B. Koprach, J. M. Brotchie, K. V. Toyka, A. Reif, and J. Volkmann. 2016. 'Tor1a $\pm$  mice develop dystonia-like movements via a striatal dopaminergic dysregulation triggered by peripheral nerve injury', *Acta Neuropathol Commun*, 4: 108.

Hofmann, U., **S. Knorr**, B. Vogel, J. Weirather, A. Frey, G. Ertl, and S. Frantz. 2014. 'Interleukin-13 deficiency aggravates healing and remodeling in male mice after experimental myocardial infarction', *Circ Heart Fail*, 7: 822-30.

Oral presentation

**Knorr S.**, Rauschenberger L., Ramirez Pasos U., Vitale F., Grundmann-Hauser K., Ott T., Volkmann J., Ip C.W. (2019) Multiscale characterization of a symptomatic DYT1 dystonia rat model. 7<sup>th</sup> Biennial Workshop on Dystonia, Rome, Italy

## Poster presentations

**Knorr S.**, Rauschenberger L., Grundmann-Hauser K., Higuchi T., Volkmann J., Ip C.W. (2019) Peripheral nerve crush injury as a trigger for a dystonic phenotype in an asymptomatic transgenic DYT1 rat model. IZKF Retreat, Kloster Banz, Germany

Rauschenberger L., Stengl A.F.R., **Knorr S.**, Grundmann-Hauser K., Volkmann J., Ip C.W. (2019) Development of a dystonic phenotype and striatal dopaminergic alterations in a DYT1 mouse model after peripheral nerve crush. 7<sup>th</sup> Biennial Workshop on Dystonia, Rome, Italy

Rauschenberger L., Stengl A.F.R., **Knorr S.**, Grundmann-Hauser K., Volkmann J., Ip C.W. (2019) Striatal dopaminergic dysregulation and dystonia-like movements induced by peripheral nerve crush in a transgene DYT1 mouse model. 23<sup>rd</sup> International Congress of Parkinson's Disease and Movement Disorders, Nice, France

Rauschenberger L., Stengl A.F.R., **Knorr S.**, Grundmann-Hauser K., Volkmann J., Ip C.W. (2019) Dystonia-like movements and altered striatal dopaminergic neurotransmission elicited by peripheral nerve crush in a DYT1 mouse model. 4<sup>th</sup> International Congress on Treatment of Dystonia, Hannover, Germany

Rauschenberger L., **Knorr S.**, Al-Zuraiqi Y., Volkmann J., Ip C.W. (2019) Abnormal plasticity, stress-dependent dopaminergic and glutamatergic dysregulation in the striatum of a DYT12 mouse model. Deutscher Kongress für Parkinson und Bewegungsstörungen, Düsseldorf, Germany

Stengl A.F.R., Rauschenberger L., **Knorr S.**, Grundmann-Hauser K., Volkmann J., Ip C.W. (2019) Striatal monoamine analysis hints at dopaminergic dysregulation in a phenotypic DYT1 mouse model. Deutscher Kongress für Parkinson und Bewegungsstörungen, Düsseldorf, Germany

Stengl A.F.R., Rauschenberger L., **Knorr S.**, Grundmann-Hauser K., Volkmann J., Ip C.W. (2018) Peripheral trauma elicits a dystonic phenotype in a DYT1 transgenic mouse model. 22<sup>nd</sup> International Congress of Parkinson's Disease and Movement Disorders, Hongkong, China

Rauschenberger L., **Knorr S.**, Al-Zuraiqi Y., Volkmann J., Ip C.W. (2018) Striatum of the ouabain-induced pharmacological DYT12 mouse model is affected by structural and metabolic abnormalities. 22<sup>nd</sup> International Congress of Parkinson's Disease and Movement Disorders, Hongkong, China

Rauschenberger L., **Knorr S.**, Al-Zuraiqi Y., Volkmann J., Ip C.W. (2018) Dopaminerge und mikrostrukturelle Veränderungen im Striatum eines pharmakologischen DYT12-Mausmodells. DGN-Kongress, Berlin, Germany

**Knorr S.**, Grundmann-Hauser K., Volkmann J., Ip C.W. (2017) Dystonia-like movements (DLM) in genetically predisposed DYT1 rats after peripheral nerve injury. EUREKA, Würzburg, Germany

**Knorr S.**, Grundmann-Hauser K., Volkmann J., Ip C.W. (2017) Dystonia-like phenotype in a DYT1 rat model after peripheral trauma. 21<sup>st</sup> International Congress of Parkinson's Disease and Movement Disorders, Vancouver, Canada

**Knorr S.**, Grundmann-Hauser K., Volkmann J., Ip C.W. (2017) Peripheral trauma triggers dystonia-like movements in genetically predisposed DYT1 rats. 6<sup>th</sup> Biennial Workshop on Dystonia, Rome, Italy

**Knorr S.**, Grundmann-Hauser K., Volkmann J., Ip C.W. (2016) DYT1 transgenic rats evolve dystonia after peripheral nerve injury. SfN Neuroscience Meeting, San Diego, USA

Karikari A.A., Gehmeyr M., Ribechini E., Maltese V., **Knorr S.**, Volkmann J., Brotchie J.M., Koprach J.B., Lutz M.B., Ip C.W. (2016) Lymphocytes contribute to motor deficits in the AAV1/2 A53T alpha-synuclein mouse model of Parkinson's disease. SfN Neuroscience Meeting, San Diego, USA

**Knorr S.**, Grundmann-Hauser K., Volkmann J., Ip C.W. (2016) Dystonia after peripheral nerve injury in DYT1 transgenic rats. 20<sup>th</sup> International Congress of Parkinson's Disease and Movement Disorders, Berlin, Germany

**Knorr S.**, Grundmann-Hauser K., Volkmann J., Ip C.W. (2016) Peripheral nerve injury leads to dystonia in DYT1 transgenic rats. 3<sup>rd</sup> International Congress on Treatment of Dystonia, Hannover, Germany

## 9 Danksagung

An dieser Stelle möchte ich mich bei Herrn Prof. Dr. Jens Volkmann ganz herzlich bedanken für die Möglichkeit meine Doktorarbeit an der Neurologischen Klinik im Team der Bewegungsstörungen absolvieren zu dürfen. Vielen Dank für Ihre Unterstützung, Betreuung und das Vertrauen in meine Arbeit.

Mein größtes Dankeschön geht an Herrn PD Dr. Chi Wang Ip für die Bereitstellung des sehr interessanten und intensiven Themas, die hervorragende Betreuung, die Diskussions- und Gesprächsbereitschaft. Du hattest immer ein offenes Ohr und konntest mich stets ermutigen, wenn Dinge auch mal suboptimal gelaufen sind. Auch deine positive Einstellung und das Vertrauen in meine Arbeit waren von unschätzbarem Wert, vielen herzlichen Dank dafür.

Zudem möchte ich mich bei Herrn Prof. Dr. Rudolf Martini und Herrn PD Dr. Robert Blum für die Betreuung und die Unterstützung meiner Doktorarbeit bedanken. Eure wissenschaftlichen Ratschläge, konstruktive Kritik und neue Ideen habe ich sehr geschätzt.

Weiterhin möchte ich mich bei Prof. Dr. Matthias Gamer für die Übernahme des Prüfungsvorsitzes bedanken.

Großer Dank auch an unsere Kooperationspartner in Tübingen, PD Dr. Kathrin Grundmann-Hauser und PD Dr. Thomas Ott. Vielen Dank Thomas, für deine hilfreichen Ratschläge und dass du es immer ermöglicht hast, unsere Vorstellungen umzusetzen.

Lisa, dir auch ein herzliches Dankeschön. Wir haben uns zusammen durch die großen Fragen der Dystonie gekämpft und tun es auch immer noch, dass hat zusammengeschweißt. Vielen Dank für die tolle Zusammenarbeit, die Diskussions- und Gesprächsbereitschaft und deine Freundschaft.

Vielen Dank Keali, Veronika, Heike, Louisa, Andrea für eure Unterstützung im Labor und in der Tierhaltung.

Danke Aet für deine Bereitschaft uns die Mikrodialyse zu erlernen und deine stetige Unterstützung und Hilfestellung bei allen Fragen zur Mikrodialyse.

Jeder braucht ein Büro 0601. Vielen Dank Lisa, Nicolo, Virginia, Chiara, Uri, Alice, Thomas, Massimiliano und Keali für die großartige Arbeitsatmosphäre, die Gespräche und Diskussionen, den Zwang zum Kaffeekonsum und besonders für eure Geduld und Unterstützung in allen Lebenslagen. All dies ist eine wahre Bereicherung für mein berufliches und auch privates Leben.

Bedanken möchte ich mich auch noch bei anderen Mitarbeitern des Kopfklinik-Teams, insbesondere bei Helga, Lydia, Dennis und Janos. Vielen Dank für eure hilfsbereite und freundliche Unterstützung in technischen Fragen. Durch Euch war es auch wie ein „nach Hause kommen“, als ich wieder in die Kopfklinik zurückgekehrt bin. Auch dem Tierhaltungs-Team der Kopfklinik ein herzliches Dankeschön.

Ein großes Dankeschön geht an meine Freunde. Ihr wart immer für mich da und habt mich bei allem unterstützt, dafür bin ich euch sehr dankbar.

Mein liebevollster und größter Dank gilt meiner Familie. Ihr habt mich immer unterstützt, mir beigestanden und immer an mich geglaubt, nur so konnte ich meine Pläne verwirklichen und das alles hier erreichen.

Vielen lieben Dank.